66–10,438

SENICH, Donald, 1929–

X–RAY DIFFRACTION AND ADSORPTION ISOTHERM STUDIES OF THE CALCIUM MONTMORILLONITE–H_2O SYSTEM.

Iowa State University of Science and Technology
Ph.D., 1966
Engineering, civil

University Microfilms, Inc., Ann Arbor, Michigan

X-RAY DIFFRACTION AND ADSORPTION ISOTHERM STUDIES OF THE CALCIUM MONTMORILLONITE-H_2O SYSTEM

by

Donald Senich

A Dissertation Submitted to the
Graduate Faculty in Partial Fulfillment of
The Requirements for the Degree of
DOCTOR OF PHILOSOPHY

Major Subject: Civil Engineering (Soils)

Approved:

Signature was redacted for privacy.

In Charge of Major Work

Signature was redacted for privacy.

Head of Major Department

Signature was redacted for privacy.

Dean of Graduate College

Iowa State University
Of Science and Technology
Ames, Iowa

1966

TABLE OF CONTENTS

	Page
INTRODUCTION	1
THEORY AND REVIEW OF LITERATURE	4
MATERIALS	27
Calcium Montmorillonite	27
Mercury	28
Calcium Chloride	29
Distilled Water	30
METHODS OF INVESTIGATION	31
Adsorption Apparatus	31
X-ray Apparatus	36
Procedures	47
Errors	58
DISCUSSION AND PRESENTATION OF RESULTS	60
X-ray Data	60
Sorption Data	115
CONCLUSIONS	187
BIBLIOGRAPHY	191
ACKNOWLEDGEMENTS	198

INTRODUCTION

According to Taylor (75), "The structural strength of a soil has been referred to by such names as bond, congealing, the development of preferred orientations of molecules, and the squeezing of adsorbed water films from between fine material particles". Research and field investigations have established that clay, especially the colloidal size fraction, is largely responsible for the plasticity characteristics of soils under various moisture conditions. However, a true explanation of soil strength where clay is involved depends to a large degree on a basic understanding of the colloidal phenomena that govern soil particle interactions (73).

Montmorillonite is a characteristic clay mineral exhibiting large volume and physical property changes at varying moisture content. The phenomena of clay-water interaction are of great interest in such fields as the ceramic industry where montmorillonite is used in manufacture of ceramics and binding of core sands, and in the petroleum industry where the important uses are as muds for drilling oil wells and as absorbents for purifying of petroleum products (21). In soil mechanics, clay-water suspensions have been extensively investigated in relation to strength, load bearing capacity, swelling and shrinkage, and consolidation. However, the direct application of the colloidal principles of surface chemis-

try has not progressed sufficiently to give the engineer much aid in his interpretations of various curious behaviors observed in clay materials. At the present time, engineers rely to a great extent on purely empirical tests for the indication of the surface chemical characteristics. Many problems of soil mechanics, such as secondary consolidation and cohesion, can not be solved by the basic mechanical approach. As a result many construction failures occur and continue to occur because the strength and sensitivity of the soil materials could not be predicted adequately from the empirical laboratory testing data (73).

It has been generally accepted that clay strength relates to the water films surrounding the individual grains (69). The amount of water normally associated with cohesive soils is characterized by the associated cation, the surface activity of the clay, and the type of clay mineral. Water can be held rigidly to the surface as surface film water, or in the case of expanding minerals, to internal surfaces as interlamminar water. When the associated surface films are so thick as to allow individual or groups of particles to slip past each other, the cohesive attraction is reduced. If, however, the water is removed as by evaporation, the surface tension forces at the air-water interface are increased and the water becomes more viscous until such a time as only solid or highly viscous water remains, effectively cementing parti-

cles together (58, 67). An understanding of the relationship between clay and water is essential for a proper appreciation of water retention and the basic mechanism of soil strength and soil structure.

Since natural soil clays are predominantly calcium saturated and because montmorillonites are perhaps the most abundant as well as being the most troublesome in engineering, a montmorillonite saturated with calcium ions was selected for this investigation. The objectives were to obtain a complete adsorption-desorption water vapor isotherm, and to obtain analogous X-ray diffraction data during adsorption and desorption of water on calcium montmorillonite; to determine the surface free energy changes during adsorption, expansion energies and swelling pressures, and by applying the BET theory and other accepted adsorption models, if possible suggest possible mechanisms of adsorption.

THEORY AND REVIEW OF LITERATURE

Clay mineralogy suddenly progressed from an art to a science with the adoption of X-ray camera and goniometric techniques. In 1930, Pauling (67) proposed a crystal structure for the mineral pyrophyllite. Hofmann, Endel, and Wilm (42), using an X-ray camera, were the first to demonstrate that the clay mineral montmorillonite has a layer lattice similar to pyrophyllite in chemical composition and crystal structure, but different in that the inner layer distances are variable and depend upon the water content. It is now generally accepted that montmorillonite is composed of unit layers -- a central alumina octahedral sheet sandwiched between two silica tetrahedral sheets. All tetrahedra are oriented pointing towards the center of the unit, and the tetrahedral and octahedral sheets are so combined that the tips of the tetrahedrons of each silica sheet and part of the hydroxyls of the octahedral sheet form a common layer, the atoms common to both the silica and alumina sheets being oxygens (Figure 1). The layers are continuous in the a and b directions and stacked above one another in the c direction (36, 77). They are held together by van der Waals forces, which are weak compared to the primary valence and ionic forces which hold the atoms in the unit layer together. Consequently, cleavage parallel to the unit layers is relative-

Figure 1. Atom arrangement in the unit cell of a three layer mineral (schematic)

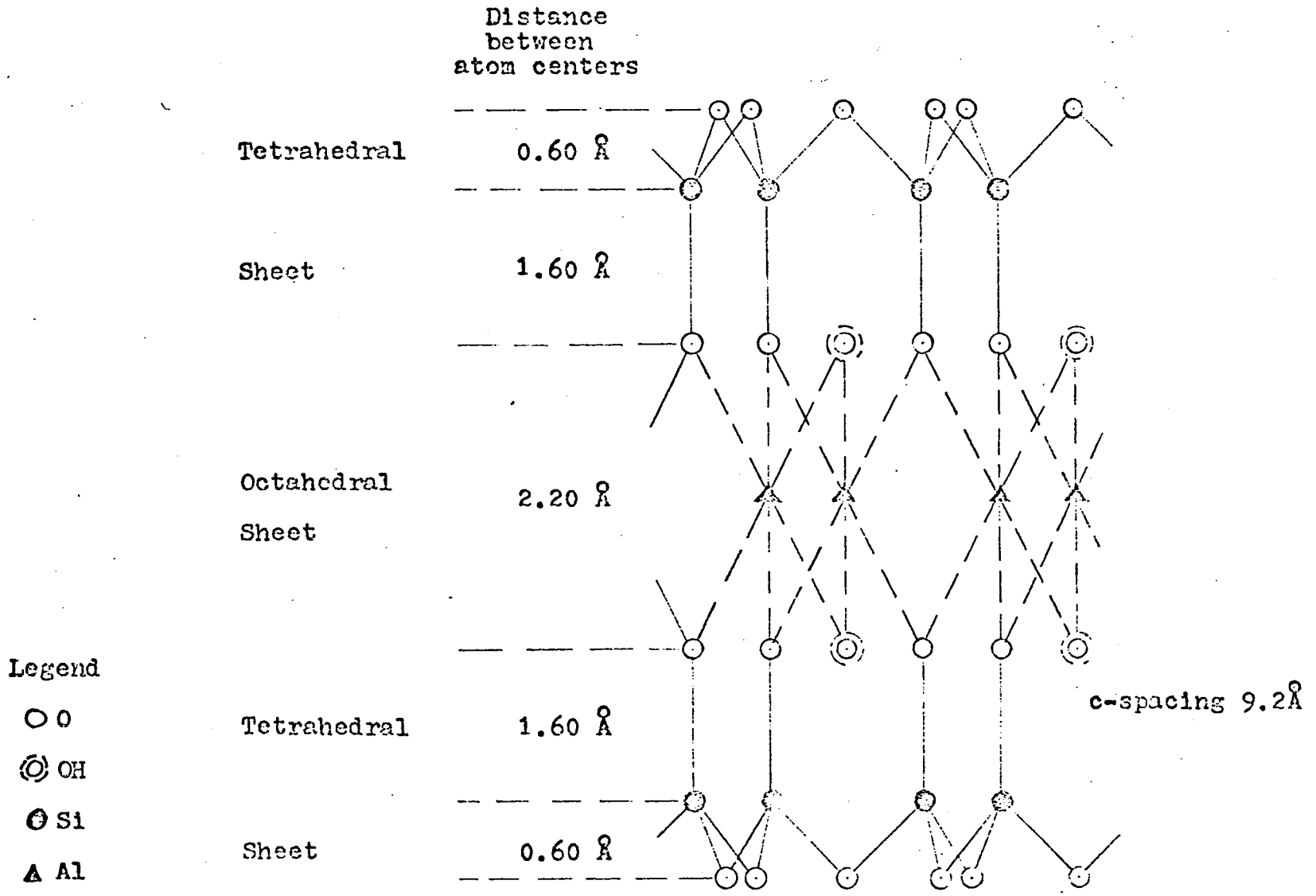
Distance between atom centers
Tetrahedral
0.60 Å
Sheet
1.60 Å
Octahedral Sheet
2.20 Å
Tetrahedral
1.60 Å
Sheet
0.60 Å
c-spacing 9.2Å
Legend
O
OH
Si
Al

ly easy. Figure 1 is a schematic atom arrangement of the montmorillonite structure (77).

Figure 2 is an electron micrograph of a typical calcium montmorillonite. As can be seen from electron diffraction pattern in the upper left-hand corner, and from a careful examination of the micrograph, the material is hexagonal or psuedohexagonal. The montmorillonite appears fluffy or cloudlike and shows only slight evidence of crystallinity, in contrast to sharp crystal outlines of clay minerals such as kaolinite or dickite. The fluffy thin flakes with irregular outlines would appear to be entirely commensurate with high adsorptive properties (24). The dark thin lines may be curled-up edges of montmorillonite sheets, although presently there is no conclusive evidence of this.*

The theoretical formula for zero lattice change montmorillonite is:

$$\left[Al_2 (OH)_2 (Si_2O_5)_2\right]_2 \cdot nH_2O \text{ (interlayer)}$$

Marshall (56) points out that the theoretical formula is altered by substitutions of Al^{+3} for Si^{+4} in the tetrahedral coordination and/or Mg^{+2} or Fe^{+2} for Al^{+3} in the octahedral coordination within the lattice. This substitution, called isomorphous substitution, tends to produce an electrically

---

*(Personal Communication Dr. E. A. Rosauer, Department of Ceramic Engineering, Iowa State University of Science and Technology, Ames, Iowa, 1966.)

Figure 2. Electron micrograph of calcium montmorillonite. Inset in upper left corner is a diffraction pattern of the material

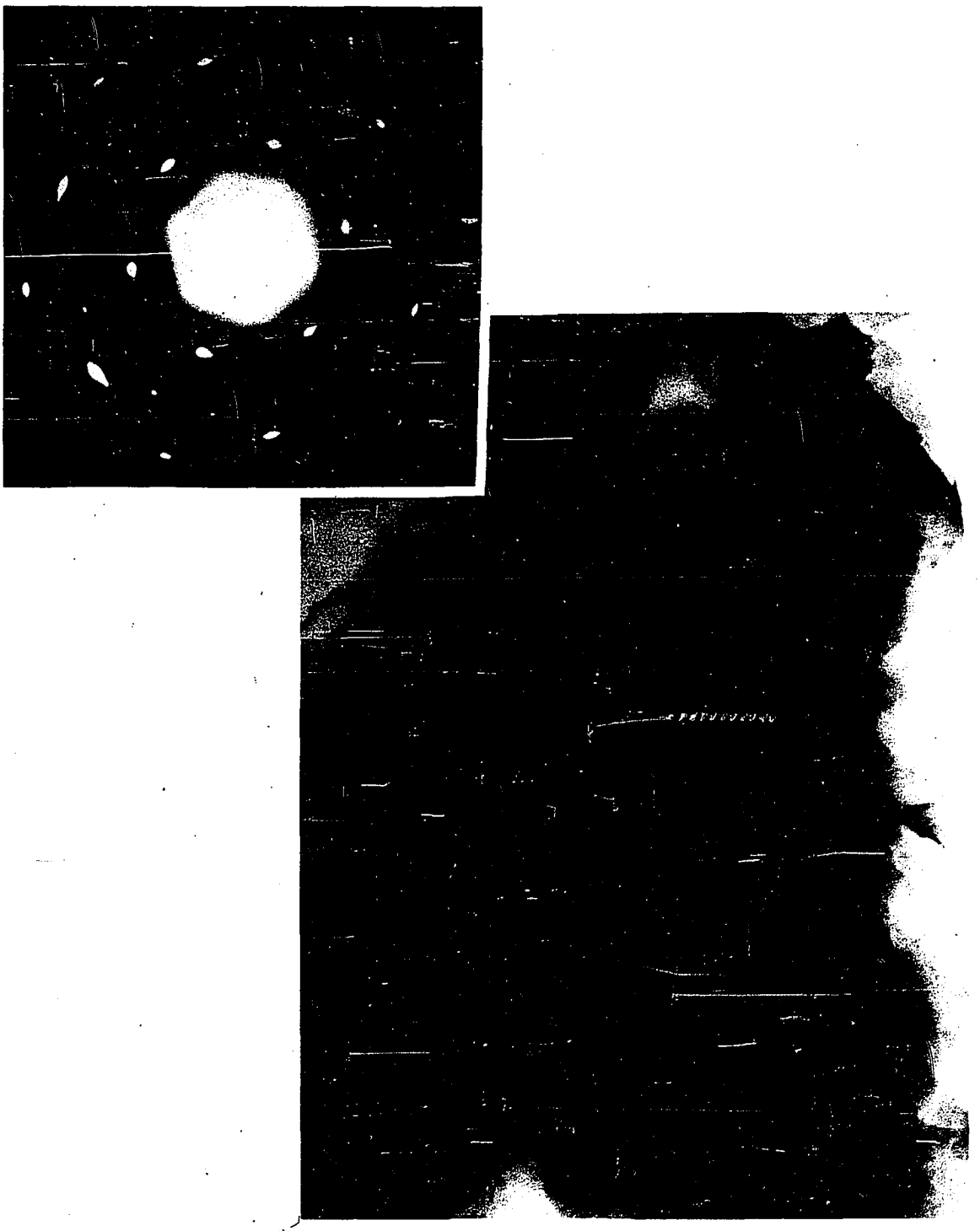

negative charge on the clay. The excess of negative lattice charge is compensated by adsorption of cations on the interlayer surfaces. The size and charge of the exchangeable cation and the charge density of the clay surface both affect the collapsed lattice spacing of a montmorillonite, as well as its swelling properties.

Montmorillonite is almost unique among the clay minerals in that it has an expanding c axis (64). Whereas in the mineral pyrophyllite the distance between related and identical planes of atoms is approximately 9.2 Å,* in the case of montmorillonite this distance will vary due to the cation adsorbed between the platelets as well as associated water molecules retained as interlayer water. Hofmann, Endel and Wilm (42) first determined that swelling of montmorillonite is a one-dimensional phenomenon and that the lattice separation in the c direction is not constant but varies with water content.

Maegdefrau and Hofmann (55) used samples of Ca-montmorillonites from Unterrupsroth, Rhoen, and Montmorillon, France, and determined that swelling takes place in a continuous manner and that the interlayer adsorption of water molecules takes place in discrete jumps indicative of water layers. Nagelschmidt (62) sealed and equilibrated the above-referenced Unterrupsroth montmorillonite in glass capillaries

---

*1 Angstrom = 10^{-8} cm.

and determined that there was a gradual proportional change in basal spacing from 10.5 Å to 15.4 Å as the water increases to four water molecules per unit cell. Adsorption of the next six molecules of water per unit cell was accompanied by a slight change of 0.4 Å in the basal spacing. On further increasing water, up to 40 molecules per unit cell, the spacing went up to 18.4 Å. Nagelschmidt concluded that the basal spacing at high water content depends upon the cation present. However, Bradley, Grim, and Clark (12) reached a different conclusion: After equilibrating Wyoming hydrogen bentonite over salt solutions they concluded that there was no evidence of gradual swelling, but that the hydrates have 2, 8, 14, 20, and 26 water molecules per unit cell corresponding to 10.6 Å, 12.4 Å, 15.4 Å, 18.4 Å, and 21.4 Å respectively. They further concluded that the first adsorbed water layer occupies 2.8 Å vertically and that the unit cell heights in the c direction vary due to water molecules hexagonally close-packed around the adsorbed cation. Quirk and Aylmore (68) point out that in calcium montmorillonite-water systems a basal spacing of 19 Å is always found. Although authors disagree as to the manner in which water is adsorbed, it is now generally accepted that the observed changes in basal spacing (d_{001}) can be attributed to a discrete number of molecular water layers adsorbed on interlayer surfaces.

Brunauer (16) states that "The term physical adsorption

may be defined as the disappearance of molecules from the gas phase and the remaining of these molecules attached to the surface of the solid and there held in place by a weak interaction between the solid and the gas" (16). Physical adsorption takes place spontaneously. The process is reversible and the adsorbate may be removed by lowering the pressure and is then recovered unchanged chemically (1). Other terms associated with physical adsorption are low temperature adsorption, secondary adsorption, and capillary condensation.

Atoms or molecules constituting a solid are held together by different forces: van der Waals or ionic forces or chemical bonds are involved. Whatever the nature of these forces, an atom located within the body of the solid is subjected to balanced forces in all directions or it would move out. An atom in the plane of a surface is subjected to unbalanced forces, the inward pull being greater than the outward pull, creating a surface energy or surface tension. The unbalanced forces of a solid surface tend to be decreased by the adsorption of molecules of a gas, and therefore all adsorption phenomena result in a decrease in the free energy of the system.

In 1915, different theories were proposed by Polanyi, Zsigmandy, and Langmuir in order to satisfy theoretical treatments of surface adsorption of gases and vapors.

Brunauer (16) has stated that "The Langmuir equation

is perhaps the most important single equation in the field of adsorption." Using the assumption that the molecules striking the bare surface condense on the solid and the other molecule-molecule actions result in an elastic reflection, and secondly, that there is no interaction between neighboring adsorbed molecules, Langmuir (47) derived the following:

$$\frac{p}{q} = \frac{1}{ab} + \frac{p}{b} \qquad (1)$$

where q is the volume of gas adsorbed at pressure p, a is the adsorption coefficient, and b is the volume of gas adsorbed when the surface is covered by a complete condensed single layer of molecules. When p/q is plotted as a function of p, a straight line is obtained with a slope of 1/b and having the intercept 1/ab on the vertical axis. These constants are neither arbitrary nor empirical constants, but well defined physical quantities, as seen in the equation.

The multimolecular adsorption (BET) theory was developed in 1938 by Brunauer, Emmett, and Teller (16, 19) is based on the following assumptions:

a. The same forces that produce condensation are also chiefly responsible for the binding energy of multimolecular adsorption.

b. The first adsorbed layer is attracted strongly by

the surface, the second layer essentially not by the surface but by the first adsorbed layer, and the adsorption thus propogates from layer to layer. Their derivation is a generalization of the Langmuir treatment of unimolecular adsorption and is based on a detailed balancing of forward and reverse rates of reaction (16). For adsorption on a free surface, they derived the equation:

$$v = \frac{v_m C p}{(p_o - p)\left[1 + (C - 1)p/p_o\right]} \qquad (2)$$

which can be more easily handled with relative vapor pressure in the form:

$$\frac{\frac{p}{p_o}}{v(1 - p/p_o)} = \frac{1}{v_m C} + \frac{C - 1}{v_m C}\,\frac{p}{p_o} \qquad (3)$$

In the above equations v is the volume of vapor adsorbed at pressure p, v_m the volume of the vapor adsorbed when the surface of the adsorbant is covered by a unimolecular layer of adsorbate, and p_o is the saturation pressure.

The constant C can be determined by the equation:

$$C = k\, e^{(E_1 - E_L)/RT} \qquad (4)$$

Since it can be shown that k does not differ much from unity, C is approximately given by the equation:

$$C = e^{(E_1 - E_L)/RT} \tag{5}$$

where E_1 is the average heat of adsorption in the first layer and E_L is the heat of liquification. Equation 3 becomes:

$$\frac{\frac{p}{p_o}}{q\,(1 - p/p_o)} = \frac{1}{q_m C} + \frac{C - 1}{q_m C}\,\frac{p}{p_o} \tag{6}$$

when the amount of vapor adsorbed is determined in terms of mass where q is the mass of the vapor adsorbed at pressure p, and q_m is the mass adsorbed at monolayer coverage at the adsorbant surface.

The multimolecular adsorption equation was developed assuming no capillary condensation. However, a more generalized isotherm equation which considers factors limiting the number of layers that can be adsorbed and also includes capillary condensation has been developed by Brunauer, Deming, Deming, and Teller (18) pointing out that there is a range of abnormally high adsorption and this adsorption is due to a higher heat of vaporiation of the last adsorbed layer than for preceding layers.

This more generalized equation reduces to equations 3 or 6 at low values of relative pressures.

According to the BET theory, physical adsorption may

be characterized at low pressures by the two parameters q_m and C. The isotherm equation of multimolecular adsorption taking place on a free surface is a linear equation; that is, the plot of $\frac{p/p_o}{q(1 - p/p_o)}$ versus p/p_o should give a straight line. The intercept of the straight line on the vertical axis is $1/q_m C$, and the slope is $C-1/q_mC$. One can therefore obtain the two constants q_m and C. Brunauer (16) points out, however, that "It may be worth emphasizing that the correctness of the theory is not proven with a plot of the data according to the isotherm equation that gives a straight line. It is also necessary that the evaluated constants should have reasonable values."

The values of E_1, the average heat of adsorption in the first layer calculated by equation 5 are less than measured heats of adsorption but of the same order of magnitude (17). Clampitt and German (23) point out that the assumption is commonly made in gas adsorption theories that the heat of adsorption of the second and higher layers of molecules is equal to the heat of vaporization of the bulk liquid and is independent of the number of adsorbed layers. This assumption fails to take into account that even if the molecules behave as if they were in a true liquid, the heat of vaporization is dependent upon the number of layers of liquid present. The heat of vaporization of the final layer is substantially different from the bulk liquid; this causes the

total heat of vaporization of the liquid above the first layer to be a function of the thickness. Clampitt and German (23) rederived the constant C from the BET equation, and although the form is the same, the constant C assumed a new meaning. C is:

$$C = e^{(E_1 - E_L) + (\Delta H_s - E_L)/RT} \qquad (7)$$

where ΔH_s is the heat of vaporization of the surface layer. The correction term $(\Delta H_s - E_L)$ accounts for the difference in the heat of vaporization of successive layers. The heat of vaporization of the liquid may be considered as a measure of the ease with which the molecules may be removed from the liquid, and the ratio between the heats of vaporization of the surface and the bulk molecules should represent the measure of the strength of the bonding between the molecules in the condensed states. By applying this correction, they obtained much better agreement between $(E_1 - E_L)$ values determined from adsorption data and heat of immersion experiments (17, 23). The correction value for water $(\Delta H_s - E_L)$ is equal to -1.7 kCal/Mole.

Goates and Hatch (35), using a slightly different approach, also developed a multimolecular adsorption equation. Although the form of the equation remains the same, the constant C is given by:

$$C = e^{(\Delta F_1^{\circ} - \Delta F_L)/RT} \qquad (8)$$

where ΔF_1° is the standard Gibbs free energy of adsorption (standard adsorption potential) of the gas on the bare solid surface and ΔF_L is the standard Gibbs free energy of the adsorbate.

Ross (72) compared the multi-molecular adsorption theory of Huettig with that of Brunauer and coworkers. Huettig's derivation assumes that the rate of evaporation of molecules in the first layer is proportional to the total number of molecules of that layer minus a certain effect produced by those molecules that are covered by one or more higher layers. In the BET theory, this effect is powerful enough to prevent evaporation of the first layer of molecules, whereas Huettig uses the opposite viewpoint, namely that molecules covered by second and higher layers still play a role in evaporation as freely as if the higher layers were not present. In general, from Huettig's equation the values of the specific surface of adsorbants agree rather well with those calculated using the BET theory, while the values of C are higher by as much as two or three times that of the BET. Deitz (25) has pointed out that the study of multi-molecular adsorption has developed in several directions since the BET theory was proposed, but, "...Other than to demonstrate the great complexity of the problem, there has been no real breakthrough since the BET theory was formulated".

A direct method for the determination of the surface

area of a powdered solid from the adsorption isotherm for a gas or a vapor on a solid has been suggested by Brunauer, Emmett and Teller on the basis of their multimolecular theory. When the data are plotted, the weight of vapor may be determined at which the surface of the solid is covered with a monomolecular layer of the vapor.

$$\sum = \frac{N_A\, q_m\, s}{M} \qquad (9)$$

where N_A is Avogadro's number, M is the molecular weight of the adsorbate, s is the area of an adsorbed molecule, and q_m is expressed for one gram of the adsorbant. Assuming that the adsorbed molecules have the same packing on the surface as the molecules of the liquified or solidified gas have in their plane of closest packing, we can obtain for the area covered by a molecule:

$$\text{Area } (s) = 4(0.866)\left(\frac{M}{4\sqrt{2}\, N_A \zeta s}\right)^{2/3} = 1.091\left(\frac{M}{N_A \zeta s}\right)^{2/3} \qquad (10)$$

where ζ_s is the density of the solidified or liquified adsorbate. Livingston (49) has defined the coefficient 1.091 as the packing factor and its value can vary from one adsorbant to another depending on the packing and adsorbant pores. Thus the equation $\sum = \frac{N_A\, q_m\, s}{M}$ can be used to deliver the

specific surface areas of adsorbents if the cross sectional area of the adsorbate molecules is known, or the equation can be used to determine the area occupied by an adsorbate molecule if the specific surface is known.

For clays with platelike particles, the total surface area per gram of clay may be computed from the unit cell dimensions. In montmorillonites, this total unit-layer surface area per gram of clay represents both the external and internal area which is accessible to exchange ions and to water or other polar molecules. Water is able to penetrate between the layers of montmorillonite while nitrogen and oxygen merely measure the external surface areas of the organized crystal particles. Therefore, the use of nitrogen can give us a good ideal of the external surface area.

Using water vapor, Emerson (28) determined by use of the BET equation that the total surface area of the calcium montmorillonite system was 710 m^2/gm. Nitrogen adsorption indicated that the external surface as 38 m^2/gm, giving a calculated internal surface of 672 m^2/gm. Aylmore and Quirk (4) determined a total crystallographic surface area of 760 m^2/gm and 112 m^2/gm for the external area using nitrogen adsorption. Therefore, the calculated internal surface area was 648 m^2/gm.

Hendricks, Nelson, and Alexander (39) investigated the effect of various chemisorbed cations on the adsorption of

water by the clay mineral montmorillonite. The different samples of montmorillonite had the same specific surface areas and the same number of equivalent weights of positive ions adsorbed, but differed from each other with the respect to the nature of the positive ions. They found that the adsorption of water at equal relative pressures depended strongly on the nature of the positive adsorbed ions, particularly at low relative pressures. Brunauer (16), using the water adsorption data of Hendricks et al. (39), calculated a specific surface of 400 m^2/gm. Zettlemoyer, Young, and Chessick (82) used ammonia adsorption on Wyoming bentonite and obtained a value of 556 m^2/gm, and 34.5 m^2/gm with nitrogen as the adsorbate. Mooney, Keenan, and Wood (60) used water desorption data to obtain values of about 800 m^2/gm, but could not obtain similar values during a later study (61). Goates and Hatch (35) found a value of 303 m^2/gm using water adsorption data for montmorillonite.

The above specific surfaces calculated from ammonia and water adsorption data assumed a closest packing of the adsorbate on the clay surface, and except for the data of Mooney et al. (60), are less than those which may be calculated from crystallographic data, which give a total surface as high as 800 m^2/gm (77).

It is possible to determine the free surface energy changes that occur during adsorption of vapors on solid sur-

faces using the Gibbs equation. This indirect method was first proposed by Bangham and Razouk in 1937 (5, 6). Their treatment was rigorously applied to nonporous solids (11, 45), and later the method was shown to apply for porous adsorbent and not to depend on the degree of compression (9, 27, 33). Inness and Rowley (43) have shown that the free energy of immersion of a solid in saturated vapor can be calculated from vapor adsorption data. A thermodynamic relationship between the spreading force and the data from adsorption isotherms was derived considering two reversible processes whereby the surface film could be formed. Jura and Harkins (45) pointed out that in order to obtain the value of the decrease of the free surface energy of the surface of a solid caused by the presence of a thin film adsorbed from a vapor, it is necessary to gather a considerable amount of experimental data in the low pressure region, which give the pressure of the vapor and the amount of vapor adsorbed when the temperature is constant. They further point out that, when expanded, the Gibbs equation for the free energy of a solid surface in saturated vapor is identical to that proposed by Bangham for the free energy of a solid surface.

Boyd and Livingston (11) have shown that if the adsorption isotherm for a vapor on a crystalline nonporous powder is obtained and if the specific surface area determined by the BET method (16) is employed, the change in free energy

of a clean solid surface upon immersion in a saturated vapor can be calculated. Using the Gibbsian adsorption equation, Boyd and Livingston (11) derived an equation for the free energy of immersion of a nonporous wettable surface in a saturated vapor. It can be made to read:

$$\Delta F = (\gamma sl - \gamma so + \gamma lv) = - \frac{RT}{M\Sigma} \int_{o}^{p_o} \frac{q}{p} \, dp \qquad (11)$$

where γ_{sl} is the solid liquid interfacial tension, γ_{so} the surface tension of the solid in a vacuum, γ_{lv} the surface tension in contact with its own vapor; q is the mass of the vapor adsorbed by a unit mass of the solid and the saturation pressure, respectively.

Demirel (26) has presented a somewhat simpler derivation based on thermodynamics, by considering that when a vapor at pressure p is in equilibrium with an adsorbed layer, the differential free energy change involved in isothermal transfer of one mole of saturated vapor onto a solid surface of unit area is equal to the difference between the chemical potential of the vapor at pressure p and at saturation pressure. The transfer involves the compression of the vapor, and the expansion of the adsorbed layer. He further points out that by substituting $p_o \, d(p/p_o)$ for dp, the expression may be changed to the following:

$$\Delta F = - \frac{RT}{M\Sigma} \int_o^1 \frac{q}{p/p_o} d\left(\frac{p}{p_o}\right) \qquad (12)$$

which is a more convenient form to use when relative vapor pressures are employed.

The value for ΔF, the free energy change accompanying the process of transferring the saturated vapor onto a unit area of solid surface can be calculated from equation 12. This transfer is completed when the equilibrium relative vapor pressure p/p_o equals one. Boyd and Livingston (11) and Jura and Harkins (45) recommend graphical integration of this equation as a simple and accurate means of determining F. Boyd and Livingston (11), and Jura and Harkins (45) calculated the free energy change by extrapolating the adsorption isotherm to saturation pressure with the assumption that no capillary condensation occurs. They make a correction which amounts to subtracting the surface tension of the liquid (γ_{lv}) from the equation for ΔF for obtaining the free energy of wetting, which presumes a zero contact angle. However, Craig et al. (22) have pointed out that this method leads to difficulties for nonporous powders because it is not possible to accurately extrapolate the adsorption isotherm to a definite limiting value, and a "nonporous" powder acts as a porous solid so that large numbers of capillary spaces are actually formed due to particle-to-particle contacts. The main difference in behavior between porous and nonporous solids is that dur-

ing adsorption of a vapor on a porous solid, the solid-vacuum interface is replaced by a liquid-vapor interface and a solid-liquid interface, and at $p/p_o = 1$ because of filling of the pores, the liquid-vapor interface is completely destroyed. In the case of a vapor on a nonporous solid, the area of liquid-vapor interface at $p/p_o = 1$ is not destroyed, and the area is considered to be essentially equal to that of the solid-vacuum interface (22). Because of the difficulties outlined above, a determined effort was made in this experiment to reach saturation as outlined later in procedures.

If the adsorbent is a non-interacting fine particle wettable by the liquid, capillary condensation in the contact zones of the particles would theoretically fill the voids with the liquid before final saturation is attained. In these cases, the change in free surface energy may be calculated by the equation:

$$\Delta F = (\gamma_{sl} - \gamma_{so}) \qquad (13)$$

where ΔF would be the free energy of immersion of a unit area of solid surface in a bulk liquid. Craig et al. (22), Dobay et al. (27), and Fu and Bartell (33) concur in this viewpoint. The free energy of wetting was calculated from the equation:

$$\Delta F = \frac{-RT}{M\Sigma} \int_0^1 \frac{q}{p/p_o} \, d\left(\frac{p}{p_o}\right) \qquad (14)$$

and the values determined by graphical integration.

In this study, the clay mineral being investigated consists of a solid powder adsorbent that has a rigid structure. This structure is not influenced by the adsorption of water vapor except as far as the adsorbate enters the interstices of the interacting solid surface and causes swelling between the platelets. This separation is manifested in separation against the forces of interaction (45) and the equation for the free surface energy must be modified as given by Demirel (26).

$$\Delta F = (\gamma sl - \gamma so) + \propto \Delta V \qquad (15)$$

The ΔF is the free energy of wetting of the solid by the liquid, ΔV is the change in potential energy of interaction, or the free energy per cm^2 of the intersticial surface due to the separation of particles against the force of interaction, and $\propto$ is the interfacial surface area per cm^2 of total surface (66, p. 253). The free energy change given by equation 15 for the clay mineral being investigated.

MATERIALS

Calcium Montmorillonite

To eliminate any difficulties that might arise from the introduction of foreign matter, the clay used was of a highly purified nature. The clay selected was a commercially available Wyoming bentonite known by the trade name Volclay-SPV, a product of the American Colloid Company. The major clay mineral which constitutes 90% of the Volclay is essentially sodium montmorillonite. The other 10% of the Volclay includes such materials as feldspar, quartz, and volcanic glass. The Volclay-SPV material was further purified from coarse-grained impurities by sedimentation. This sedimentation process was repeated for twelve cycles until the suspended material was less than one micron diameter and practically freed from coarse impurities.

Calcium montmorillonite was prepared by mixing a 100 cu cm saturated solution of calcium chloride (1,100 milliquivalents of calcium ions per 100 cu cm) with the 200 gm per liter clay suspension obtained after the last sedimentation cycle. Calcium chloride was slowly added to 3.5 liters of the suspension and was stirred constantly for 24 hours. The amount of calcium ions added by this process was about 16 times as much as required to satisfy the cation

exchange of the montmorillonite in suspension. The clay was then separated from the solution by means of a Sharples supercentrifuge. The clay was then redispersed in 3.0 liters of distilled water and again treated with 100 cu cm of the calcium chloride solution. This procedure was repeated five times to insure that the calcium ions replaced all the cations normally associated with the montmorillonite. The effective diameter of the material suspending in the water was 0.3 micron. The clay was washed free of all free electrolyte by dispersion in distilled water and centrifuging until a silver nitrate test showed the rinse water was free of all chloride ions. The calcium montmorillonite was then dried in a 40° C oven and ground to pass a No. 140 sieve. The physical and chemical properties were determined by standard procedures and are presented in Table 1.

Mercury

Mercury used in the manometers was C.P. grade triple-distilled mercury.

Table 1. Properties of the mineral used

Mineral	Calcium montmorillonie
Physical properties	
Liquid limit, %[1]	341
Plastic limit, %[2]	46
Plasticity index, %	295
Shrinkage limit, %[3]	34
Centrifuge moisture equivalent, %[4]	173
Chemical properties	
Cation exchange capacity, m.e./100 gm[5]	103
pH[6]	6.60

[1]Source (2: pp. 1286-1290).

[2]Source (2: pp. 1291-1293).

[3]Source (2: pp. 1297-1300).

[4]Source (2: pp. 1294-1296).

[5]Ammonium acetate method.

[6]Glass electrode method using suspension of 1 gm soil in 30 cc distilled water.

Calcium Chloride

The calcium chloride used was reagent-grade calcium chloride dihydrate meeting A.C.S. specifications.

Distilled Water

Throughout the laboratory work the distilled water used was obtained from a steam-heated type SLH-2 Barnstead Automatic Still. This still produces practically carbon dioxide-free distilled water with a pH approaching 7. The principle of operation is for all purposes a double distilling process: Incoming steam is condensed in coils; after cooling, the liquid is passed around the outside of the steam-condensing coils and is redistilled. In addition, for the adsorption experiments the distilled water was triple-distilled just before introduction into the apparatus.

METHODS OF INVESTIGATION

The adsorption and desorption isotherms were determined gravimetrically (by weighing). X-ray diffraction was used for studying the interlayer spacings at varying relative vapor pressures of water.

Adsorption Apparatus

A schematic diagram of the adsorption apparatus is shown in Figure 3. The adsorption apparatus employed consisted of an electrobalance system comprised of a beam balance (s), control unit (p), and vacuum flask (G), connected to a Sargent model SR recorder (R). The electrobalance was connected to the vacuum train by means of a large ground glass stopcock (S-1) and a mercury dual-limb cut-off (K). The sample (C), suspended from the electrobalance in a hangdown tube (F), and the water reservoir (A), were both suspended in a constant-temperature bath (B) having a capacity of 16 liters.

The vacuum train was a portable unit consisting of a rotary single stage forepump, an air-cooled oil diffusion pump, a dry ice-acetone cold trap, and a Cenco vacuum discharge gauge, all mounted on a rolling cart.

The constant temperature bath was equipped with a tap water cooling coil, a Beckman thermometer reading to 0.01°C,

Figure 3. Schematic drawing of adsorption apparatus

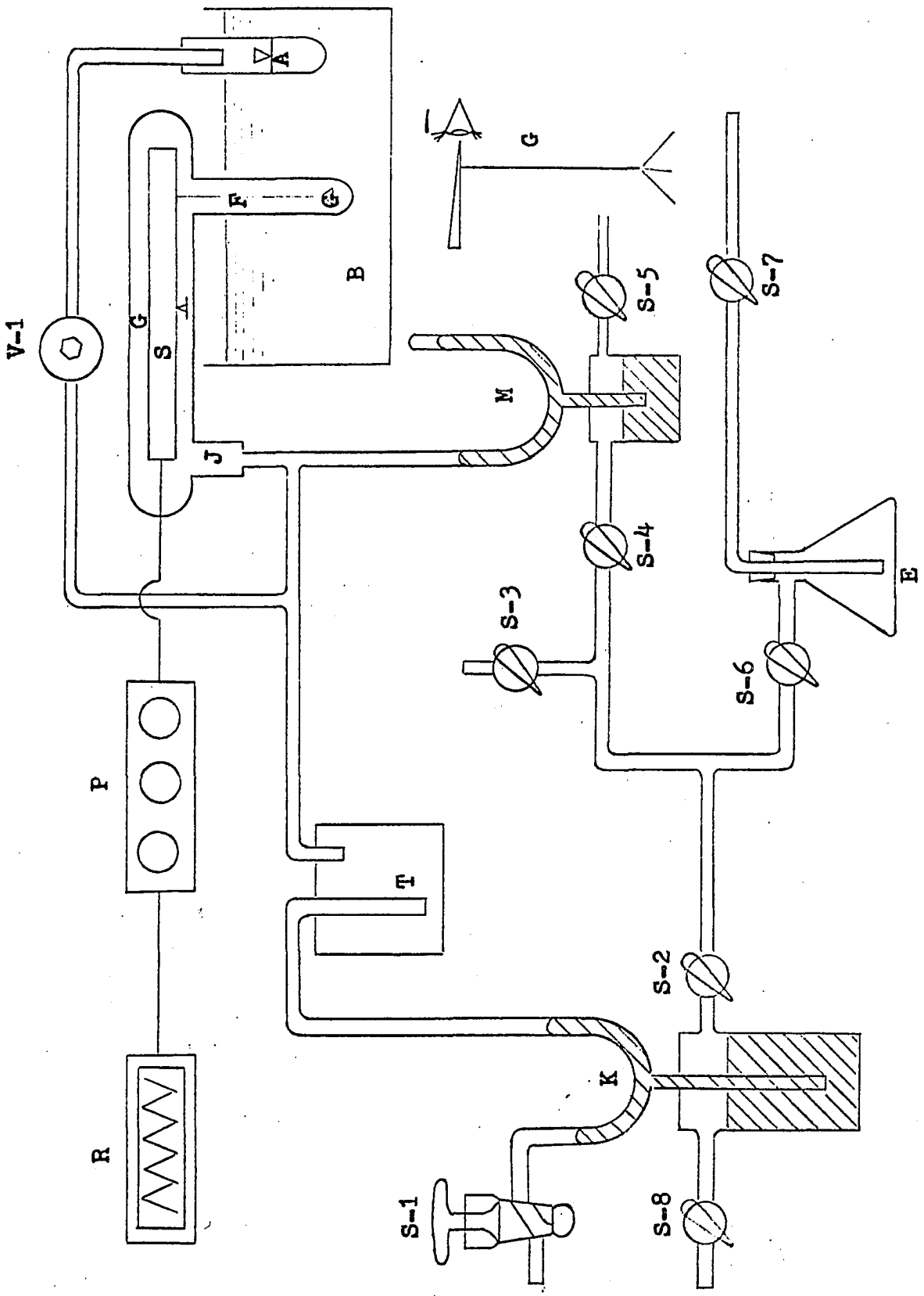
A
B
C
D
E
F
G
H
J
K
M
P
R
S
V-1
S-1
S-2
S-3
S-4
S-5
S-6
S-7
S-8

a continuous heater, and an intermittent heater-mercury regulator-relay circuit. The Beckman thermometer was calibrated against a N.B.S. certified thermometer at the thermostat temperature. The immersed heaters were two 100-watt light bulbs with variable transformer voltage control. Room temperature was maintained at about 2° C above that of the thermostat by using an air conditioner, electric space heater and normal room steam heat. Temperature variation in the thermostat (B) was not more than plus or minus 0.02° C throughout the entire investigation.

The tube A was the water reservoir used for introducing water into the system, and was attached to the system by means of an ultra-high vacuum valve V-1, obtained from the Granville-Phillips Company of Boulder, Colorado. The leak rate of the valve can be controlled from 1 liter/sec to 1×10^{-14} liters/sec. M is a simple mercury manometer used to determine the pressure in the adsorption chamber. The level of the mercury in the manometer was maintained by use of a mercury reservoir, the water aspirator and stopcocks (S-4) and (S-5). D is a mercury reservoir used to supply the cut-off K, stopcocks S-2 and S-8 being used to control the level of the mercury in the cut-off. A cold trap (T) was used during degassing to trap mercury vapor in the system. Stopcocks (S-2, S-4, and S-6 isolated the system from the water aspirator. All glass parts in the system were Pyrex, and a high-

vacuum silicone grease was used for all joints.

A cathetometer (E) used to read the manometer (M) was rigidly mounted on a soapstone table top tied to a steel framework to eliminate any movement during unattended periods. The electrobalance was supplied by the Cahn Instrument Company of Paramount, California and was afixed to a ten inch steel pipe which extended through the floor and was embedded at the bottom in several feet of chipped hard rubber to eliminate room vibrations. The load capacity of the balance is 1.0 gm. The smallest weight that can be reliably detected depends on the total load and the magnitude of the weight change; for the small sample used 10^{-6} gm was the precision of the balance, representing a balance sensitivity of 0.05% change in weight. The method of operation of the balance was essentially as follows: Changes in the sample weight cause the beam S to deflect momentarily; this motion changes the phototube current which is amplified and applied to the coil attached to the beam. The coil is in a magnetic field, so the current passing through it exerts a moment on the beam, restoring it to balance. The current is an exact measure of the sample weight. A signal is sent to the control unit P where it is amplified and the final signal is fed to the automatic recorder R.

Item J attached to the electrobalance is a cadmium trap whereby small strips of cadmium were placed in this well to

trap any mercury vapor from the manometer. This was found to be necessary to prevent mercury adsorption on the beam balance. The stopcocks in the system were sealed with mercury, and ground joints were sealed with Viton "O" rings to reduce the possibility of leaks into the system.

Figures 4 and 5 are photographs of the adsorption apparatus.

X-ray Apparatus

A special adsorption accessory for use with a General Electric XRD-5 diffractometer consisted of a Rigaku-Denki controlled-atmosphere high temperature X-ray diffractometer furnace modified to serve as an adsorption chamber and equipped with a mercury manometer and a water reservoir (Figures 6, 7, and 8). Figure 9 is a schematic diagram of the X-ray apparatus. The furnace heating element and element base were removed and a stainless steel sample holder was put in their place. This sample holder was so constructed that the clay adsorbent sample could be positioned in proper orientation by using the translation, rotation, and inclination controls provided for the alignment of the original furnace. Also, a constant temperature bath could be used to maintain the temperature in the adsorption chamber and in the water reservoir vapor source, since the original furnace in-

Figure 4. Equipment for adsorption measurements

Figure 5. Sorption isotherm equipment--thermostat and electrobalance in the foreground with the automatic recording device in the background

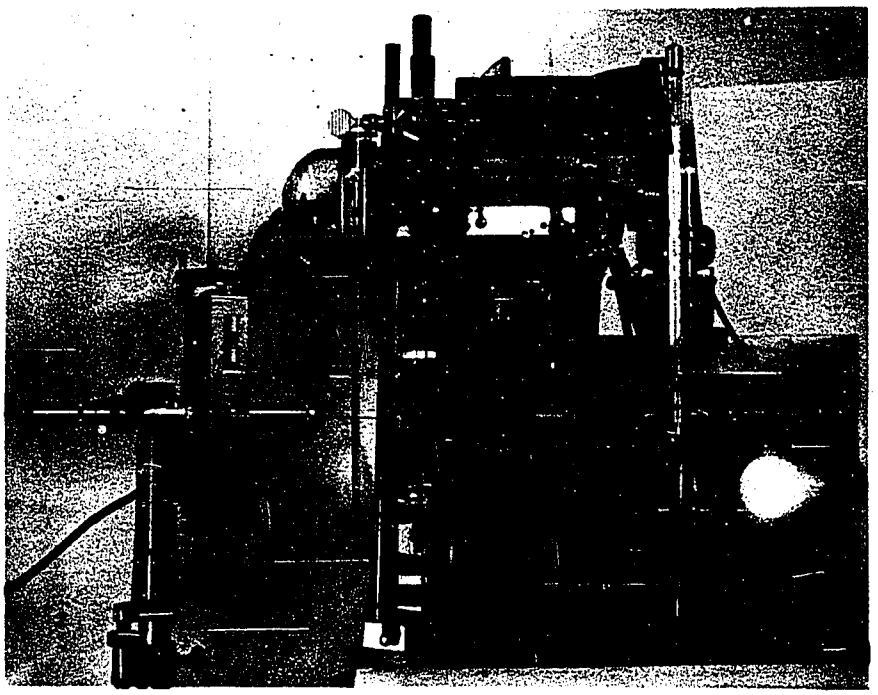

Figure 6. X-ray adsorption chamber mounted on the diffractometer with immersion cooler bath installed

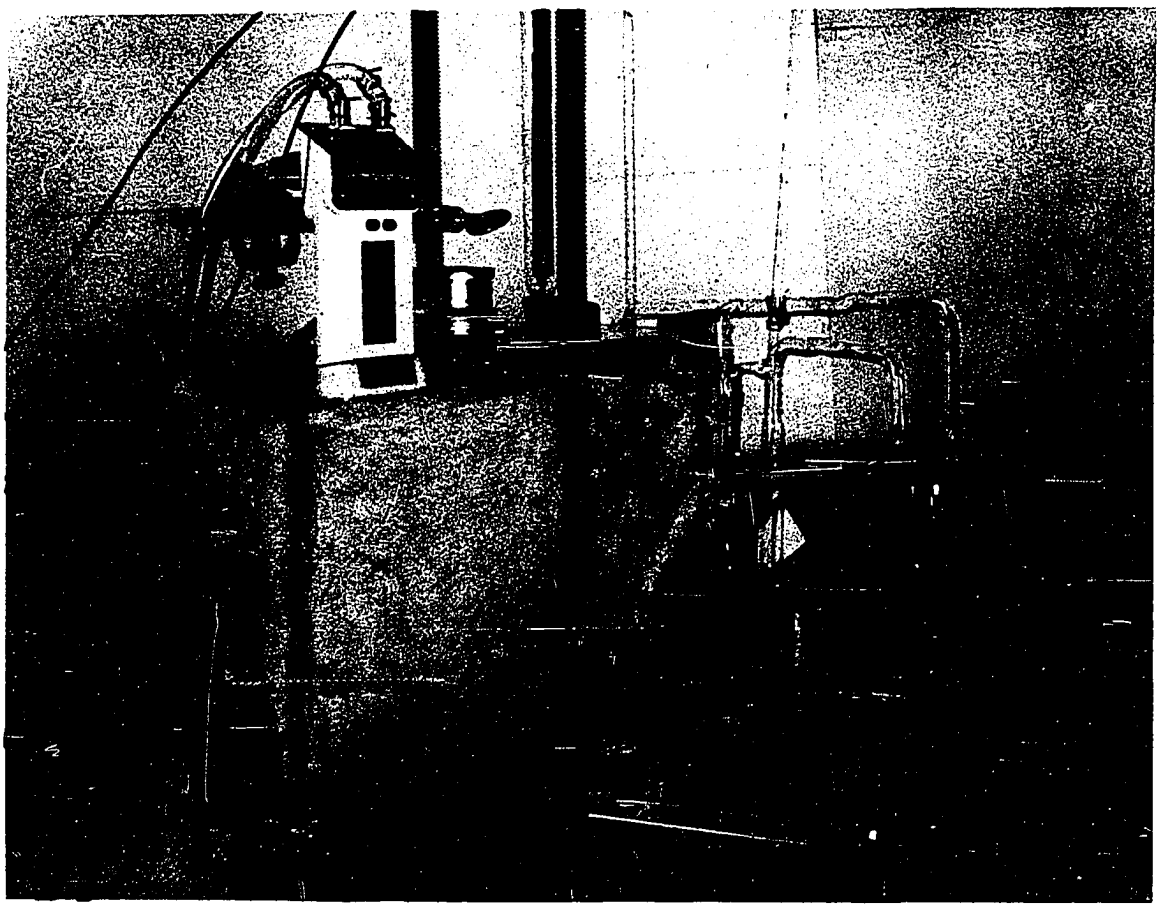

Figure 7. X-ray adsorption apparatus

Figure 8. X-ray adsorption chamber base showing sample holder

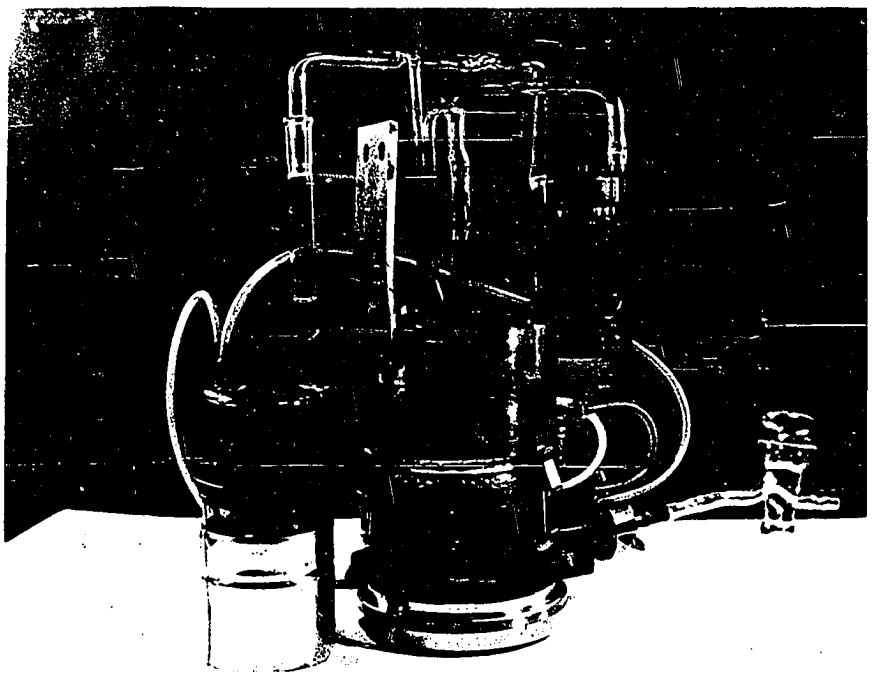

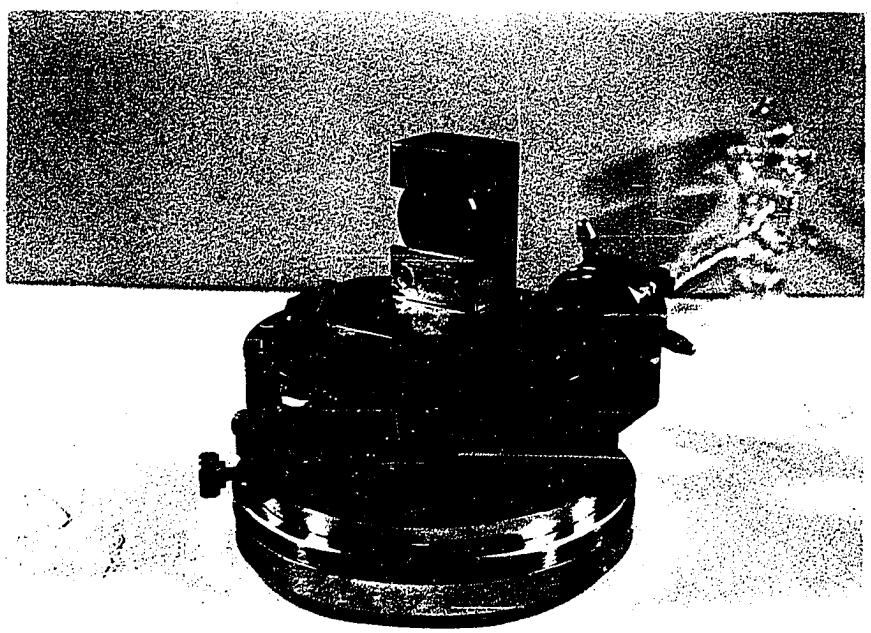

Figure 9. Schematic drawing of X-ray apparatus

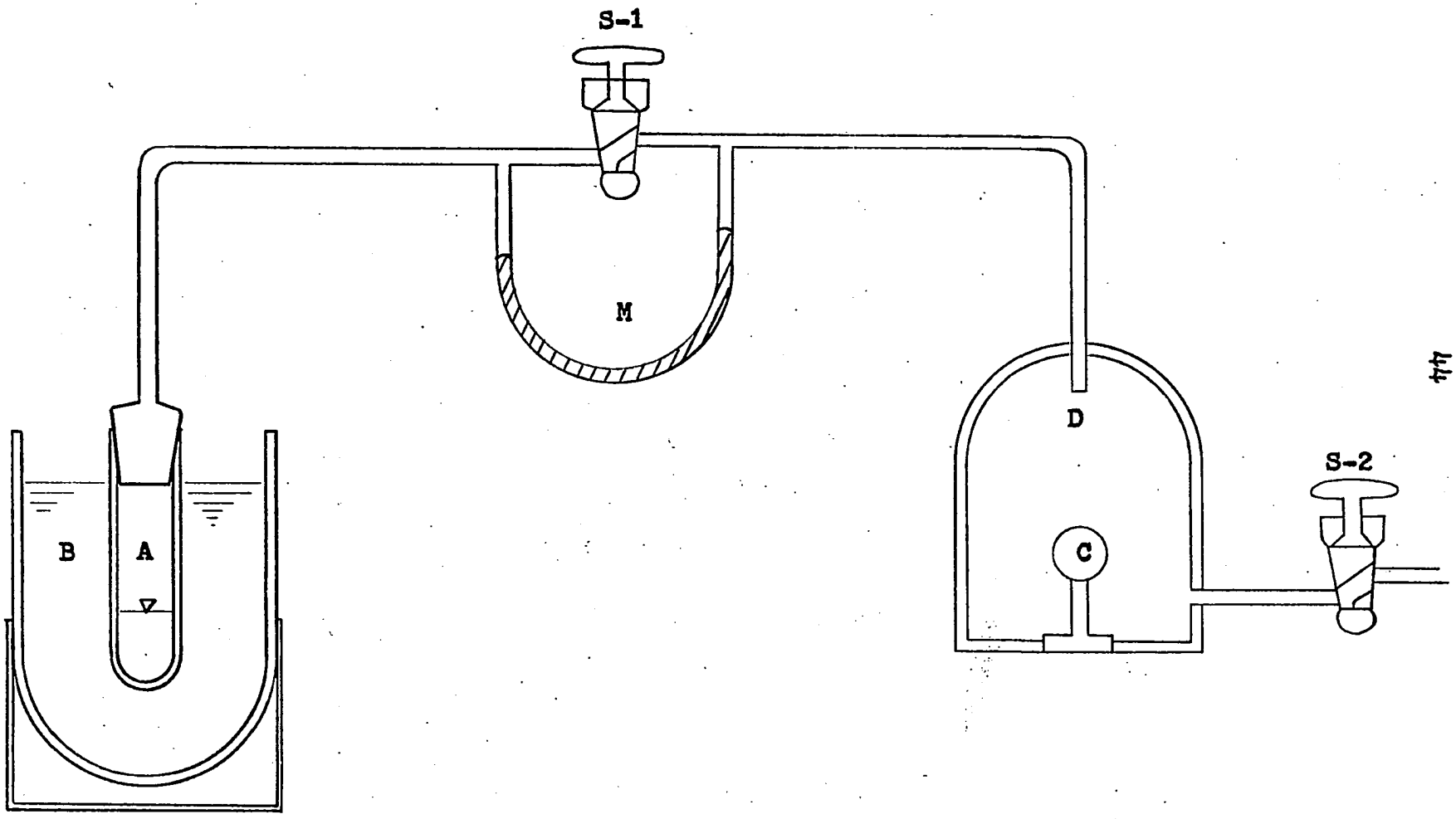
S-1
M
D
S-2
C
B
A

corporated cooling coils. The bath consisted of a polystyrene picnic cooler equipped with a circulating pump, a motor stirrer, a tap water cooling coil, intermediate and continuous immersion heaters with variable transformer voltage controls, a mercury thermoregulator-electronic relay circuit to control the intermediate heater, and a Beckman thermometer reading to 0.01° C. The constant temperature water was circulated through the cooling coils fastened in a water-filled Dewar flask to maintain a constant temperature in the water vapor reservoir, and through the coils in the adsorption chamber. The temperature of the thermostat was maintained at 25.02° C. The measured temperature in the Dewar flask surrounding the water vapor source was 25.0° C. All glass tubing and fittings were Pyrex glass, and high vacuum silicone grease was used on all moving parts.

For introduction of water into the adsorption chamber, a glass stopcock connecting the water reservoir to the adsorption chamber was cemented with epoxy into a small brass cylinder, which in turn was bolted to a large brass cylinder tightly fit and surrounding the top of the adsorption chamber. The male portion of the glass stopcock had a small horizontal slot filed adjacent to the port so that small increments of water vapor could be introduced to the clay sample. A large knurled brass knob was attached to the stopcock. Connection between the adsorption chamber and the vacuum train was made

by another tube attached to the exhaust port coupling by a Kovar metal tube and a large stopcock.

The same portable vacuum train was used as previously described.

A cathetometer capable of reading to 0.02 mm was used in measuring the differences in the mercury levels in each limb of the manometer. A General Electric XRD-5 diffractometer using copper Kα radiation was utilized in determining basal spacing and intensity throughout the investigation. The X-ray window on the adsorption chamber was formed by a 1/2 mil "Mylar" polyester film necessary to prevent pinhole corrosion of the aluminum foil by water.

Correction of mercury manometers for temperature and gravity

Vapor pressure determinations were converted to the standard scale by the relationship: $h_o\ g_o\ d_o = h\ g\ d$ where h_o is the corrected manometer reading, g_o and g are standard and local acceleration of gravity in cm/sec^2, and d_o and d are the density of mercury at 0^o C and at the test temperature in gm/cm^3. Values of $g_o = 980.665\ cm/sec^2$, and $d_o = 135{,}951\ gm/cc$ were used. Values of d at test temperatures were obtained from the literature (41). The local value of the acceleration of gravity is $g = 980.297\ cm/sec^2$ (26). When these values are substituted in the above relationship, the following correction value was obtained:

$$h_o = 0.75353\ d\ h$$

for both the adsorption apparatus and the X-ray apparatus.

Meniscus correction for observed mercury levels

The mercury levels in each limb of the manometers for both the adsorption apparatus and the X-ray chamber were corrected for capillary depression of the apex of the mercury columns, since water vapor caused the meniscus heights to differ slightly. After the inside diameter of the manometer limbs was determined, data from the International Critical Tables (63) were used to construct graphs of apex depression versus meniscus height (Figures 10 and 11). The corrected meniscus height was determined for each mercury level by adding to the measured meniscus height the correction factor corresponding to apex depression.

Procedures

Determination of the adsorption-desorption isotherm

Three hundred five mg of calcium montmorillonite were placed in a stainless steel ring (I.D. 0.375 inch) and then equilibrated under a bell jar containing hot water for two hours. The final humidty recorded under the bell jar was 91% as measured by a dial type Air Guide room humidity indicator. The loose sample and the ring were removed from the

Figure 10. Capillary depression of the apex of a mercurial column in a glass tube ten millimeters in diameter versus meniscus height for the adsorption chamber

Figure 11. Capillary depression of a mercurial column in a glass tube four millimeters in diameter versus meniscus height for the X-ray apparatus

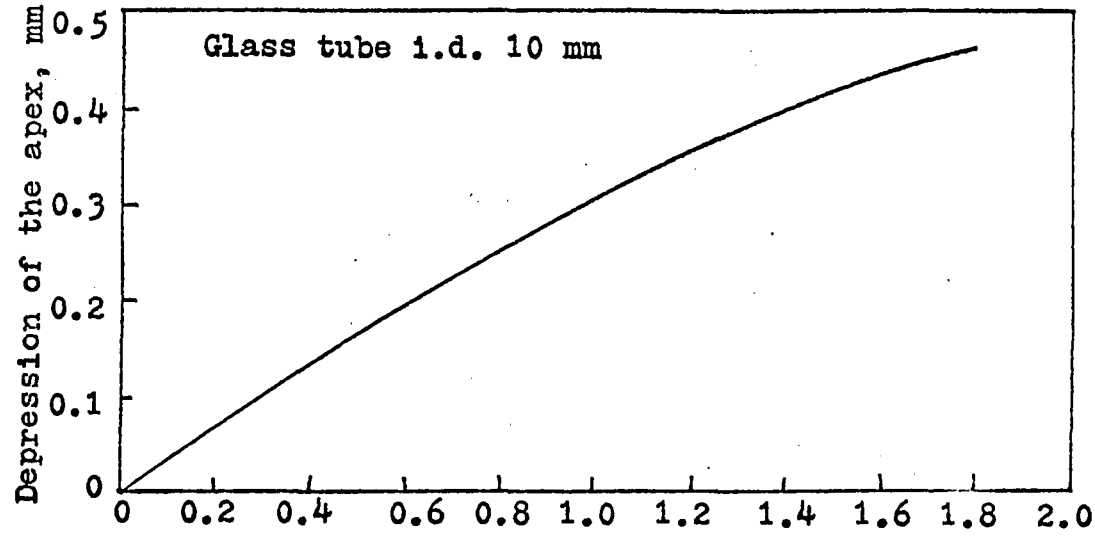
Glass tube i.d. 10 mm
Depression of the apex, mm
0.5
0.4
0.3
0.2
0.1
0
0 0.2 0.4 0.6 0.8 1.0 1.2 1.4 1.6 1.8 2.0

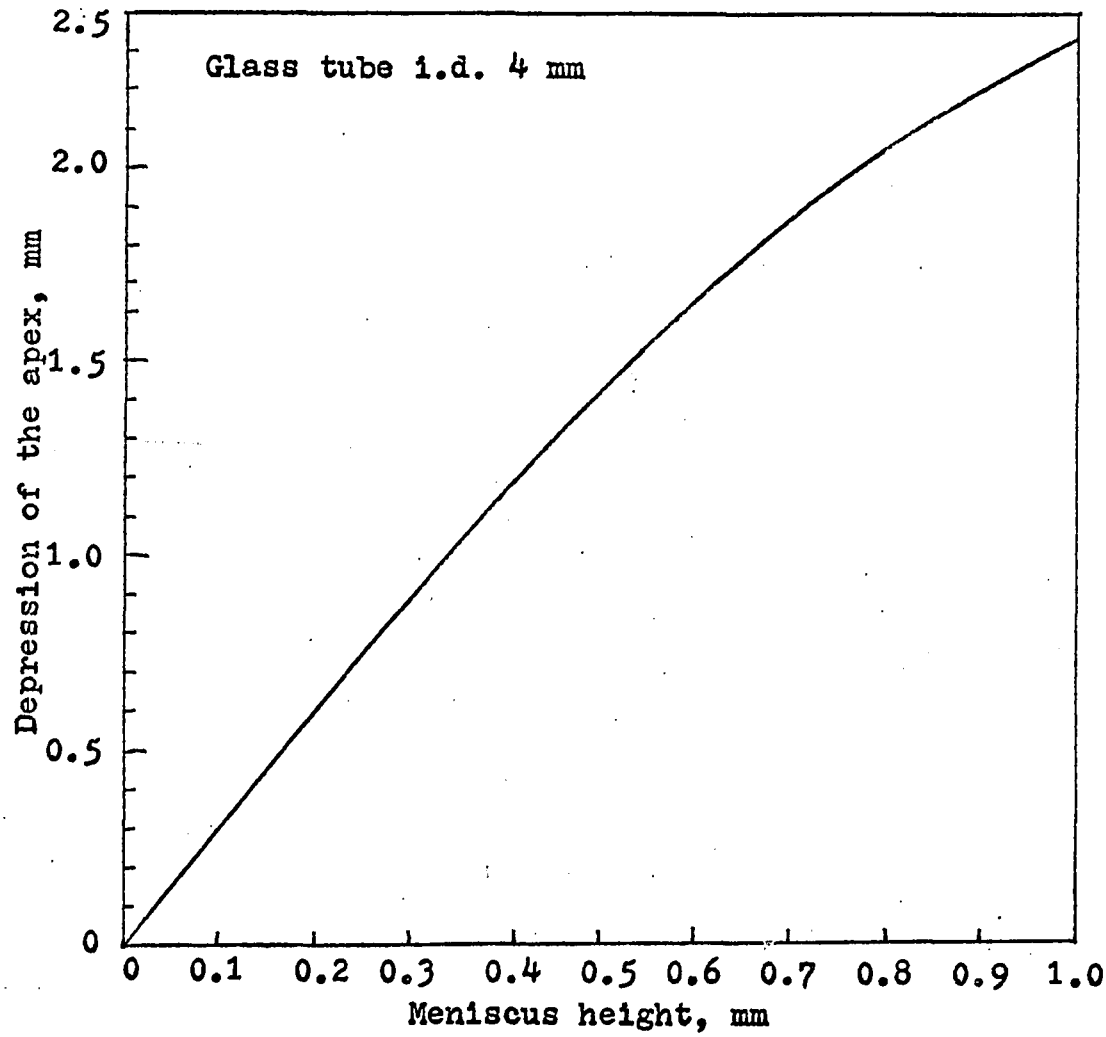
Glass tube i.d. 4 mm
Depression of the apex, mm
2.5
2.0
1.5
1.0
0.5
0
0 0.1 0.2 0.3 0.4 0.5 0.6 0.7 0.8 0.9 1.0
Meniscus height, mm

bell jar and placed on a press where the sample was subjected to a load of 25 Kg/cm^2 for two hours under ambient conditions of 23° C and 27% relative humidity. After removal of the load, the sample was extruded from the mold and the weight was found to be 300.52 mg. The sample was allowed to air dry for one day. Freshly boiled, triple-distilled water was introduced into the reservoir A; the reservoir was attached to the adsorption chamber and the pill-shaped sample was placed on the electrobalance pan. The thermostat water was brought to 25.00° C immediately after placing the sample in the hang-down tube of the electrobalance. The level of the mercury in cut-off K was lowered by means of the water aspirator and stopcock S-2, and the sample and balance were evacuated by using the aspirator through stopcock S-2. After evacuating the system with the water aspirator for one day, the sample weight was measured on the electrobalance and found to be 287.0 mg. Stopcock S-2 was closed and the system was connected to the high vacuum train; stopcock S-1 opened the system to the vacuum train. The system was pumped for 37 days with the mechanical and oil diffusion pumps.

To degas the water reservoir, the water in the reservoir was quickly frozen with a mixture of dry ice and acetone with valve V-1 closed. The valve V-1 was opened and the gases in the water reservoir and the sample were evacuated for 15 minutes. A pressure of 4.5×10^{-5} mm Hg was recorded on the

Cenco vacuum gage. After 15 minutes, valve V-1 was closed and the water allowed to thaw and release its trapped gases. This procedure for degassing of the water in the reservoir was repeated five times.

After 37 days of pumping, the weight of the sample and the pressure on the vacuum gage were 265.04 mg and 4×10^{-5} mm Hg respectively. Throughout the entire pumping period with the forepump and oil diffusion pump, cold traps were employed to trap moisture and mercury vapor in the lines. During the degassing as much of the apparatus as possible was heated with a hand torch, but because of the sensitivity of the balance and the clay to heat, they were not heated. During this period, mercury in the manometer M and in the cut-off K was deaired several times by raising and lowering the mercury. After degassing, the mercury level in the manometer M and in the cut-off K was raised and the main stopcock S-1 joining the adsorption chamber and the vacuum train was closed. Manometer readings were taken as soon as the evacuation was completed. Three readings of both the apex and lower edge of the mercury of both the left and right limbs of the manometer were taken and averaged to determine the pressure in the system. After correcting for temperature, gravity, and meniscus depression, the pressure was found to be 0.00 mm Hg. Immediately after taking the manometer readings, a reading of the automatic recording device was made

to determine the equilibrium weight in milligrams.

Vapor was transferred to the adsorption chamber in the following manner: Valve V-1 was opened slightly by use of a torque wrench, to allow a small increment of water vapor to enter the adsorption chamber. Valve V-1 was then closed with the torque wrench, and the weight automatically recorded on the apparatus as adsorption proceeded on the sample. Very small increments of water vapor were introduced in order to obtain the maximum number of points during adsorption. It was found that the equilibrium condition of adsorption on the sample was attained about three to four hours after introduction of the vapor. However, pressure readings and weight readings were recorded for a period of from four to eight hours. Equilibrium readings were taken intermittantly between four and eight hours and immediately prior to an additional transfer of vapor. In this manner, more and more vapor was introduced into the adsorption chamber and the pressures up to saturation at constant temperature were investigated.

In the vicinity of saturation two additional techniques were used to insure complete saturation. The high vacuum valve V-1 was left open and after there was no additional rise in weight of the sample, a small amount of ice-water was introduced against the side of the hangdown tube (F) containing the sample. This produced a small amount of dew

on the hangdown tube, and the time for the dew to disappear was observed. At pressures below saturation the dew disappeared rapidly, whereas at saturation the time of disappearance sharply increased. The weight as recorded on the automatic recorder showed very little change in the weight of the sample while the dew persisted on the side of the chamber. Secondly, at saturation, the room temperature was raised one degree centigrade. This slightly higher temperature in effect forced a condensation on the sample due to increase in pressure. This was continued until there was no further increase in the weight of the sample.

The desorption process was performed by cooling a dewar flask bath immediately surrounding the water reservoir A with chipped ice. When the dewar flask temperature reached equilibrium, valve V-1 was opened and small amounts of water that had been adsorbed on the sample were redistilled back into the water reservoir. A point at a saturation pressure of $p/p = 0.9994$ was selected as the point of departure for the desorption isotherm. It was possible to cause the return of water to the reservoir from saturation to a $p/p_o = 0.30$ in this manner. For a p/p_o 0.3 to 0.15, a dry ice trap was applied to the Pyrex tubing near the water reservoir. For p/p_o of 0.15 to 0.00, the water reservoir was cooled with a dry ice-acetone mixture. For the final removal of adsorbed water from the sample, the water bath was removed and the sys-

tem was again pumped by using the vacuum train.

Determination of interlayer spacing

Approximately 1.0 gm of calcium montmorillonite was dispersed in 250 ml of distilled water and then placed on a mechanical shaker and gently shaken at two-hour intervals for two days. A thin layer of clay was deposited on a 30 mm diameter fritted medium-porosity glass disk by pulling the clay suspension through the disk using a water aspirator. The sample was set aside to air dry for one day; on the following day it was placed in a desiccator containing phosphorous pentoxide, and the system was evacuated. After five days, the sample was removed from the desiccator and placed in the sample holder of the X-ray adsorption apparatus and the top was fastened into place. All joints were lubricated with high-vacuum grease to eliminate leaks. Freshly boiled, triple distilled water was placed in the water reservoir, the water reservoir attached to the apparatus, and the system degassed. Stopcock S-1 connecting the water reservoir and the chamber was closed and the water in the reservoir was quickly frozen by immersion of the reservoir in a dewar flask containing a mixture of dry-ice acetone. Stopcock S-1 was then opened and the sample and frozen water were evacuated with the forepump of the vacuum train to a vacuum of 10^{-3} mm Hg. Stopcock S-1 was then closed and the ice allowed to melt and release the

dissolved gases in the water. This degassing cycle was repeated three times with the forepump of the vacuum train immediately after attaching the water reservoir to the apparatus, and subsequently repeated three more times with the oil diffusion pump two days prior to the start of testing. Immediately after the initial degassing of the water reservoir with the forepump, stopcock S-1 was closed and the sample was continuously pumped for 26 days. A dry-ice acetone cold trap was utilized in the evacuation line. During the last eight days of degassing of the system, a vacuum of 5×10^{-5} mm Hg was maintained.

A constant temperature bath was prepared and brought to 25.02° C. After the 26-day evacuation period, stopcock S-2 was closed and the suction line between ground glass stopcock S-2 and the vacuum train was cut and sealed with a torch, and the adsorption apparatus was disconnected from the vacuum train. The adsorption apparatus was then connected to the constant temperature water circulating system, placed on the X-ray diffractometer and the sample was aligned according to the manufacturer's procedures. As soon as the system came to thermal equilibrium, the sample was X-rayed using copper K radiation, and a series of five diffractometer traces of the initial 001 peak was made. During the X-ray period, manometer readings were taken twice and corrected for temperature, gravity, and meniscus. The values obtained agreed with water

vapor pressures given in the literature (41). The initial 001 traces indicated a peak position at 10.15 Å, and a line breath at half-maximum intensity of B_o = 0.98 degrees at a calculated relative vapor pressure equal to zero.

Immediately after obtaining the traces of the original peak and determining the pressures, stopcock S-1 was partially opened to allow a small increment of water vapor to be distilled into the adsorption chamber. X-ray traces were then run at four-minute intervals for a period of 40 minutes, during which most change occurred. Traces of the 001 peak positions and pressure readings were recorded a minimum of four more times in the 24 hour period between the introduction of water vapor, and the equilibrium peak was recorded after 24 hours. The equilibrium peak was recorded five times and the manometer readings were recorded twice during each X-ray period and the equilibrium pressures and p/p_o were calculated as before: This procedure was repeated, with water being transferred from the water reservoir to the adsorption chamber in small increments, until saturation pressure was obtained.

In the vicinity of saturation, the following technique was employed to determine the position of the 001 peak spacing: The ground glass stopcock S-1 was left open and the water allowed to transfer over to the sample very slowly. This stopcock was not closed during the entire period of 334

hours. Traces were run of the 001 peak intermittantly and with a six hour maximum time interval between readings. After 242 hours, no shift in peak position was observed. A small amount of ice was applied to the Pyrex tubing extending from the water reservoir A to the adsorption chamber D; a small dew was produced in the Pyrex tubing, and since the dew did not disappear quickly, saturation had in fact been completed in the system.

Immediately prior to the start of the desorption studies, the Dewar flask surrounding the water reservoir was removed from the adsorption apparatus and the water reservoir A was immersed in a constant temperature bath (Figure 6). The thermostat consisted of the following: a 3.5 liter Plexiglass container insulated with two inch glass wool; a solid-state immersion cooler-heater purchased from the Chemical Rubber Company, Cleveland, Ohio; a motor-driven stirring device with a Plexiglass screw type paddle; a thermoregulator; a micro-relay; and a 25 ampere power source. The bath was filled with an ethylene glycol automobile antifreeze to allow the investigation to be carried out below freezing temperatures. With stopcock S-1 left open, the bath temperature was lowered in small increments, causing the water to redistill from the adsorption chamber back into the water reservoir A. X-ray traces of the equilibrium peak were taken a minimum of 24 hours after each thermal equilibrium was established. The

temperature of the bath was recorded for ten minutes during the X-ray period by means of a cathetometer and thermometer suspended in the bath immediately adjacent to the water reservoir A. This procedure was continued until a temperature of -15.8° C was attained, corresponding to a relative vapor pressure of 0.048. For values of p/p_o less than 0.048, the thermostat was removed and the water in the water reservoir quickly frozen by use of a dry ice-acetone mixture, finally, the vacuum train was used to obtain a relative vapor pressure of zero.

Errors

Experimental error in determining p/p_o

The errors in determining p/p_o for the electrobalance adsorption chamber were determined as follows: The readings of the mercury manometer were made with a cathetometer the reproducibility of which is ±0.005 mm. The maximum error in the value of p_o due to temperature variations was estimated to be 0.02 mm. The error in p/p_o was obtained through the use of the following relationship (76, p. 20):

$$\left(\delta \frac{p}{p_o}\right) = \left(\frac{\partial \frac{\Delta p}{p_o}}{\partial \Delta p}\, \delta \Delta p\right)^2 + \left(\frac{\partial \frac{\Delta p}{p_o}}{\partial p_o}\, \delta p_o\right)^2$$

which can be made to read:

$$\delta\frac{p}{p_o} = \pm \left[\left(\delta\frac{\Delta p}{p_o}\right)^2 + \left(1 - \frac{p}{p_o}\right)^2 \left(\delta\frac{p_o}{p_o}\right)^2 \right]^{1/2} \quad (16)$$

where $\delta p/p_o$, δp_o, and $\delta \Delta p$ are the errors in p/p_o, p_o, and the pressure difference respectively. The error in p/p_o calculated by this expression was found to be ± 0.0004 for all pressure ranges.

The error in determining p/p_o for the X-ray apparatus was determined from the equation 16 above: The readings of the cathetometer was found to be reproducible within ± 0.02 mm, and the maximum error in the value of p_o due to temperature variations was estimated to be ± 0.006 for all pressure ranges.

The experimental error in determining q

The automatic recording device had a reliability of 0.05% at the range selected. The error in grams of water vapor adsorbed per gram of clay specimen was estimated to be a maximum of $\pm 2 \times 10^{-5}$ gm/gm as determined from an average of four series of 20 recordings at selected equilibrium conditions.

DISCUSSION AND PRESENTATION OF RESULTS

X-ray Data

The accuracy in determination of X-ray diffraction peak positions depended on the angle at which the peak position appeared, the relative sharpness of the peak, the accuracy in alignment of the sample, and the alignment of the instrument. Ordinary commercial diffractometers incorporate a small misalignment because the sample is flat and is penetrated a certain distance by the X-rays, so part of the sample is struck by the beam beyond the instrument axis or outside the parafocusing circle. For best intensity, it is essential that the sample be of sufficient length to intercept the full incident beam at the lowest angle to be recorded; therefore, with the 30 mm diameter sample holder, a 1^{o} beam slit was used in conjunction with a medium resolution soller slit and a 0.2^{o} detector slit.

The alignment of the instrument and effect of systematic errors were tested by X-raying an Ethylene Diamine-d-Tartrate (EDDT) crystal and an Ammonium Dihydrogen Phosphate (ADP) crystal with copper radiation at 40 KV and 20 ma and a 0.007 inch Ni filter. These crystals normally are used for X-ray fluorescence analysis. Table 2 shows the results of the tests.

For highly precise lattice parameters one would plot the

Table 2. Calculated d_{001} spacings for the EDDT crystal and ADP crystal from secondary reflections

Sample	2θ	d, Å*	hKl	Calculated d_{001}, Å
EDDT	20.15	4.4382	001	4.4382
	40.95	2.2196	002	4.4392
	63.40	1.4776	003	4.4328
	88.95	1.1082	004	4.4328
ADP	16.62	5.3753	001	5.3753
	33.52	2.6901	002	5.3802
	51.30	1.7936	003	5.3808
	70.50	1.3453	004	5.3812

*The "d" value was calculated using unresolved $K\alpha$ doublet wavelength of 1.5418 Å.

calculated d_{001} versus a function of θ and extrapolate to $\theta = 90^\circ$, at which misalignment errors would disappear. However, the values for d_{001} in the Table agree within ± 0.003 Å, so no correction was made.

A standard deviation, σ, for the sample d_{001} was evaluated at one relative vapor pressure, and found to be $\pm 0.03^\circ$. In terms of basal spacing, this gives ± 0.03 Å at 9° 2θ and ± 0.10 Å at 5° 2θ.

The variations of measured line breadths from the average values were from $\pm 0.01^{\circ}$ to $\pm 0.10^{\circ}$ 2θ. The line breaths were determined as in Figure 12.

Intensities were measured by peak area measurement with a planimeter, and by digital counting and print-out during the scans. Peak intensities at selected equilibrium pressures were evaluated by averaging three peak areas. It was found that for the basal spacing pattern run prior to the introduction of the first increment of water vapor, the differences between the digital printer counts and planimetering method were $\pm 5\%$. Therefore, the intensities indicated in Figure 12 and in Tables 3 and 4 were measured by planimetering the diffraction patterns, and then corrected for the Lorentz-polarization factor by use of the International Tables for X-ray Crystallography (44, p. 270) and expressed relative to the starting intensities.

Figures 13 and 14 are plots of the apparent first order basal spacings versus the relative vapor pressure at which they were observed. The upper plots of Figures 13 and 14 are the line breadths and intensities versus the selected relative vapor pressures, respectively, expressed relative to the reference line breadth and intensity observed prior to the introduction of water vapor into the system. The data for these curves are presented in Tables 3 and 4.

As can be seen from the curves, the changes in average

Figure 12. Sketch showing the determination of X-ray diffraction peaks

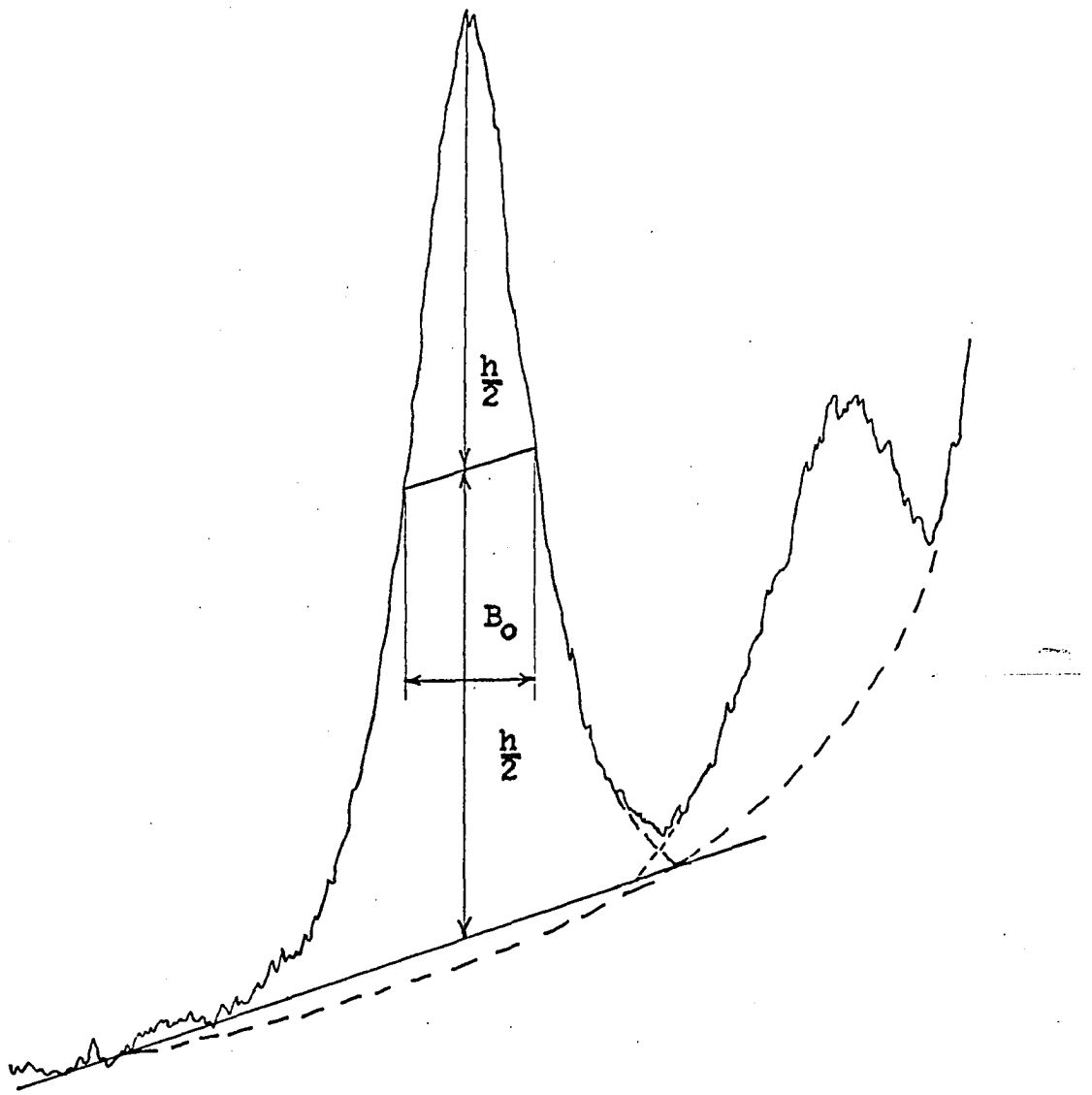
h/2
B₀
h/2

Table 3. X-ray diffraction data during adsorption

p, mm Hg	p_o, mm Hg	p/p_o	Apparent basal spacing, d_{001}, Å	Intensity of d_{001}, $in^2 \times 10^{-4}$ I	Relative intensity, $\frac{I}{\bar{I}}$	Line breadth B_o degrees	Relative line breadth $\frac{B}{B_o}$
0.00	23.756	0.000	10.15	5.65	1.00	0.98	1.00
0.31		0.013	10.39	8.38	1.48	1.12	1.14
0.52		0.022	11.18	9.59	1.70	1.22	1.24
1.09		0.046	11.78	9.65	1.71	1.20	1.22
1.61		0.068	11.93	10.98	1.94	1.23	1.25
2.19		0.092	12.32	11.32	2.00	1.20	1.22
3.30		0.139	12.58	11.32	2.00	1.23	1.25
3.78		0.159	12.62	12.56	2.22	1.30	1.33
4.13		0.174	12.68	12.41	2.20	1.36	1.39
4.47		0.188	12.79	11.50	2.04	1.35	1.38
4.60		0.194	12.98	10.71	1.90	1.44	1.47
5.32		0.224	13.54	11.66	2.06	1.49	1.52
5.46		0.230	13.66	12.40	2.19	1.43	1.46
6.04		0.254	14.08	11.47	2.03	1.42	1.45
6.49		0.273	14.54	11.81	2.09	1.35	1.38
7.15		0.301	14.85	12.77	2.26	1.16	1.18
7.41		0.312	14.93	12.90	2.28	1.12	1.14
7.91		0.333	15.01	13.17	2.33	1.06	1.08
8.48		0.357	15.05	12.94	2.29	1.02	1.04
9.10		0.383	15.16	13.48	2.39	0.97	0.99
9.48		0.399	15.35	10.30	1.82	0.91	0.93
9.86		0.415	15.46	10.85	1.92	0.88	0.90
9.98		0.420	15.49	10.79	1.91	0.88	0.90
10.41		0.438	15.55	10.88	1.93	0.87	0.89
10.67		0.449	15.60	10.93	1.93	0.84	0.86
10.79		0.454	15.63	10.42	1.86	0.84	0.85

Table 3. (Continued)

p, mm Hg	p_o, mm Hg	p/p_o	Apparent basal spacing, d_{001}, Å	Intensity of d_{001}, $in^2 \times 10^{-4}$ I	Relative intensity, $\frac{I}{\bar{I}}$	Line breadth B_o degrees	Relative line breadth $\frac{B}{B_o}$
11.00		0.463	15.57	10.07	1.78	0.84	0.85
12.09		0.509	15.66	10.67	1.89	0.80	0.82
12.19		0.513	15.63	11.00	1.95	0.79	0.80
12.90		0.543	15.63	11.15	1.97	0.77	0.78
13.47		0.567	15.66	11.13	1.97	0.74	0.76
14.71		0.619	15.66	11.52	2.04	0.68	0.69
14.97		0.630	15.69	11.39	2.02	0.68	0.69
15.85		0.667	15.69	11.76	2.08	0.68	0.69
17.01		0.716	15.79	12.00	2.12	0.66	0.67
18.32		0.771	15.94	11.64	2.06	0.64	0.66
19.13		0.805	16.03	11.86	2.10	0.64	0.66
20.31		0.855	16.03	11.78	2.08	0.62	0.64
21.41		0.901	16.08	11.52	2.04	0.63	0.65
21.91		0.922	16.26	11.70	2.08	0.66	0.68
22.19		0.934	16.23	11.49	2.03	0.64	0.65
22.83		0.961	16.41	11.63	2.04	0.70	0.71
22.90		0.964	16.31	11.52	2.06	0.67	0.68
23.50		0.989	16.63	11.40	2.02	1.32	1.35
23.47		0.988	17.25	10.92	1.93	1.38	1.41
23.50		0.989	18.02	9.89	1.75	1.27	1.30
23.50		0.989	18.95	9.20	1.63	0.98	1.00
23.756		1.000	19.25	7.92	1.40	0.68	0.69

Table 4. X-ray diffraction data during desorption

p, mm Hg	p_o, mm Hg	p/p_o	Apparent basal spacing, d_{001}, Å	Intensity of d_{001}, $in^2 x 10^{-4}$	Relative intensity, $\frac{I}{I_o}$	Line breadth B_o degrees	Relative line breadth $\frac{B}{B_o}$
22.71	23.756	0.956	19.23	7.97	1.41	0.73	0.74
21.38		0.900	19.19	8.56	1.52	0.76	0.77
20.01		0.842	19.07	8.95	1.58	0.76	0.77
19.25		0.810	19.15	8.63	1.53	0.76	0.77
17.96		0.756	19.19	12.10	2.14	0.76	0.78
16.70		0.703	19.10	8.38	1.48	0.82	0.84
15.63		0.658	18.95	8.64	1.53	0.86	0.88
14.42		0.607	16.14	12.12	2.14	0.78	0.80
13.16		0.554	15.77	11.85	2.10	0.63	0.65
12.07		0.508	15.77	12.15	2.15	0.62	0.64
11.07		0.466	15.73	12.18	2.16	0.64	0.65
10.00		0.421	15.60	12.41	2.20	0.65	0.66
9.08		0.382	15.52	12.73	2.25	0.67	0.68
8.41		0.354	15.44	12.05	2.13	0.67	0.68
7.89		0.332	15.41	12.26	2.17	0.69	0.69
7.01		0.295	15.39	12.45	2.20	0.71	0.72
6.11		0.257	15.23	12.35	2.18	0.72	0.74
4.66		0.196	14.97	12.76	2.26	0.94	0.95
3.42		0.144	14.27	13.17	2.33	1.43	1.46
2.95		0.124	13.82	13.41	2.37	1.48	1.51
1.95		0.082	13.16	14.63	2.59	1.46	1.49
0.000		0.000	10.70	10.60	1.82	1.41	1.43

Figure 13. Variations in the first order basal spacings and relative line breadths versus relative vapor pressure for calcium montmorillonite

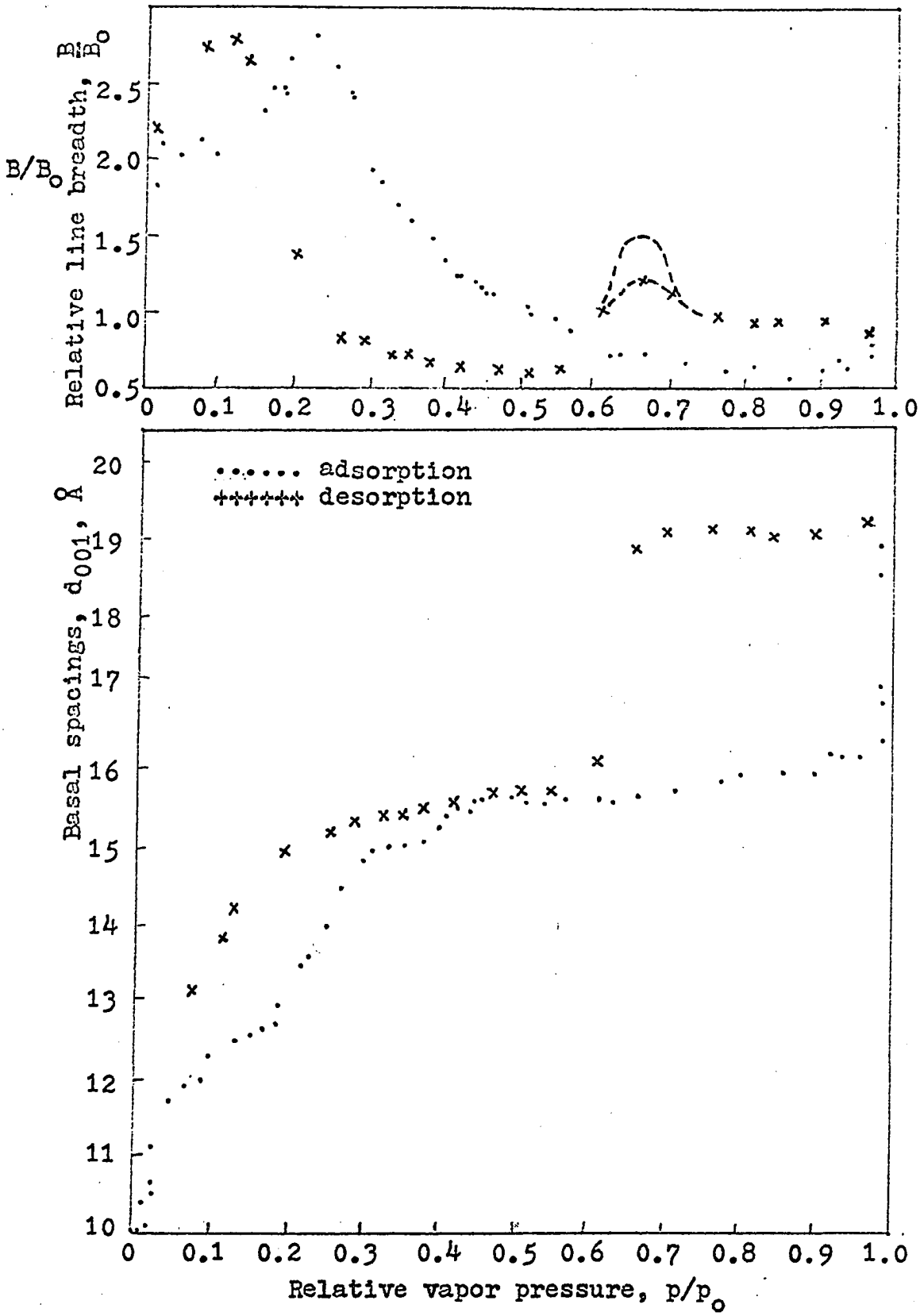
B/B$_o$
Relative line breadth, $\frac{B}{B_o}$
2.5
2.0
1.5
1.0
0.5
0
0.1
0.2
0.3
0.4
0.5
0.6
0.7
0.8
0.9
1.0
adsorption
desorption
Basal spacings, d_{001}, Å
20
19
18
17
16
15
14
13
12
11
10
Relative vapor pressure, p/p_o

Figure 14. Variations in the first order basal spacings and relative intensities versus relative vapor pressure for calcium montmorillonite

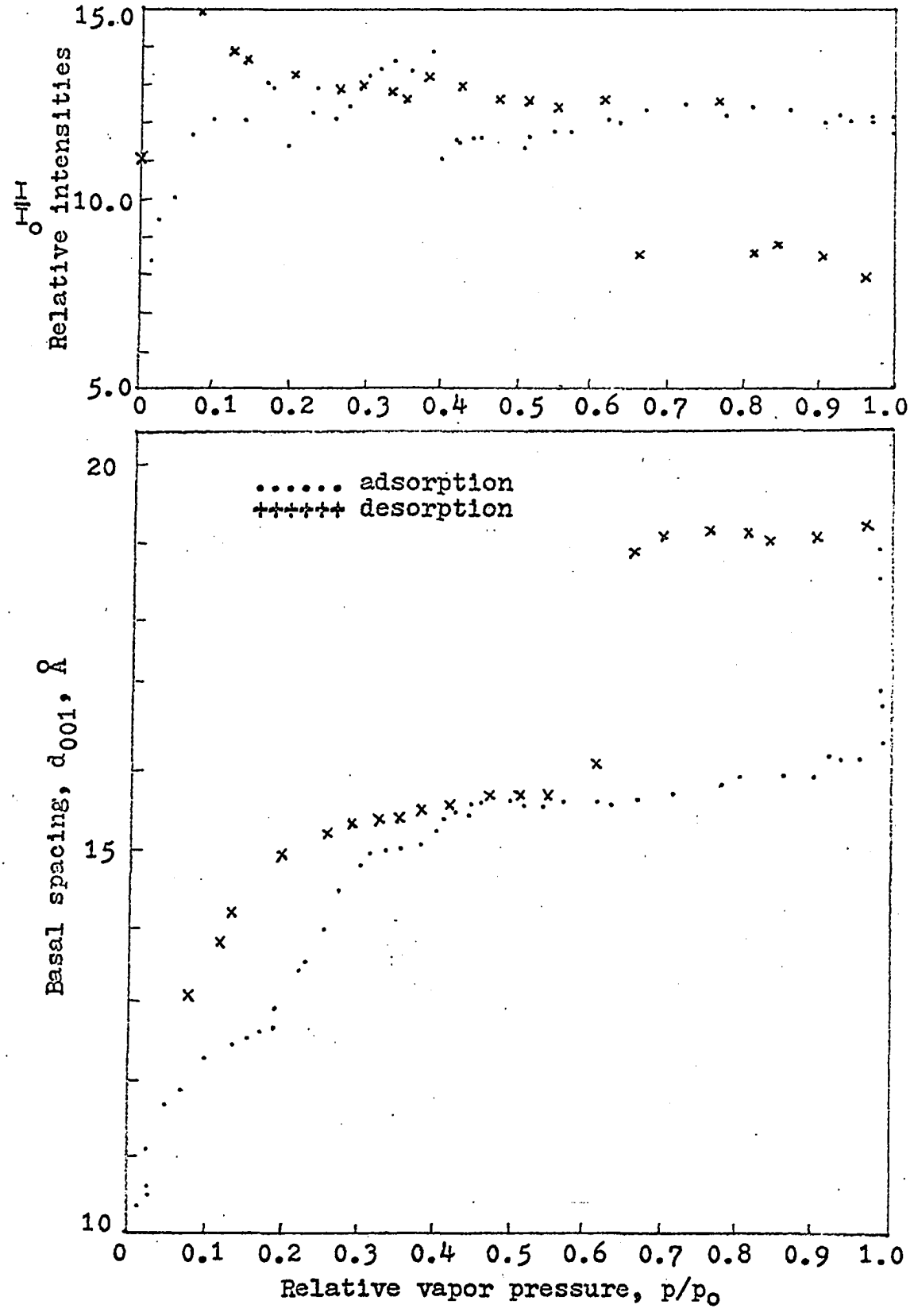
15.0
10.0
5.0
Relative intensities
0
0.1
0.2
0.3
0.4
0.5
0.6
0.7
0.8
0.9
1.0
20
15
10
adsorption
desorption
Basal spacing, d_{001}, Å
Relative vapor pressure, p/p_o

basal spacing take place in a continuous but non-uniform manner with changes in relative vapor pressure. Hendricks and Jefferson (38) hypothesized that the X-ray diffraction patterns from an expanding powder should show that the basal spacing would vary continuously with water content. As the relative vapor pressure is increased from zero, there is a slight increase in d spacing up to $p/p_o = 0.015$. This would seem to indicate that only a small portion of vapor is adsorbed in the interlayer region, while the rest is adsorbed on the external surfaces. The expansion then rapidly increases to 11.9 Å between $p/p_o = 0.015$ and p/p_o 0.08, indicating an expansion equivalent to one molecular layer of water when 1.8 molecules per unit cell are adsorbed, Figure 15. There is a small hump in the curve between $p/p_o = 0.08$ and $p/p_o = 0.11$, perhaps associated with the space occupied by a calcium cation. The d spacing is stable from $p/p_o = 0.11$ to $p/p_o = 0.19$; then the second major expansion from 12.6 Å to 15.1 Å occurs between $p/p_o = 0.19$ to $p/p_o = 0.30$ with the uptake of 5.5 molecules per unit cell, Figure 15.

There is a second hump in the curve between $p/p_o = 0.38$ and $p/p_o = 0.42$ perhaps associated with the coordination of molecules of water with the cation. The total uptake of water necessary to attain the stable 15.6 Å configuration is 7.5 molecules per unit cell. Between $p/p_o = 0.42$ and $p/p_o = 0.98$, there is a stable range of d spacing where the

spacing increases only 0.8 Å while adsorbing twelve molecules of water per unit cell. The final increment of expansion occurred between a relative vapor pressure p/p_o of 0.99 and saturation. This final expansion to 19.26 Å requires the adsorption of approximately 14 molecules per unit cell and required 242 hours to attain equilibrium. The 19.26 Å was the maximum spacing that could be obtained with this interlayer cation (59).

The desorption curve experienced two hysteresis loops, the first occurring between saturation and $p/p_o = 0.60$, and the second, which is less pronounced, between $p/p_o = 0.3$ and zero. Figure 16 is a plot of the molecules of water adsorbed during desorption.

The effect of time and pressure gradient were evident in the final expansion during adsorption, and the first collapse during desorption. The pressure gradient for the last expansion was very small (0.24 mm), corresponding to $p/p_o = 0.99$ to $p/p_o = 1.00$, and full expansion took place after 242 hours. Prior to this point, all expansion had been completed almost immediately after introduction of each increment of water vapor. The equilibrium pressures and peak positions were determined after twenty-four hours, although the expansion had been completed within the first 30 minutes. During desorption, all collapse was completed not later than 16 hours after the water bath temperature had reached the

Figure 15. Plot of the number of water molecules adsorbed per unit cell versus the basal spacing, first adsorption cycle

Figure 16. Plot of the number of water molecules adsorbed per unit cell versus the basal spacing, first desorption cycle

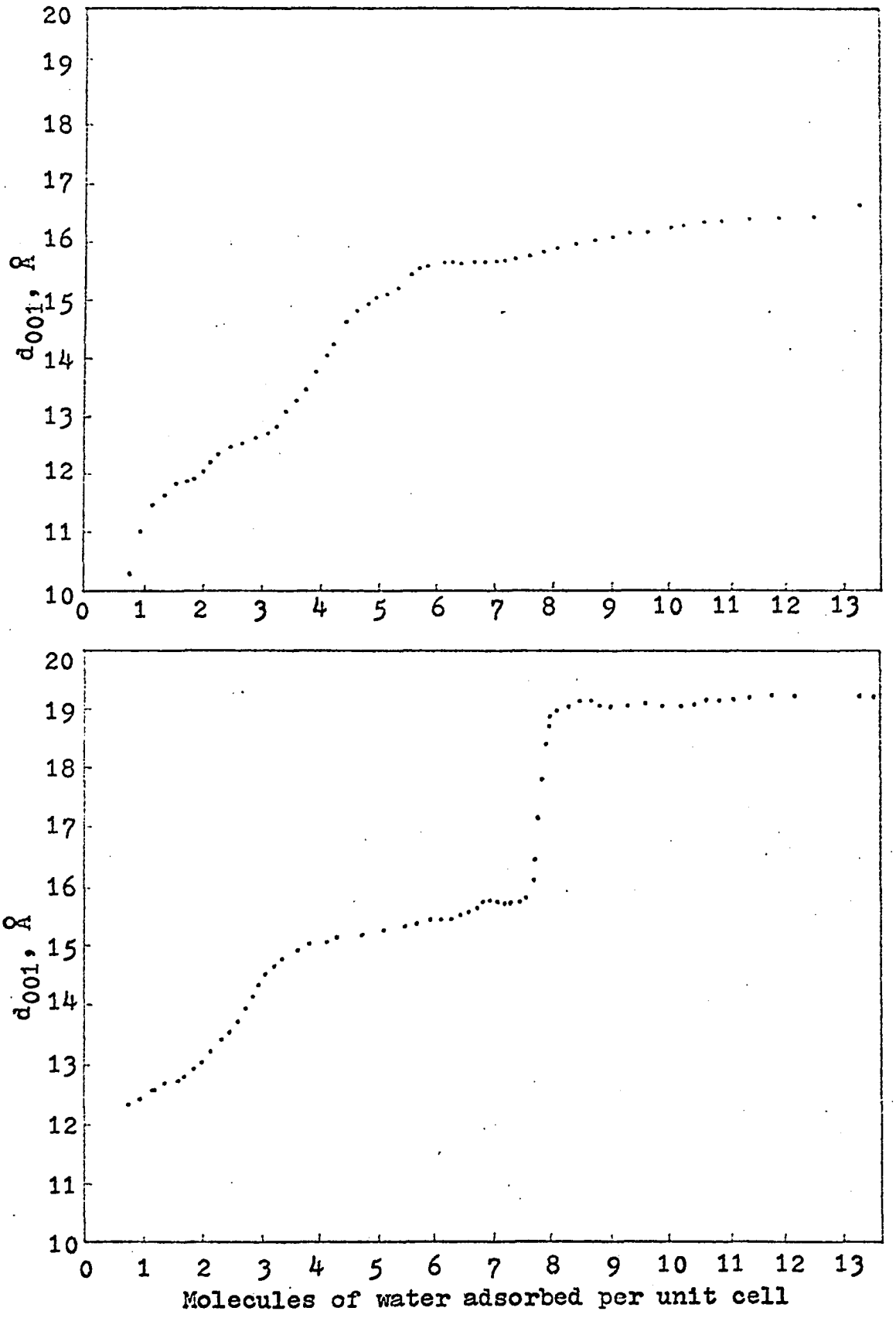
20
19
18
17
16
15
14
13
12
11
10
d_{001}, Å
0 1 2 3 4 5 6 7 8 9 10 11 12 13
Molecules of water adsorbed per unit cell

equilibrium temperature. The first collapse of the platelet system took place between $p/p_o = 0.65$ and $p/p_o = 0.60$, but the desorption curve did not return to the original d spacing. This suggests that interlayer water was trapped in the pores or remained associated with the cation. A pumping period of ten days utilizing a dry-ice acetone bath surrounding the water reservoir produced a shift from 11.5° Å to 10.7° Å, but the relative line breadth increased as water was removed, indicating a disordered system. It is reasonable to visualize that the isolated water islands are well within the platelet structure, their exit being blocked or impeded as the clay surfaces on each side of the islands move more closely together.

The plot of the X-ray line breadth versus relative vapor pressure, Figure 12, tends to substantiate the conclusion that there are varying numbers of molecular interlayers, i.e. 0, 1, 2, etc., and that an octahedral coordination of water around the cation may exist within the interlaminar spaces. Between a relative vapor pressure of zero and $p/p_o = 0.08$, the line breadth increases corresponding to an uptake of water, indicating non-uniform spacing in the interlayer regions. We may note that line breadth reaches a maximum near the center of the steeper portions of the basal spacing plot, and then decreases to a minimum value or remains constant as the basal spacing plot approaches flatter

sections. A low value of line breadth is indicative of a uniform spacing (15).

When d_{001} was between 10.5 Å and 15 Å, a broad peak appeared at approximately twice the d_{001}, indicating a possible repeating double layer structure (superlattice) including water molecules. The clean porous disc on which the clay sample was deposited, had been tested using copper radiation, and gave a typical amorphous pattern expected from a glassy material with no indication of the peaks obtained with the calcium montmorillonite sample. A superlattice has been reported by Brindley (13, p. 151) for chlorites, Brindley (13, pp. 93-96) for serpentine, and Gillery (34) and Demirel (26) for calcium montmorillonite. Demirel suggests that the offset stacking of platelets to match the water molecules with oxygen atoms of the silica surfaces must repeat in an organized manner in the c direction. Gillery attributes the diffuse band to a two-layer natural stacking of the layers which may be due to a tendency to form two types of montmorillonite lattices which alternate, or hydration tending to take place in alternate layers. Using copper radiation and the beam slit-detector slit configuration in this investigation, the diffuse band could not be clearly resolved. In future experiments, chromium and iron radiation should be used to resolve the peak and obtain more evidence and information on the possible superlattice.

Comparison with work of other investigators

Nagelschmidt (62) dried calcium montmorillonite samples in a furnace at temperatures between 85° C and 245° C, rehydrated them over salt solutions, sealed them in capillaries of 0.77 mm internal diameter, and took X-ray photographs. He noted a proportional increase in the basal spacing from 10.5 Å to 15 Å during the uptake of the first four molecules of water per unit cell, and an increase of 0.6 Å during the uptake of the next ten molecules of water. He explained that the small increase in d spacing was due to the adsorption only on the external surfaces.

Mooney et al. (60, 61) used a Wyoming bentonite, Volclay-SPV, obtained from the American Colloid Company, and prepared a homionic calcium montmorillonite from this bentonite. The sample was sealed in a Pyrex capillary and placed in a X-ray camera and irradiated with copper K radiation. The system was maintained at 20° C. In a plot of d spacing versus relative vapor pressure, they found that the spacing levelled off between 12 Å and 13 Å and between 15 Å and 16 Å, which values corresponded to integral number of layers of water molecules between platelets. They obtained a spacing of 16.5 Å, which was apparently ignored in their conclusions, but were not able to obtain a 19 Å spacing, perhaps due to insufficient time for hydration. They reported no hysteresis in their curves although they appar-

ently completed their adsorption cycle at a relative vapor pressure of approximately 0.90. In the present study, the last platelet separation occurred between p/p_o = 0.98 and saturation; the present data indicate that if Mooney et al. (60, 61) actually began their desorption at p/p_o = 0.90 and the second desorption equilibrium pressure point was lower than p/p_o = 0.60, no hysteresis would have been observed. These data illustrate the importance of obtaining complete evacuation of the system prior to adsorption, and complete adsorption to saturation prior to desorption.

Gillery (34) used a natural Wyoming bentonite supplied by the National Lead Company. After running adsorption studies on sodium montmorillonite, he resaturated the material with $CaCl_2$ and obtaining a homoionic calcium montmorillonite. The relative humidity was controlled by passing compressed air through appropriate saturated salt solutions and into the sample chamber; humidities were measured with wet and dry thermocouples. The type of X radiation was not specified and the sample was investigated during the desorption phase. Gillery states that the plot of basal spacing versus percent relative humidity suggests a mixture of sodium and calcium cations. He suggests that the adsorbed cation effects the characteristics of adsorbed water by showing hydrates of 12.3 Å over a very small stability range of about 5% relative humidity, while the second hydrate of 15.5 Å

has a stability range from about 35% relative humidity to saturation. He suggests that a hydrate of 18 Å exists, but that $p/p_o = 1.00$ is not sufficient water vapor pressure to produce this hydrate in a pure form, and the final hydrates exists only in a mixed layer form with the 15.5 Å hydrate. The present study indicates that if sufficient time is allowed for hydration, the 19.2 Å hydrate can be obtained.

Hendricks et al. (39) used montmorillonites from California, Mississippi and Wyoming, saturated with various cations. The Wyoming material was the Wyoming bentonite sold under the trade name "Volclay". Their material was equilibrated over salt solutions and the samples selected for X-ray investigation were sealed in glass capillary tubes to prevent loss of water. The samples were placed in X-ray cameras for diffraction measurements for periods of ten to 48 hours. There was considerable scatter in the data. The relative humidities reported were those determined while the samples were in the adsorption chamber or desiccator. No reference was made to any method for temperature control, which may account for the scatter.

Demirel (26) equilibrated his dry samples at room temperature in vacuum desiccators maintained at the desired relative humidities by appropriate salt solutions. A plexiglass hood equipped with a Mylar X-ray window covered the sample and salt solution during X-ray studies. Although

only four points were obtained for adsorption, he was able to attain full expansion at saturation by immersing his sample in distilled water. His data compare favorably with the data in the present study, including the desorption hysteresis.

The data of these various investigators are presented in Figure 17 for comparison to the present study.

Color changes during irradiation

Upon completion of the X-ray studies, the sample had been under copper irradiation for approximately 1,000 hours. When it was removed from the apparatus, a very distinct color change was evident; whereas the sample had been a yellowish white prior to testing, it was a dark greenish blue after irradiation. Normal chemical tests and fluorescent analysis were performed to determine if some impurities' may have been in the sample or if copper contamination from the adsorption chamber had taken place. The latter is completely lined with stainless steel, and the sample holder is manufactured out of stainless steel. The cooling coils are copper but are imbedded into the walls of the original furnace and completely shielded from the sample by a stainless steel lining of the chamber.

A strip of pure copper was placed in a watch glass containing a suspension of calcium montmorillonite, and the

Figure 17. Variations in the first order spacings versus relative vapor pressure for calcium montmorillonites reported by various authors

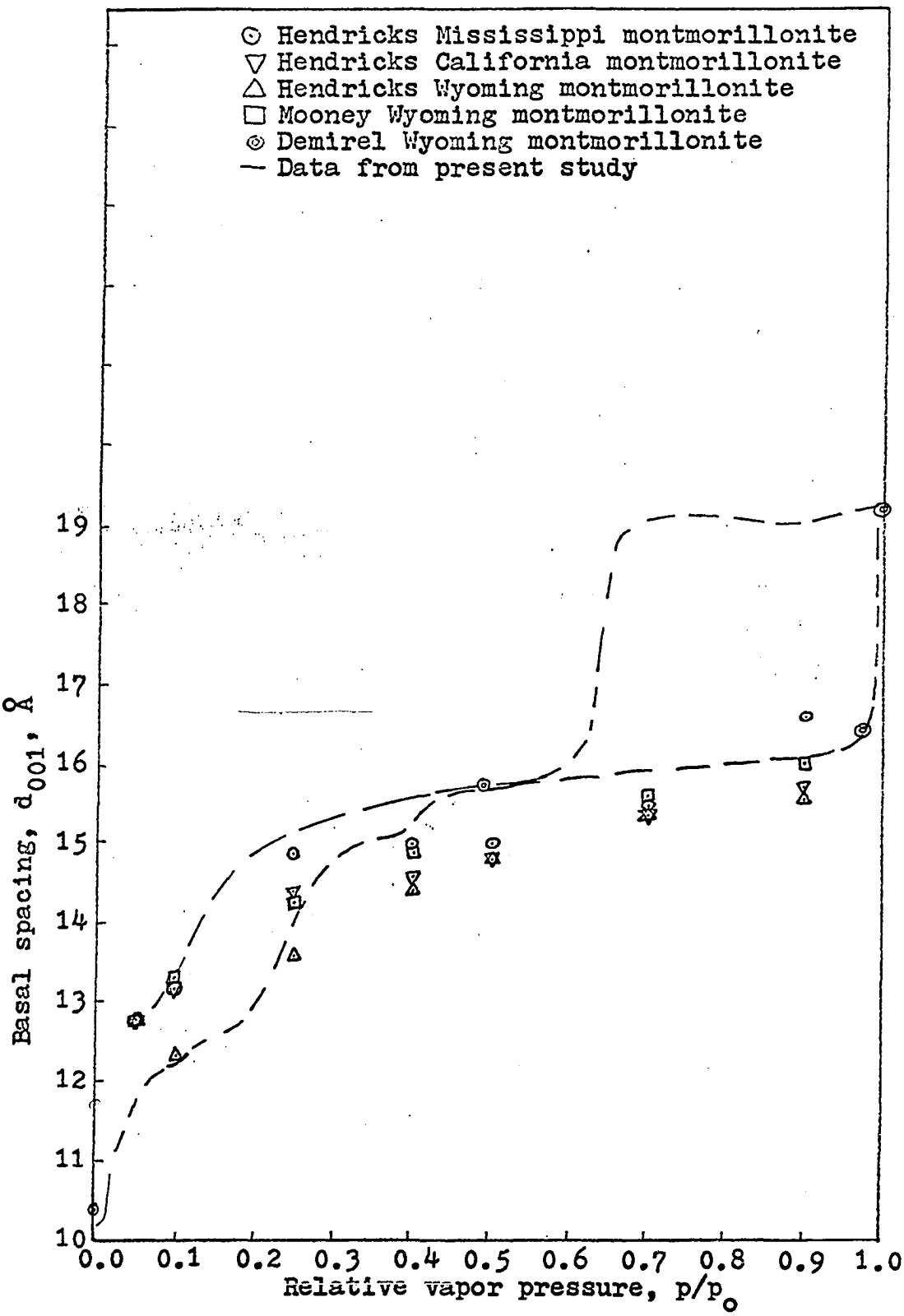
Hendricks Mississippi montmorillonite
Hendricks California montmorillonite
Hendricks Wyoming montmorillonite
Mooney Wyoming montmorillonite
Demirel Wyoming montmorillonite
Data from present study
Basal spacing, d_{001}, Å
Relative vapor pressure, p/p_o
10
11
12
13
14
15
16
17
18
19
0.0
0.1
0.2
0.3
0.4
0.5
0.6
0.7
0.8
0.9
1.0

watch glass was placed in a 100% relative humidity room. After more than 700 hours no change in color was observed. Later, a portion of the irradiated sample was placed in a 50 ml beaker and a solution of $NH_4C_2H_3O_2$ and ammonium hydroxide was added. The resulting solution was clear while a small piece of copper in a similar solution caused the solution to turn blue.

The fluorescent analysis was run using tungsten radiation with LiF, NaCl, and EDDT analyzing crystals on four different specimens: a) the 1,000 hour irradiated sample, b) a sample that had been evacuated to 10^{-5} mm Hg for 20 days and irradiated with copper radiation for 26 hours, c) an air-dried sample of calcium montmorillonite, and d) a plain fritted porous disc similar to that used in the sample holder of the apparatus. None of the four specimens showed any trace of copper.

The fluorescent diagrams did show small traces of tungsten and iron; the tungsten was attributed to tungsten used in the manufacture of the porous disc, and the iron peaks in all three clay samples were of the same magnitude of intensity and can be attributed to the iron substitution in the octahedral layer (isomorphous substitution).

The only other material that could come into contact with the clay specimen is mercury from the manometer. The possibility mercury contamination was eliminated for two

reasons: a) no traces of mercury were found during fluorescent analysis, and b) the clay specimen in the electrobalance was exposed to a greater surface area of mercury in the limbs of the manometer attached to the electrobalance than the surface of the limbs of the manometer attached to the X-ray apparatus, this sample was under investigation and vacuum for approximately 5,500 hours, and no discoloration occurred in the sample.

Therefore, the discoloration can be due to: a) a change in the valence state of a naturally occurring metallic impurity in the host crystal (e.g. Fe in MgO is a known example of this) or b) a radiation-induced color center in the crystal (e.g. electron trapped at a halogen ion vacancy in an alkili halide). In either case, about ten ppm could produce the observed effect.[1]

A series of short experiments were conducted subsequently to determine possible color changes by different forms of X radiation. A 99.6% sample of pure NaCl meeting A.C.S. specifications, was irradiated using copper radiation, and a dull yellow-white was observed after 26 hours of radiation. Later a porous disc 1/2 of which was covered by a thin layer of calcium montmorillonite and the other 1/2 left

---

[1]Dr. D. W. Lynch, Department of Physics, Iowa State University of Science and Technology, Ames, Iowa, 1966.

undisturbed, was irradiated using copper and tungsten radiation. Using copper radiation, there was no noticeable color change after 26 hours of irradiation on the undisturbed section of the plate or in the clay specimen. However, while using tungsten radiation, the porous disc turned brown after four hours at any section through the entire thickness where the radiation was impinging on the plate. There was no discoloration of the clay specimen after four hours or after 26 hours. After 26 hours, the plate became slightly darker brown. From the above observation, it can be deduced that the color change is a function of the length of exposure, the type of radiation employed, and the atoms and structure of the material irradiated.

Reflection intensity during transfer of vapor

Intensity data from the X-ray diffraction study during adsorption and desorption of water vapor on calcium montmorillonite are presented in Tables 5 and 6. The Tables include intensities of observed first, second, third, fourth, fifth, and sixth order spacings, when observed. As can be seen from Figures 18 and 19 and the data, the peaks of the secondary reflections disappear and reappear throughout the study. MacEwan et al. (51) point out that peaks migrate between positions as the relative proportions of the two species change. This investigation shows that during migration, the

Table 5. X-ray diffraction intensity data during adsorption*

p/p_o	(001)		(002)		(003)		(004)		(005)		(006)	
	d	$Ix10^2$	d	I	d	I	d	I	d	I	d	I
0.000	10.15	5.65	4.92	1.80			3.07	6.27				
0.013	10.39	8.38	5.15	1.50			3.09	7.07				
0.022	11.18	9.59	5.47	2.20			3.10	8.67				
0.046	11.78	9.65	5.70	1.80			3.12	3.30				
0.068	11.93	10.98	5.86	1.90			3.12	3.01				
0.097	12.32	11.32	6.06	1.10			3.12					
0.139	12.58	11.32	6.30	0.60	4.23		3.12					
0.159	12.62	12.56	6.30	0.50	4.43							
0.174	12.68	12.41	6.23	0.40	4.27							
0.188	12.79	11.50	6.30	0.30								
0.194	12.98	10.71										
0.224	13.54	11.66			4.90	0.90						
0.230	13.66	12.40			4.95	1.20						
0.254	14.08	11.47			4.97	1.50						
0.273	14.54	11.81			4.97	1.60						
0.301	14.85	12.77			4.97	2.20						
0.312	14.93	12.90			4.97	2.50						
0.333	15.01	13.17			4.97	2.80						
0.357	15.05	12.94			5.00	3.20						
0.383	15.16	13.48			5.00	3.00						
0.399	15.35	10.30			5.03	2.80						
0.415	15.46	10.85			5.06	2.50			3.04	5.00		
0.420	15.49	10.79			5.06	2.80			3.04	8.00		
0.438	15.55	10.88			5.06	3.00			3.03	6.67		
0.449	15.60	10.93			5.09	3.30			3.03	7.00		
0.454	15.63	10.42			5.09	2.50			3.06	10.00		

*d is the apparent spacings of the reflections, Å; I is the intensity of the reflections, $in^2 \times 10^{-4}$.

Table 5. (Continued)

p/p_o	(001)		(002)		(003)		(004)		(005)		(006)	
	d	$Ix10^2$	d	I	d	I	d	I	d	I	d	I
0.463	15.57	10.07			5.09	2.70			3.06	7.33		
0.509	15.66	10.67			5.09	2.70			3.06	8.00		
0.513	15.63	11.00			5.12	3.40			3.07	7.67		
0.543	15.63	11.15			5.12	3.00			3.07	8.67		
0.567	15.66	11.13			5.12	3.20			3.07	8.33		
0.619	15.66	11.52			5.12	3.10			3.07	7.66		
0.630	15.69	11.39			5.13	3.00			3.08	7.33		
0.667	15.69	11.76			5.15	3.00			3.08	6.33		
0.716	15.79	12.00			5.15	3.20			3.09	7.33		
0.771	15.94	11.64	8.03		5.18	3.10			3.10	7.33		
0.805	16.03	11.86	8.03		5.20	2.60			3.11	7.00		
0.855	16.03	11.78	8.03		5.20	2.60			3.11	8.00		
0.901	16.08	11.52	8.03		5.21	2.10			3.12	7.33		
0.922	16.26	11.70	8.03		5.24	2.60			3.13	7.33		
0.934	16.23	11.49	8.03		5.24	2.20			3.13	6.67		
0.961	16.41	11.63	8.03		5.24	2.60			3.14	6.33		
0.964	16.31	11.52	8.03		5.27	2.20			3.15	6.33		
0.989	16.63	11.40	9.60	0.32	5.27	1.80			3.14	5.66		
0.988	17.25	10.92	9.60	0.44	5.27	1.10			3.14	5.33		
0.989	18.02	9.89	9.60	0.58	6.19	1.60			3.13	5.00		
0.989	18.95	9.20	9.50	0.76	6.30	0.90	4.76	0.60			3.14	5.66
1.000	19.25	8.89	9.60	1.22	6.32	1.20	4.76	0.60			3.14	4.33

Table 6. X-ray diffraction intensity data during desorption*

p/p_o	(001)		(002)		(003)		(004)		(005)		(006)	
	d	$Ix10^2$	d	I	d	I	d	I	d	I	d	I
0.956	19.23	7.97	9.62	1.09	6.23	1.00	4.74	0.20			3.13	3.33
0.900	19.10	8.56	9.55	1.32	6.23	1.40	4.72	0.40			3.13	3.33
0.842	19.07	8.95	9.50	1.36	6.27	1.00	4.69	0.40			3.13	3.33
0.810	19.15	8.63	9.50	1.24	6.23	1.20	4.76	0.50			3.14	4.33
0.756	19.19	12.10	9.60	1.34	6.26	1.60	4.74	0.50			3.15	6.66
0.703	19.10	8.38	9.62	1.02	6.27	1.00	4.74	0.10			3.14	5.66
0.658	18.95	8.64	9.50	1.00	6.26	1.50	4.71	0.30			3.13	4.33
0.607	16.14	12.12	9.30		5.24	2.30			3.13	8.00		
0.554	15.77	11.85	8.00		5.21	2.50			3.07	8.33		
0.508	15.77	12.15			5.15	3.00			3.07	8.33		
0.466	15.73	12.18			5.12	3.00			3.06	7.66		
0.421	15.60	12.41			5.09	2.60			3.04	7.33		
0.382	15.52	12.73			5.09	2.80	3.78	0.10	3.04	7.33		
0.354	15.44	12.05			5.06	2.70	3.78	0.20	3.03	6.00		
0.332	15.41	12.56			5.06	2.60	3.77	0.30	3.02	6.66		
0.295	15.39	12.45			5.03	2.60	3.75	0.30	3.02	5.66		
0.257	15.23	12.35			5.03	2.20	3.72	0.40	3.00	6.00		
0.196	14.97	12.76			4.98	1.70			2.98	3.00		
0.144	14.27	13.17	6.23	0.70	4.92	0.50						
0.124	13.82	13.41	6.27	1.00	4.92	0.50						
0.082	13.16	14.63	6.18	1.60					2.99	1.66		
0.000	10.70	10.60	5.36	3.50								

*d is the apparent spacings of the reflections, Å, I is the intensity of the reflections, $in^2 \times 10^{-4}$.

Figure 18. Variation in normalized intensity of various reflections versus basal spacing during adsorption of calcium montmorillonite

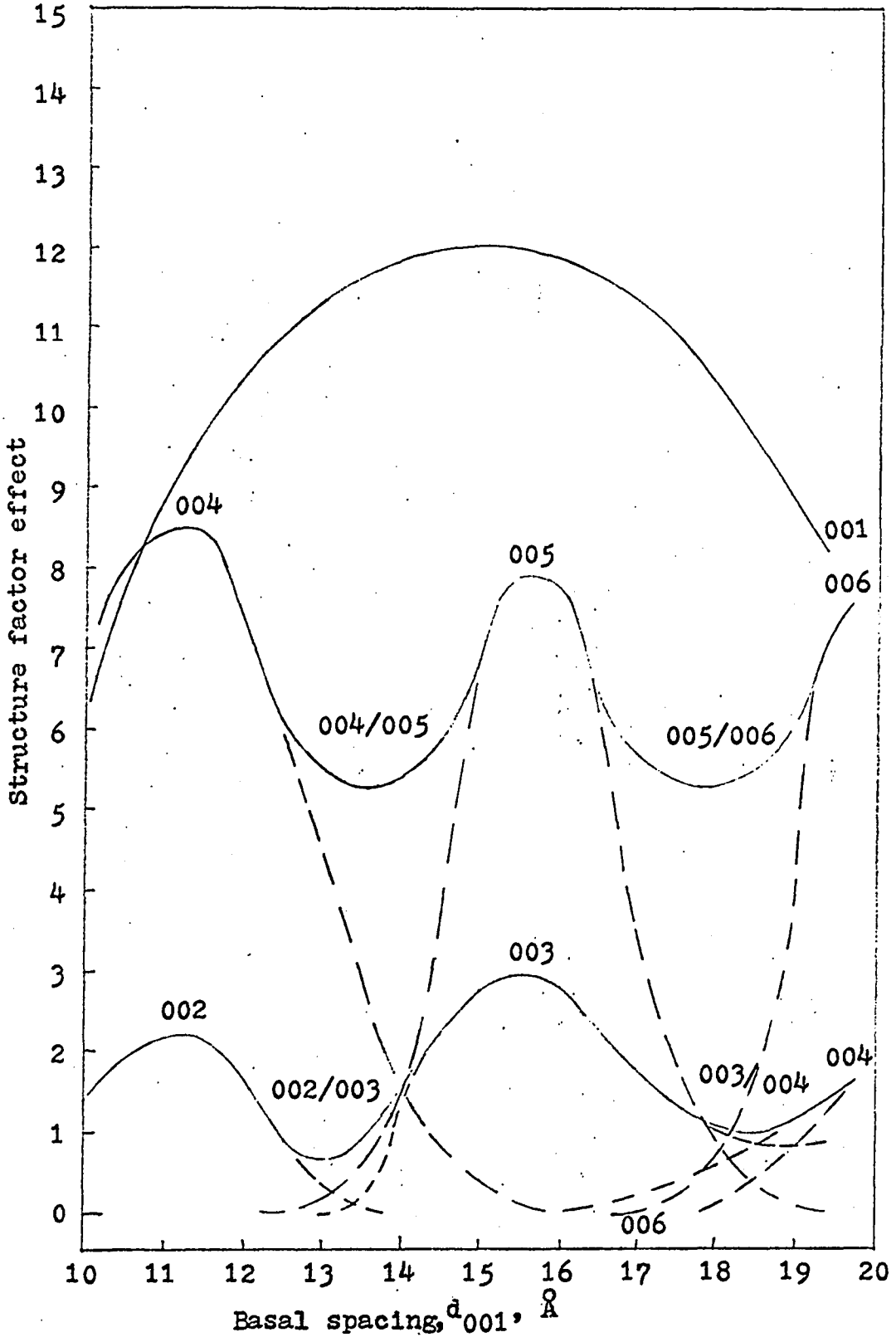
Structure factor effect
Basal spacing, d_{001}, Å
001
002
003
004
005
006
004/005
005/006
002/003
003/004
004
006

Figure 19. Variation in normalized intensity of various reflections versus basal spacing during desorption of calcium montmorillonite

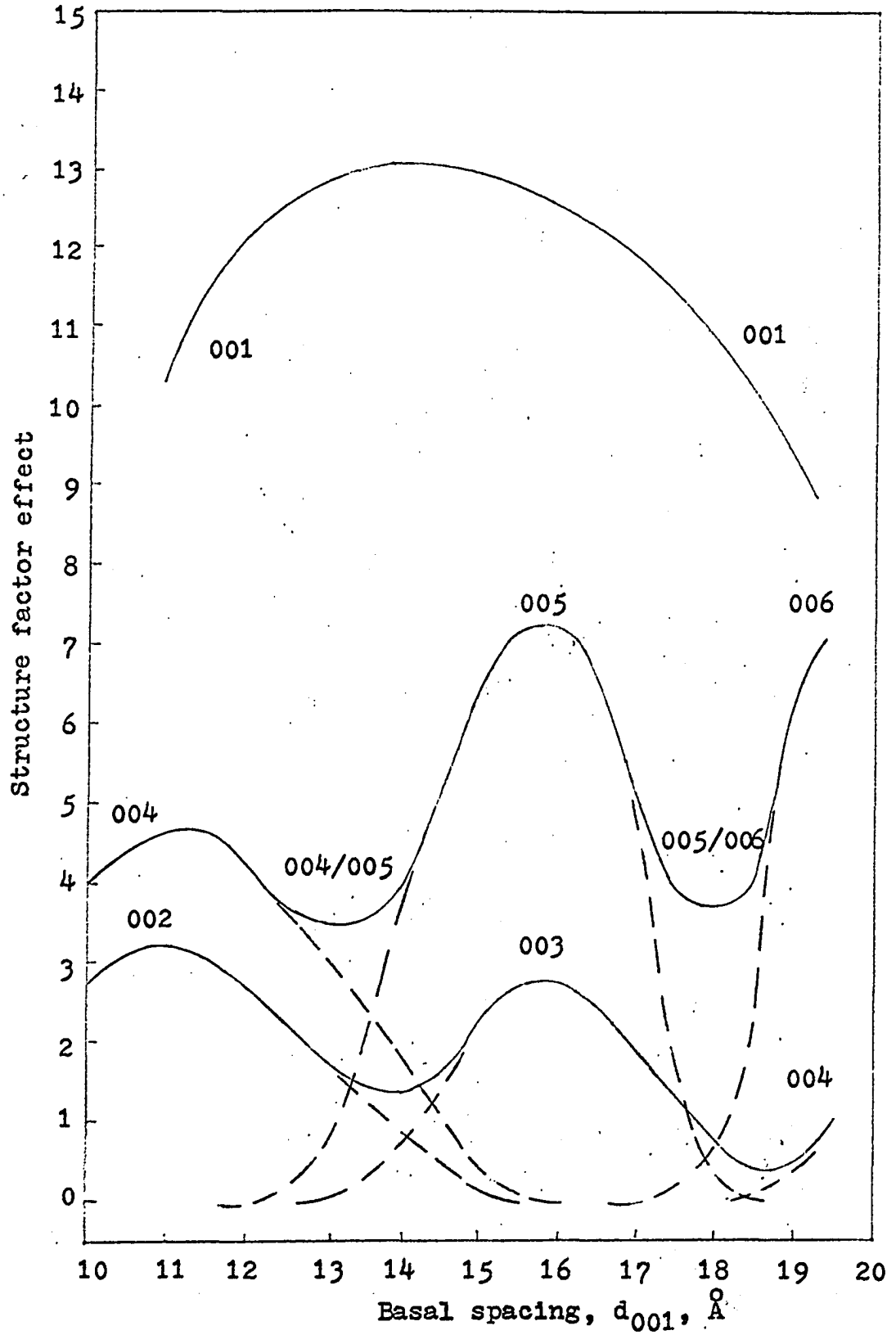
Structure factor effect
Basal spacing, d_{001}, Å
001
001
005
006
004
004/005
005/006
002
003
004
0
1
2
3
4
5
6
7
8
9
10
11
12
13
14
15
10
11
12
13
14
15
16
17
18
19
20

peaks pass through a phase of extreme diffuseness and apparently disappear in certain composition ranges. In some cases, no indicies could be assigned to the peaks of the mixture in the system studies. For ease in tabulating the spacings, the data were placed in the columns according to the reflection orders, and can be conveniently labelled by the order or combination of orders, e.g. 005 or 005/006.

MacEwan, Amil, and Brown (51) have shown that the intensity of diffraction is given by:

$$I = \theta \left|F_1\right|^2 \psi \qquad (17)$$

where θ is the Lorentz-polarization factor, $\left|F_1\right|$ is the layer structure factor and ψ is the mixing function.

The Lorentz-polarization factor depends on the experimental technique. The combined factor increases with decreasing angle, and should cause a 17 Å peak to be nearly three times as intense as a 10 Å reflection. The intensities of all reflections were corrected using the data in the International Tables for X-ray Crystallography (44, p. 270).

The mixing function ψ is dependent on the spacings of the constituent phases and the probability of occurrence of these spacings. The influence of a mixing function was observed in that peaks did migrate within certain limits; in Tables 5 and 6, the peak position migrated in the 3 Å and in the 5 Å ranges. However, only during the final transfer was

the mixing function pronounced, shown by the 002 and 003 peaks. During this transfer of vapor, the 002/003 peak shifted from a 2θ of 16° to a 2θ of 14°. At approximately 80 hours after the transfer, the higher peak was fairly strong in the area of 16°, whereas the peak at 14° was barely observed. At 196 hours, the peak had shifted to the 14° position and was fairly strong. Thus, no definite pattern could be determined, but, this shows it is important to recognize that, in general, the more intense observed spacings of the 3 Å and 5 Å would present intense reflections for the third, fourth, fifth, or sixth order reflections.

The structure factor is a complex quantity whose magnitude is the amplitude of the scattered wave, and whose direction is determined by the phase of the scattered wave. No matter how complicated a crystal, one may picture it as a series of simple interpenetrating simple lattices, one for each different kind of atom in the crystal. Klug and Alexander (46) have shown that the reflection geometry is determined entirely by the lattice dimensions and not by the complexity of the diffraction pattern. The effect of the atomic arrangement on the diffraction intensity from a plane are taken into account by the structure factor. However, the problem of evaluating the structure factor can be considered to be that of compounding several wave motions, all of the same period, but different in phase and amplitude.

Figures 18 and 19 are plots of the basal spacing versus the second, third, fourth, fifth, and sixth order reflections during adsorption and desorption, respectively. The dashed lines indicate reflections were not observed. As can be seen, d_{001} is the most intense peak throughout the entire range. The 002 reflection is observed when d_{001} is between 10 Å to 13 Å and again from 17 Å to 19 Å. The 003 and 005 reflections were prevalent in the mid-range from d_{001} = 13 to 17 Å . At final expansion, the 005 reflection could not be observed. The 004 reflection was observed in the range from 10.5 to 13 Å and again from 17 to 19 Å, in conjunction with the 006 reflection.

In general, as the first order basal spacing increases the higher order basal reflections decrease in intensity. These reflections are strongest at 3 Å and 5 Å. The mixing function would tend to decrease the intensity when several species comprise the system, but at stable positions this decrease in intensity would not completely extinguish the position. All the reflections have been corrected for the Lorentz-polarization factor, but this can not explain the strong reflections occurring only at 3 Å and 5 Å. Therefore, the strong reflections are due to reflection planes approximately overlaping planes in the montmorillonite structure.

The systematic absence of reflections depends on the atomic parameters and the size of the crystallite. In the

present study, the size of the crystallite is sufficient to give strong reflections and was not considered an influential factor. Buerger (20) points out that in general, the structure factor may be expressed as:

$$\left|F_{hkl}\right| = \Sigma_j \, f_j \, e^{\,i\phi_j} \qquad (18)$$

where f_j represents the scattering factors, and may be expressed as:

$$\phi_j = 2\pi(hx_j + ky_j + lz_j)$$

where ϕ_j is the phase angle expressed as the fractional coordinates (x_j, y_j, z_j) of the atoms of the unit cell. The summation must be taken over all the atoms in the unit cell and if any symmetry occurs, it can be significant in determining the form of the structure factor.

The importance of the structure factor in the clay mineral system can be illustrated by analogy to sodium chloride, which is a face-centered cubic structure. By applying equation 18, above, to the sodium chloride system in Figure 20, it can be seen that the orthogonal planes of the unit cell are interleaved exactly halfway by identical planes. For diffraction from either the C or C' planes, the phase difference must be an integral multiple of 2π. Therefore, no first order reflection will be expected because planes C and C are exactly out of phase (one half wavelength apart) and

Figure 20. The structure of sodium chloride (face-centered cubic)

Figure 21. Idealized electron density curve, number of electrons per plane in the mica-like structure versus atomic plane separation

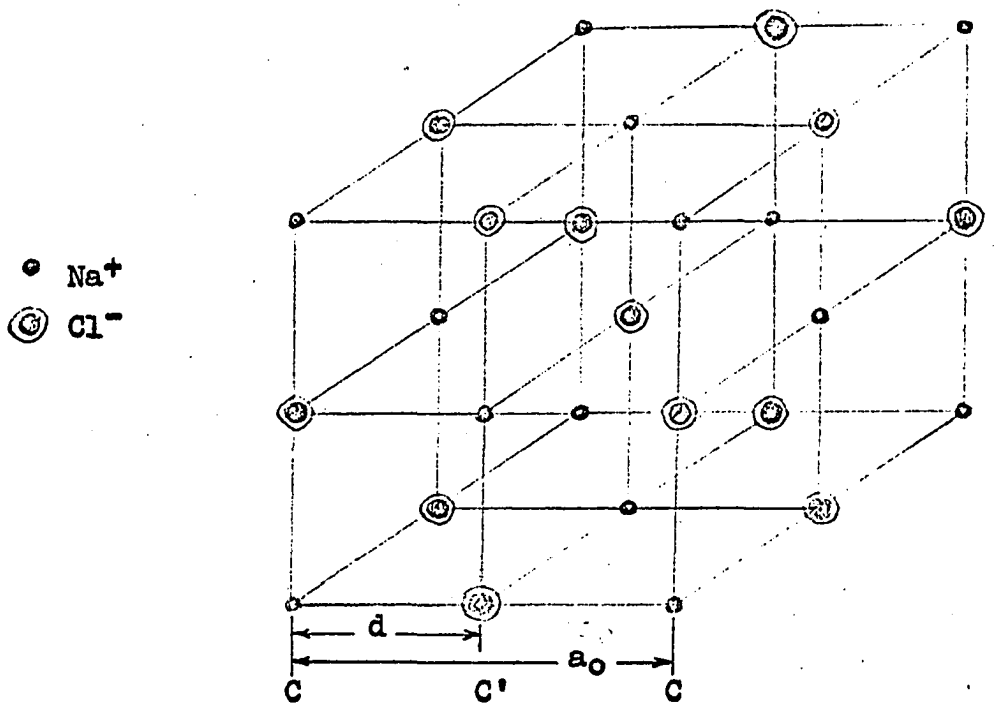
Na+
Cl−
d
a0
C
C'
C

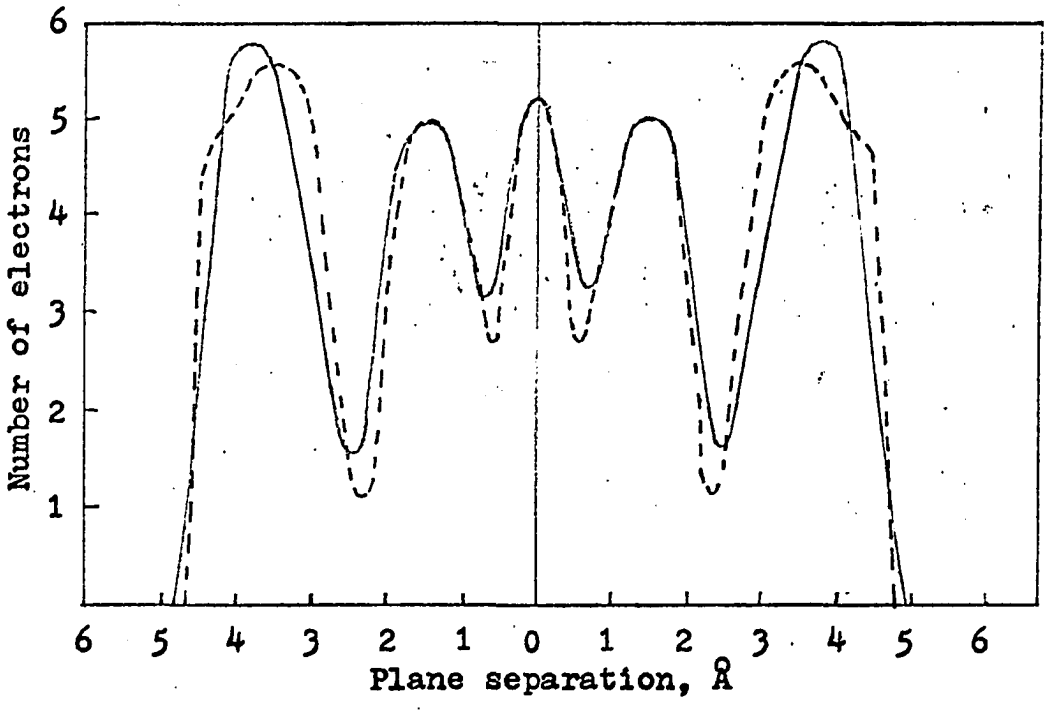
Number of electrons
1
2
3
4
5
6
6 5 4 3 2 1 0 1 2 3 4 5 6
Plane separation, Å

will exactly cancel each other since their amplitudes are identical. There will be a strong second order reflection because the distance CC corresponds to a phase difference of 4π (two wavelength) and CC' is half this distance 2π (one wavelength). The two reflected waves C C' and C'C will be exactly in phase and will reinforce each other.

Figure 21 is an idealized curve of electron population or density in the basic pyrophyllite structure, and it was drawn by plotting the total number of electrons available in each plane of the unit cell versus the plane location using the structure illustrated in Figure 1. Since the inner orbital electrons are chiefly responsible for diffraction, the effective electron populations are centered at each plane location. The curve was symmetrically drawn about the central plane, which is aluminum ions. Crests and troughs of the curve were determined by using the intensity data and a trial and error procedure. The curve appears similar to the one-dimensional Fourier syntheses of the basal reflections of Allevardite, a mica type mineral (51, p. 426).

The swelling of the montmorillonite presents a distortion of the normally expected definition of a space lattice and unit cell. By definition, a unit cell is the smallest portion of a space lattice that contains a complete repeating unit of the crystal pattern. In the swelling montmorillonite system, each mica like sheet is separated from the

next by n·H_2O molecules and interlayer cations; if this separation is repeated in an orderly geometric fashion, a diffraction pattern may be expected when the Bragg equation is satisfied. The thickness of the unit cell then must include at least one mineral sheet and one water-cation layer; boundaries of the unit cell then can be drawn anywhere--through the mineral sheet or through the water--so long as they are the proper distance apart.

If the unit cell is symmetric and expands only in the c direction, the structure factor F_{hkl} may be simplified. In equation 18, the structure factor was defined as:

$$\left|F_{hkl}\right| = \sum_j f_j \, e^{i\phi j}$$

This expression may be expanded to the following:

$$F_{hkl} = \left[\sum f_j \cos 2\pi(hx_j + ky_j + lz_j)\right] + i\left[\sum f_j \sin 2\pi(hx_j + ky_j + lz_j)\right]$$

which upon using the symmetry conditions of the crystal, may be simplified to:

$$\left|F_{001}\right| = 2\sum_{j=1}^{J/2} f_j \cos 2\pi(lz_j)$$

Therefore the intensity is effected as follows:

$$I \cong \left[2\sum_{j=1}^{J/2} f_j \cos 2\pi(lz_j)\right]^2 \qquad (19)$$

where f_j is the layer structure factor of scattering obtained from the curve in Figure 21, and lz_j represents locations of the reflecting imaginary plane.

In order for symmetry to occur, the unit cell boundary may be taken as half way through the water layer. The primary contribution to the reflections may be assumed to occur from the center of the unit cell, since this has the maximum electron density. The behavior should be similar to that of the sodium chloride structure whenever clay lattice expansion is such that the central plane is located exactly out of phase (one half wavelength) from the silicon-oxygen planes forming the tetrahedral layers.

Figure 22 is an electron population curve with the positions of the reflecting planes superimposed for the 10.1 Å, 12.6 Å. 15.6 Å, and 19.2 Å basal spacings. Table 7 is the calculated values of the structure factor contribution for the spacings listed above for the first, second, third, fourth, fifth, and sixth order basal reflections. The structure factors are always applied as the square of the function, equation 17, so that any negative values calculated merely represent the contribution from the wave motion in the second and third quadrants of a unit circle.

No quantitative values can be taken from the Table to directly determine the actual intensity. However, it can be seen from Figure 22 and Table 7, that when the structure fac-

Figure 22. Electron density curve of basic mica-like structure with reflection planes superimposed.

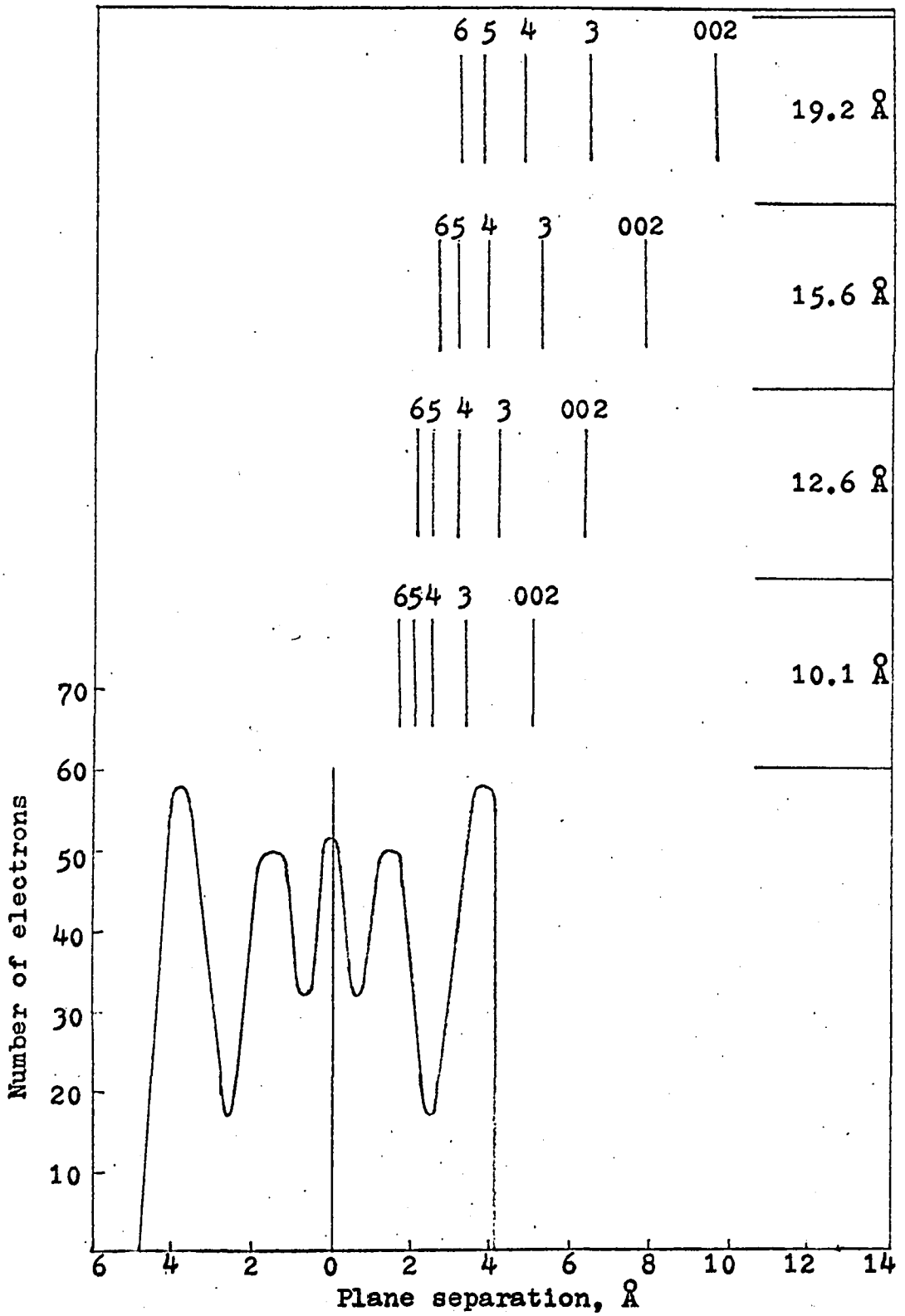
6 5 4 3 002
19.2 Å
65 4 3 002
15.6 Å
65 4 3 002
12.6 Å
654 3 002
10.1 Å
Number of electrons
70
60
50
40
30
20
10
6 4 2 0 2 4 6 8 10 12 14
Plane separation, Å

Table 7. Calculated values of the structure factor effect on the intensity of reflections from the calcium montmorillonite-water system*

	001	002	003	004	005	006
d_{001}						
10.1 Å	29.7	-11.9		3.1	-0.1	
12.6	41.4	-6.3	1.5	-12.9	-3.9	0.8
15.6	50.4	10.0	-11.2	-0.8	14.1	3.0
19.2	57.8	21.9	4.6	10.3	1.0	12.3

*The underlined reflections indicate those reflections actually observed on the diffractions traces.

tor values were small (0-4) the intensity of the observed peak was small or the reflection was extinct. If the calculated value was four or greater, the diffraction peak was observed and its intensity could be measured by planimetry.

Figures 18 and 19 show that the reflections occurring at 3 Å are the most intense higher order peaks; this can be attributed to the fact that at the 3 Å position, the imaginary reflection plane corresponds to a real plane of high electron density and the overall effect is a reinforcement of the intensity.

No attempt was made for the construction of the curve in Figure 21 to include diffraction effects of the cations or water molecules between the platelets, which may account for the spread in the data. Although it appears that the latitude allowed is extremely large, Lipson and Cochran (48) have pointed out that errors in the order of 20% are acceptable. The accuracy of measurement was not high, and in general, accuracy of not much better than 5-10% can be claimed for individual structure amplitudes. Secondly, the scattering factor curves are affected by electrons which participate in bonds between the atoms, and these effects were ignored in construction of Figure 21.

Possible configuration of interlayer water

Hendricks and Jefferson (38) have suggested that because

of the dipole character of the water as well as the lattice characteristics of the clay mineral surface, water molecules are joined by hydrogen bonding into groups of extended hexagonal networks. By assuming a 3.0 Å separation of oxygen, such a water network has a and b dimensions of the clay minerals, and every other water molecule in the net has one hydrogen available for bonding to an oxygen of the clay mineral surface. Successive hexagonal nets build up on one another and are hydrogen bonded to one another. This hypothesis leads to a laminar stacking of hexagonal water molecule network with a vertical separation of 2.76 Å for each layer. In this configuration each water molecule in a monomolecular layer occupies an area of about 11.5 $Å^2$.

Macey (52) pointed out that there is a similarity between the basal plane of ice and the oxygen layer of the basal plane of clay mineral. In the clay interlayer oxygen surface, the oxygen atoms are 4.51 Å apart, whereas the oxygens of the basal plane of ice are 4.52 Å apart. Assuming an ice configuration, there are 2 2/3 molecules of water per unit cell, and each water molecule covers an area of about 17.5 $Å^2$. Macey suggests that the ice structure develops on clay mineral surfaces with the hexagonal molecular configuration of the basal plane of ice and tends to build outward from the surface. This configuration was supported by Forslind (30) using the Edelman-Favejee clay lattice structure.

Barshad (8) has postulated various configurations for the water molecules adsorbed. He suggests for a monomolecular layer of water the maximum expansion would be 2.76 Å if the centers of the oxygens of the water molecules were vertically above the centers of oxygens in the basal plane of clay mineral lattice, whereas the separation would be only 1.78 Å if the water molecules form tetrahedra with the bases of the linked silica tetrahedra of the clay mineral lattice. Three possible arrangements may occur dependent on the manner of superposition of one monolayer of water on the other. If the water molecules form tetrahedra at the water-oxygen interface and octahedra at the water-water interface, the arrangement would give a separation of 1.78 Å + 2.09 Å = 3.87 Å. If the water molecules form tetrahedra at the oxygen-water interface but are vertically above each other at the water-water interface, this would give an octahedral arrangement with a separation of 1.78 Å + 2.76 Å = 4.54 Å. If the water molecules are vertically above and below the oxygens of the clay surface and are also above each other at the water-water interface, the arrangement would give a thickness of 2.76 Å + 2.76 Å = 5.52 Å.

When three monomolecular layers are present, three possible separations are 3.87 Å + 2.76 Å = 5.96 Å; 4.54 Å + 2.76 Å = 7.30 Å; and 5.52 Å + 2.76 Å = 8.28 Å, respectively. Depending on the arrangement at the clay surface, the area

covered per molecule may be about 11.5 Å^2 or 7.7 Å^2.

The results of Demirel's studies (26) suggest that water is adsorbed in the interlayer regions in the form of icelike structure. This agrees essentially with Macey's hypothesis that a stacking of the hexagonal rings occurs in the quartz-like structure of ice: The first and second layers form a separation of 2.76 Å each; the third and fourth layers fill in between the hexagonal networks forming tetrahedrons with the molecules of the network. The complete unit cell of ice is formed with the entrance of the fourth layer, causing a separation of 7.36 Å. The fifth and sixth layers of water enter between the unit cell of ice and the clay surfaces causing total separation of 10.12 Å and 12.88 Å, respectively. The area occupied by a water molecule in this method is approximately 17.5 Å^2.

Opposing this view, Mackenzie (53) questions the validity of an ice-like structure. Nuclear magnetic resonance studies by Wu (81) on montmorillonite at low temperatures, do not substantiate the theory of ice structure. He points out that at temperatures below 0° C, the evidence indicates that the water close to the clay has a structure but it is different from that of ice. Wu further points out that selective adsorption sites exist for the first few molecules of adsorbed water, but that the water molecules are not bound to fixed positions but are under considerable thermal agitation.

Roderick (70) gives evidence of the formation of a laminated arrangement of interlayer water rather than an ice-like structure for a sodium montmorillonite with up to three layers of water. Mering (59) performed water vapor adsorption studies on calcium montmorillonite at 30° C and deduced that initially the first stage of hydration if the formation of groups of six H_2O molecules around every cation. He further suggested that the "hydrate" with two layers of water begins to form immediately after the hydration of the cations without passing through a one layer state.

There are approximately 0.35 calcium cations per unit cell; therefore, a three unit cell system satisfied by one cation is the basic model that will be utilized. From the data available and using Figures 13 and 17, the possible uptake and arrangement of the interlayer water molecules are visualized as follows: The first layer of water forms a hexagonal network shared by two montmorillonite platelets causing a separation of 2.76 Å. In Figure 15, this point can be located at the position at which approximately two molecules of water per unit cell are adsorbed.

After the first two molecules per unit cell are adsorbed, there is a small increase which may be attributed to the space occupied by the calcium ion, and may be considered as the state in which the first monolayer is completed and the start of the hydration of the cation occurs. The observed spacing

may be explained if the water molecules are shared by the cation and are located in positions directly below oxygens of the mineral surface, while the cation is located in the base of the tetrahedron in the hexagonal framework of the mineral surface.

As the second layer of water enters and 5.5 molecules of water per unit cell are adsorbed, two hexagonal networks stacked in a laminar fashion would give the proper amount of water per unit cell and give a d spacing of 14.7 Å. The larger observed spacing 15.1 Å, can be attributed to space occupied by the cation. A straight laminar stacking including the cation would have given a spacing of 15.6 Å; it is concluded that the 15.1 Å spacing is an average value from the 14.7 Å and 15.6 Å peaks. This view is supported by the line breadths, which are very broad in this region (Figure 13).

The 15.6 Å spacing relates to the entrance of additional water, and on the basis of the subsequent structure, this spacing, which also gives a broad peak, may be the start of an ice-like configuration with the formation of tetrahedrons with the water molecules of the hexagonal network. The 15.6 Å spacing is associated with the adsorption of 7.5 molecules of water per unit cell.

A four water-layer ice-like configuration causing a separation of 7.36 Å can be obtained by the adsorption of

twelve molecules of water per unit cell, and gives a d spacing of 16.5 Å. The observed combination of minimum line breadth and maximum intensity lend credence to the hypothesis of an ice-like configuration containing least disorder. The cation in this case fits loosely in holes, and does not directly affect the spacing.

Apparently a fifth molecular layer of water enters between the configuration, giving a less ordered structure but causing a minimum line breadth at 19.2 Å. An observed decrease in the intensity of the 001 reflections in the region of saturation must be an indication that the water molecules and/or cations have some structure effect. As the relative vapor pressure increased from p/p_o 0.42 to p/p_o 0.95, the interlaminar water content increased, but there was no significant change in intensity. After p/p_o 0.95, intensity decreased. In general, the effective structure factor may be expressed as a combination of the contribution from the mineral structure plus the effect of the interlayer cations and water molecules. At large separations, the ordering effect of the mineral surface is reduced and there is a build-up of electron population of water and the cations midway between the two sheets. Therefore, the 001 reflection would be reduced because the electron density would be exactly out of phase, although of a much reduced amplitude. The decreased intensity suggests that the cations may now be centrally lo-

cated, and prevention of further expansion is by symmetrical ion-dipole linkages between the layers.

As pointed out, the ice-like configuration is completed in a very limited range of relative vapor pressure near saturation. The configuration proposed in this study is not in basic contradiction with the ice-structure proposed by Macey (52) and Demirel (26) nor with the Nuclear Magnetic Resonance studies of Wu (81). At the present time there have been no Nuclear Magnetic Resonance studies published concerning work conducted at relative humidities at which the ice-like configuration results. Perhaps future studies can be conducted so as to bring more light upon the interlayer water theories.

Other alternatives for the arrangement of water were also considered. In the case of laminated stacking, a separation of 2.76 Å would be caused by the adsorption of each additional molecular layer of water. Table 8 indicates that the ice configuration explains the data in a better manner than does the laminated stacking concept.

The hypothesis proposed by Barshad (8) for the configuration of the interlaminar water was also examined, and the spacings proposed by him are included in the Table. As can be seen, these values can be utilized if one uses all three of his alternatives simultaneously. However, the configuration would be changed for each increment of water layers that entered. For example, alternative number one could be used

Table 8. Comparison of observed first order basal spacings of calcium montmorillonite with those calculated from montmorillonite platelet thickness (c_o) and hypothetical mechanism of the adsorption of water

	Ice configuration		Laminated stacking		Barshad's alternatives		
Number of molecular layers of water	Based on pyrophyllite thickness	Based on d_{001} of collapsed montmorillonite	Based on pyrophyllite thickness	Based on d_{001} of collapsed montmorillonite	Alternative #1[a]	Alternative #2[a]	Alternative #3[a]
0	9.14	10.1	9.14	10.1	10.16	10.16	10.16
1	11.90	12.86	11.90	12.86	11.94	12.92	
2	14.66	15.62	14.66	15.62	14.03	14.70	15.68
3	14.66	15.62	17.42	18.38	16.12	17.64	18.44
4	16.50[b]	17.46	20.18	21.14			
5	19.26	20.22	22.94	23.90			
6	22.02	22.98	25.70	26.66			

[a]Based on a minimum d spacing of 10.16 as proposed by Barshad (8).

[b]Corresponds to a single unit cell of ice like structure between platelets.

to explain the system with zero and one layer of water. Alternative number two could be used to explain the system with zero, one, and two layers. Alternative number three could be utilized to explain the system with two layers of water only. The arrangement proposed in the preceding discussion, i.e., a build-up of water in an ice-like configuration, appears to more aptly describe the observed spacings.

Sorption Data

The data utilized to define the adsorption and desorption isotherms are presented in Tables 9, 10, 11, and 12. The amount of water adsorbed, q, is expressed in mg per gm of the calcium montmorillonite. The relative vapor pressure, p/p_o, is unitless and is expressed in decimals at 25° C. Included in the Tables are the values of the function $\frac{p/p_o}{q(1-p/p_o)}$ for evaluation of the BET parameters, the function $\frac{p/p_o}{q}$ for the evaluation of the Langmuir parameters, and the function $\frac{q}{p/p_o}$ used to determine the free surface energy change.

Figures 23 and 24 are plots of the adsorption and desorption isotherms for the first and second cycles respectively. The desorption branch for the first and second branches did not return to the initial value of $q = 0$. For the entire range of the adsorption and desorption isotherms, the final point showed differences of 0.3% and 0.25% in the first and

Table 9. Adsorption isotherm data, first cycle

p mm Hg	p_o mm Hg	p/p_o	q, $\frac{gm}{gm} \times 10^{-3}$	$\frac{p/p_o}{q(1-p/p_o)}$	$\frac{q}{p/p_o}$	$\frac{p/p_o}{q}$
0.04_7	23.756	0.001_8	6.87_3	0.27_7	3.6_2	0.27_6
0.23_3		0.0097	15.45_0	0.634	1.59	0.628
0.23_8		0.010_0	15.54_3	0.649_9	1.55_4	0.643_5
0.35_4		0.014_9	18.82_4	0.803_5	1.26_3	0.791_8
0.38_8		0.016_3	18.88_6	0.877_4	1.15_9	0.862_8
0.48_7		0.020_5	21.91_7	0.954_9	1.06_9	0.935_5
0.50_4		0.021_3	22.07_3	0.986_0	1.03_6	0.965_3
0.67_4		0.028_5	25.97_9	1.12_9	0.911_5	1.09_7
0.91_4		0.038_5	30.30_2	1.32_1	0.787_1	1.27_0
0.92_0		0.038_7	31.75_9	1.26_8	0.820_7	1.21_8
1.12_2		0.0472	35.47_7	1.396	0.7516	1.330
1.49_4		0.0629	39.50_7	1.699	0.6281	1.592
1.50_6		0.0634	39.35_1	1.720	0,6207	1.611
1.51_8		0.0639	39.47_6	1.729	0.6178	1.618
2.00_7		0.0845	45.41_2	2.032	0.5374	1.861
2.05_3		0.0864	45.38_1	2.084	0.5252	1.904
2.07_3		0.0873	45.35_0	2.109	0.5195	1.925
2.20_9		0.0930	47.94_3	2.139	0.5155	1.940
2.21_3		0.0932	47.91_1	2.14_5	0.5141	1.945
2.23_4		0.0940	47.78_6	2.171	0.5084	1.967
2.45_6		0.103_4	50.47_3	2.284_9	0.4881_3	2.049

Table 9. (Continued)

p mm Hg	p_o mm Hg	p/p_o	q, $\frac{gm}{gm} \times 10^{-3}$	$\frac{p/p_o}{q(1-p/p_o)}$	$\frac{q}{p/p_o}$	$\frac{p/p_o}{q}$
2.52_2		0.106_2	50.34_8	2.360_0	0.4740_9	2.110
2.69_5		0.113_4	52.66_0	2.428_9	0.4643_7	2.153
2.77_1		0.117_2	57.31_6	2.316_3	0.4890_4	2.045
2.90_2		0.122_2	55.09_2	2.526_7	0.4508_8	2.218
2.90_6		0.122_3	57.72_2	2.414_0	0.4719_7	2.119
2.94_6		0.124_0	57.65_9	2.455_0	0.4649_9	2.151
2.96_1		0.124_6	55.03_5	2.586_3	0.4416_9	2.264
3.49_9		0.147_3	65.67_3	2.630_4	0.4458_5	2.243
3.61_8		0.152_3	66.06_4	2.719_5	0.4337_8	2.305
3.64_6		0.153_5	65.59_5	2.764_5	0.4273_3	2.340
3.72_2		0.156_7	67.87_6	2.737_4	0.4331_6	2.308
3.79_9		0.159_9	68.06_3	2.782_7	0.4256_6	2.349
3.91_8		0.164_9	71.42_3	2.765_2	0.4331_2	2.309
3.94_2		0.165_9	71.43_6	2.784_4	0.4306_0	2.322
3.99_2		0.168_0	71.53_1	2.822_6	0.4257_8	2.349
4.05_4		0.170_7	71.56_2	2.646_7	0.4192_3	2.386
4.19_0		0.176_4	74.93_7	2.858_5	0.4248_1	2.354
4.47_9		0.189_5	79.49_8	2.941_0	0.4195_1	2.384
4.54_5		0.191_3	79.49_8	2.976_2	0.4155_7	2.406
4.85_6		0.204_4	84.06_0	3.056_1	0.4112_5	2.431
5.01_6		0.211_2	87.87_2	3.046_6	0.4160_6	2.403

Table 9. (Continued)

p mm Hg	p_o mm Hg	p/p_o	q, $\frac{gm}{gm} \times 10^{-3}$	$\frac{p/p_o}{q(1-p/p_o)}$	$\frac{q}{p/p_o}$	$\frac{p/p_o}{q}$
5.12_7		0.215_8	87.99_6	3.127_4	0.4077_7	2.452
5.20_3		0.219_0	91.62_1	3.060_5	0.4229_3	2.365
5.21_9		0.219_7	91.62_1	3.073_7	0.4170_3	2.39_8
5.35_2		0.225_3	92.21_4	3.153_4	0.4092_9	2.442
5.35_6		0.225_4	93.90_1	3.099_2	0.4166_0	2.400
5.38_6		0.226_7	94.18_3	3.113_2	0.4154_5	2.407
5.41_8		0.228_0	92.18_3	3.203_4	0.4043_1	2.473
5.70_8		0.240_3	97.86_9	3.232_0	0.4072_8	2.455
5.73_3		0.241_3	97.74_4	3.269_4	0.4050_7	2.469
5.82_6		0.245_2	100.931	3.219_0	0.4116_3	2.429
5.92_8		0.249_5	101.43_1	3.277_1	0.4065_4	2.460
6.09_1		0.256_4	101.68_1	3.391_0	0.3965_7	2.521
6.19_4		0.260_7	104.61_8	3.370_4	0.4013_0	2.492
6.22_9		0.262_3	104.49_3	3.401_2	0.3985_2	2.509
6.23_9		0.262_6	104.30_5	3.414_0	0.3972_0	2.518
6.51_4		0.274_2	107.68_3	3.508_4	0.3927_2	2.546
6.54_1		0.275_3	107.61_7	3.530_1	0.3909_1	2.558
6.82_8		0.287_4	111.67_9	3.611_2	0.3885_8	2.591
6.91_4		0.291_0	111.46_0	3.682_0	0.3830_2	2.611
7.16_4		0.301_6	114.24_1	3.779_7	0.3787_8	2.640
7.36_7		0.310_1	117.36_5	3.829_9	0.3784_7	2.642

Table 9. (Continued)

p mm Hg	p_o mm Hg	p/p_o	q, $\frac{gm}{gm} \times 10^{-3}$	$\frac{p/p_o}{q(1-p/p_o)}$	$\frac{q}{p/p_o}$	$\frac{p/p_o}{q}$
7.43_3		0.312_9	117.36_5	3.880_1	0.3750_9	2.666
7.70_8		0.324_5	120.33_3	3.992_3	0.3708_3	2.697
7.91_3		0.333_1	126.11_3	3.950_7	0.3786_0	2.641
7.91_6		0.333_2	125.92_6	3.968_2	0.3779_3	2.646
7.95_3		0.334_8	123.08_3	4.089_1	0.3676_3	2.720
7.97_9		0.335_8	126.05_2	4.011_1	0.3753_8	2.664
8.01_7		0.337_5	123.11_4	4.162_0	0.3647_8	2.741
8.10_9		0.341_3	125.98_8	4.112_3	0.3991_7	2.505
8.37_7		0.352_6	128.67_5	4.232_4	0.3649_3	2.740
8.62_7		0.3632	131.45_6	4.339_1	0.3619_4	2.763
8.72_5		0.367_3	131.29_9	4.421_2	0.3574_7	2.797
9.10_3		0.383_2	134.45_5	4.620_9	0.3508_7	2.850
9.19_5		0.387_1	136.58_0	4.624_4	0.3528_3	2.834
9.20_6		0.387_5	136.39_2	4.642_3	0.3520_7	2.840
9.44_9		0.397_8	136.70_5	4.829_3	0.3436_5	2.910
9.75_4		0.416_9	139.42_3	5.128_3	0.3344_3	2.990
10.11_8		0.4259	141.45_4	5.2448	0.33213	3.011
10.40_8		0.4381	144.20_3	5.4070	0.32916	3.038
10.50_4		0.4422	144.51_5	5.4859	0.32681	3.060
10.62_8		0.4474	146.04_6	5.5435	0.32643	3.063
11.11_0		0.4677	148.79_6	5.9047	0.31814	3.143

Table 9. (Continued)

p mm Hg	p_o mm Hg	p/p_o	q, $\frac{gm}{gm} \times 10^{-3}$	$\frac{p/p_o}{q(1-p/p_o)}$	$\frac{q}{p/p_o}$	$\frac{p/p_o}{q}$
11.12_5		0.4683	148.79_6	5.9195	0.31774	3.147
11.20_3		0.4716	148.67_1	6.0032	0.31525	3.172
11.39_9		0.4792	150.79_5	6.1016	0.31468	3.178
11.51_2		0.4846	153.29_5	6.1333	0.31633	3.162
11.51_9		0.4849	153.23_2	6.1437	0.31601	3.164
11.86_1		0.4993	155.91_9	6.3956	0.31228	3.202
11.87_2		0.4997	155.91_9	6.4059	0.31203	3.205
12.13_8		0.5109	155.41_9	6.7212	0.30421	3.287
12.23_6		0.5151	157.98_1	6.7243	0.30670	3.261
12.28_3		0.5198	157.98_1	6.8521	0.30393	3.291
12.69_6		0.5344	161.32_4	7.1147	0.30188	3.312
12.73_1		0.5359	161.32_4	7.1576	0.30103	3.322
12.87_2		0.5418	161.26_2	7.3328	0.29764	3.360
12.97_5		0.5462	163.79_2	7.3483	0.29988	3.334
13.06_0		0.5498	163.79_2	7.4558	0.29791	3.357
13.40_0		0.5641	166.35_4	7.7792	0.29490	3.391
13.43_3		0.5655	166.35_4	7.8237	0.29417	3.399
14.14_0		0.5953	171.79_1	8.9645	0.28858	3.465
14.23_6		0.5993	170.85_3	8.7537	0.28509	3.508
14.60_8		0.6149	174.85_3	9.1317	0.28436	3.516
14.61_8		0.6153	174.85_3	9.1471	0.28418	3.519

Table 9. (Continued)

p mm Hg	p_o mm Hg	p/p_o	q, $\frac{gm}{gm} \times 10^{-3}$	$\frac{p/p_o}{q(1-p/p_o)}$	$\frac{q}{p/p_o}$	$\frac{p/p_o}{q}$
14.99_3		0.6311	179.03_9	9.5555	0.28369	3.525
15.01_5		0.6321	179.16_4	9.5896	0.28344	3.529
15.35_4		0.6463	181.72_6	9.5220	0.28118	3.556
15.46_8		0.6511	181.53_9	10.280	0.27882	3.587
15.79_4		0.6648	182.27_3	10.881	0.27418	3.647
15.84_0		0.6667	182.21_0	10.978	0.27330	3.659
16.24_9		0.6839	186.33_4	11.611	0.27246	3.670
16.53_5		0.6960	189.39_6	12.088	0.27212	3.675
16.55_1		0.6966	189.39_6	12.123	0.27189	3.678
16.88_8		0.7108	192.70_8	12.754	0.27111	3.689
16.90_9		0.7118	192.70_8	12.816	0.27073	3.694
17.34_5		0.730_1	197.20_7	13.71_7	0.2701_1	3.70_2
17.34_5		0.730_1	197.17_6	13.71_9	0.2700_7	3.70_3
17.66_7		0.743_6	200.14_4	14.49_1	0.2691_6	3.71_5
17.74_3		0.746_9	200.20_6	14.74_0	0.2680_5	3.73_1
18.14_0		0.763_6	204.95_5	15.76_0	0.2684_1	3.72_6
18.26_2		0.768_7	204.67_4	16.23_8	0.2662_6	3.75_5
18.58_2		0.782_2	209.42_3	17.14_9	0.2677_4	3.73_6
18.74_2		0.788_9	212.27_8	17.60_5	0.2690_8	3.71_6
18.74_6		0.789_1	212.45_4	17.61_1	0.2692_4	3.71_5
19.05_3		0.802_0	214.95_3	18.84_4	0.2680_2	3.73_1

Table 9. (Continued)

p mm Hg	p_o mm Hg	p/p_o	q, $\frac{gm}{gm} \times 10^{-3}$	$\frac{p/p_o}{q(1-p/p_o)}$	$\frac{q}{p/p_o}$	$\frac{p/p_o}{q}$
19.45_2		0.818_8	219.29_6	20.60_6	0.2678_3	3.73_4
19.49_0		0.820_4	219.17_1	20.84_2	0.2671_5	3.74_3
19.50_8		0.821_1	219.17_1	20.94_1	0.2669_2	3.74_7
19.80_8		0.833_8	223.32_6	22.46_4	0.2678_4	3.73_4
19.93_6		0.839_2	222.98_3	23.40_5	0.2657_1	3.76_4
20.32_8		0.855_7	229.26_3	25.86_6	0.2679_2	3.73_3
20.54_5		0.864_8	232.85_6	27.46_9	0.2692_6	3.71_3
20.57_5		0.866_1	232.98_1	27.76_3	0.2690_0	3.71_7
20.74_5		0.873_2	237.13_6	29.04_0	0.2715_7	3.68_2
20.75_9		0.873_8	237.07_3	29.20_6	0.2713_1	3.68_6
20.76_1		0.873_9	237.01_1	29.24_0	0.2712_1	3.68_7
20.91_7		0.880_5	237.07_3	31.080	0.26925	3.715
20.94_2		0.8815	237.04_2	31.382	0.26891	3.719
20.97_9		0.8831	237.04_2	31.869	0.26842	3.726
21.10_4		0.8883	239.94_8	33.143	0.27012	3.702
21.11_6		0.8889	240.26_0	33.301	0.27029	3.700
21.13_0		0.8895	240.44_8	33.478	0.27032	3.700
21.18_6		0.8918	240.79_1	34.229	0.27001	3.704
21.19_5		0.8922	241.13_5	34.323	0.27027	3.700
21.22_4		0.8934	241.32_3	34.729	0.27012	3.702
21.26_1		0.8950	242.04_1	35.216	0.27044	3.698

Table 9. (Continued)

p mm Hg	p_o mm Hg	p/p_o	q, $\frac{gm}{gm} \times 10^{-3}$	$\frac{p/p_o}{q(1-p/p_o)}$	$\frac{q}{p/p_o}$	$\frac{p/p_o}{q}$
21.43_5		0.9023	244.44_7	37.781	0.27092	3.691
21.60_5		0.9095	248.10_2	40.506	0.27279	3.666
21.62_8		0.9104	245.56_9	41.376	0.26974	3.708
21.69_6		0.9133	249.16_5	42.277	0.27282	3.666
21.70_3		0.9136	245.85_3	43.010	0.26910	3.716
21.81_0		0.9181	250.66_4	44.721	0.27302	3.663
21.88_6		0.9213	250.19_6	46.790	0.27157	3.682
21.95_0		0.9239	251.22_7	48.326	0.27192	3.678
22.05_2		0.9283	253.38_2	51.097	0.27295	3.663
22.13_0		0.9316	253.85_1	53.653	0.27249	3.670
22.15_9		0.9328	257.06_9	53.997	0.27559	3.628
22.33_7		0.9403	258.38_1	60.959	0.27479	3.639
22.35_9		0.9412	258.31_9	61.966	0.27446	3.643
22.41_7		0.9437	261.50_6	64.098	0.27711	3.609
22.50_3		0.9473	261.13_1	68.836	0.27566	3.627
22.50_9		0.9475	261.16_2	69.104	0.27563	3.628
22.65_2		0.9535	267.56_7	76.637	0.28062	3.564
23.03_4		0.9696	280.64_2	113.65	0.28944	3.454
23.04_1		0.9699	281.11_1	114.63	0.28984	3.451
23.06_4		0.9709	281.65_7	118.46	0.29010	3.447
23.07_1		0.9711	277.83_0	120.94	0.28610	3.495

Table 9. (Continued)

p mm Hg	p_o mm Hg	p/p_o	q, $\frac{gm}{gm} \times 10^{-3}$	$\frac{p/p_o}{q(1-p/p_o)}$	$\frac{q}{p/p_o}$	$\frac{p/p_o}{q}$
23.17_1		0.9754	286.42_2	138.44	0.29365	3.406
23.21_9		0.9774	292.39_7	147.91	0.29916	3.342
23.23_5		0.9781	292.33_5	152.78	0.29888	3.346
23.26_1		0.9792	291.77_2	161.35	0.29797	3.356
23.28_0		0.9800	294.70_9	166.27	0.30072	3.326
23.28_6		0.9802	287.70_3	172.07	0.29351	3.407
23.30_1		0.9805	296.70_9	169.47	0.30261	3.305
23.29_5		0.9806	287.10_9	176.05	0.29279	3.415
23.30_4		0.9810	291.772	176.96	0.29742	3.362
23.36_8		0.9837	298.58_3	202.12	0.30353	3.295
23.45_3		0.9875	303.77_0	260.07	0.30762	3.251
23.54_2		0.9910	308.95_6	356.40	0.31176	3.207
23.54_5		0.9911	305.33_2	364.71	0.30807	3.246
23.56_9		0.9921	306.26_9	410.04	0.30871	3.239
23.63_6		0.9949	309.08_1	631.16	0.31067	3.219
23.68_2		0.9969	318.17_3	1010.7	0.31916	3.133
23.71_7		0.9984	322.48_4	1935.0	0.32300	3.096
23.72_1		0.9985	311.73_7	2135.3	0.31221	3.203
23.73_1		0.9989	316.54_8	2868.8	0.31690	3.156
23.78_3		1.001	319.73_5	———	0.31942	3.131
23.78_6		1.001	319.93_0	———	0.31961	3.129

Table 9. (Continued)

p mm Hg	p_o mm Hg	p/p_o	q, $\frac{gm}{gm} \times 10^{-3}$	$\frac{p/p_o}{q(1-p/p_o)}$	$\frac{q}{p/p_o}$	$\frac{p/p_o}{q}$
23.85_3		1.004	328.38_9	———	0.32708	3.057
23.89_7		1.005	323.67_2	———	0.32206	3.105
23.90_0		1.008	322.39_1	———	0.31983	3.127
23.97_1		1.009	336.51_3	———	0.33351	2.998
23.99_4		1.010	330.79_6	———	0.32752	3.053
24.18_3		1.017	353.52_5	———	0.34762	2.877
24.26_4		1.021	360.58_5	———	0.35317	2.831
24.37_6		1.026	353.80_6	———	0.34484	2.900
24.43_6		1.028	357.93_0	———	0.34484	2.900

second desorption runs, respectively. These differences may or may not be real, since readings of the calibrated dial on the automatic recording device or marking pen position may have introduced an error. However, if this difference is real it may be attributed to trace amounts of individual or clustered water molecules that were trapped within the interlayer positions if the pumping period were insufficient in length to remove the water from within the collapsed clay structure. Hence, the values for the BET function, the Langmuir func-

Table 10. Desorption isotherm data, first cycle

p mm Hg	p_o mm Hg	p/p_o	q, $\frac{gm}{gm} \times 10^{-3}$	$\frac{p/p_o}{q(1-p/p_o)}$	$\frac{q}{p/p_o}$	$\frac{p/p_o}{q}$
23.74_1	23.756	0.9994	319.86_8	———	0.32006	3.124
23.44_8		0.9870	307.71_4	246.73	0.31177	3.207
23.42_6		0.9861	301.65_3	235.18	0.30591	3.269
23.42_0		0.9858	302.02_8	229.86	0.30628	3.264
23.06_5		0.9709	284.07_9	117.45	0.29259	3.418
22.46_6		0.9457	268.14_5	64.950	0.28354	3.527
21.72_7		0.9146	256.42_8	41.764	0.28037	3.566
21.57_1		0.9080	253.92_9	38.867	0.27966	3.575
21.45_7		0.9032	252.36_7	36.972	0.27941	3.579
20.84_1		0.8773	240.88_5	29.682	0.27458	3.642
19.66_0		0.8276	232.91_8	20.610	0.28144	3.554
19.65_8		0.8275	232.60_5	20.623	0.28109	3.557
19.12_7		0.8051	227.84_1	18.130	0.28300	3.534
18.62_7		0.7839	223.46_7	16.233	0.28507	3.508
18.19_1		0.7657	220.10_8	14.847	0.28746	3.478
17.62_8		0.7420	216.35_9	13.292	0.29159	3.429
17.59_2		0.7407	216.35_9	13.203	0.29210	3.423
17.11_8		0.7205	212.45_4	12.134	0.29487	3.391
16.62_2		0.6996	209.32_9	11.126	0.29921	3.342
16.18_8		0.6814	206.67_4	10.348	0.30331	3.297
15.53_1		0.6537	203.42_4	9.2794	0.31119	3.213

Table 10. (Continued)

p mm Hg	p_o mm Hg	p/p_o	q, $\frac{gm}{gm} \times 10^{-3}$	$\frac{p/p_o}{q(1-p/p_o)}$	$\frac{q}{p/p_o}$	$\frac{p/p_o}{q}$
14.86_9		0.6259	199.33_2	8.3935	0.31847	3.140
14.45_9		0.6086	196.39_4	7.9174	0.32270	3.099
13.83_2		0.5823	193.02_0	7.2223	0.33148	3.017
13.57_9		0.5716	191.64_6	6.9622	0.33528	2.983
13.10_7		0.5517	188.11_5	6.5420	0.34097	2.933
12.59_0		0.5300	183.74_1	6.1372	0.34668	2.885
12.55_7		0.5294	183.99_1	6.1141	0.34755	2.877
12.20_3		0.5137	180.99_1	5.8364	0.35233	2.838
11.72_9		0.4937	178.55_5	5.4611	0.36167	2.765
11.04_3		0.4649	174.52_5	4.9781	0.37540	2.664
10.62_7		0.4473	171.27_5	4.7252	0.38291	2.612
10.31_1		0.4340	168.43_2	4.5525	0.38809	2.577
9.81_2		0.413_0	164.99_5	4.264_2	0.3995_0	2.503
9.66_8		0.407_0	163.09_0	4.208_4	0.4007_1	2.496
9.32_2		0.392_4	159.90_3	4.038_8	0.4075_0	2.454
8.82_6		0.371_5	155.87_2	3.792_1	0.4195_7	2.383
8.39_5		0.353_4	150.70_2	3.626_7	0.4274_3	2.345
8.06_7		0.339_6	146.78_1	3.503_4	0.4322_2	2.314
8.06_3		0.339_4	146.78_1	3.500_3	0.4324_7	2.312
7.69_3		0.323_8	141.42_2	3.386_0	0.4367_6	2.290
7.43_4		0.312_9	136.70_5	3.331_2	0.4369_0	2.289

Table 10. (Continued)

p mm Hg	p_o mm Hg	p/p_o	q, $\frac{gm}{gm} \times 10^{-3}$	$\frac{p/p_o}{q(1-p/p_o)}$	$\frac{q}{p/p_o}$	$\frac{p/p_o}{q}$
7.30_7		0.307_6	133.76_8	3.321_1	0.4348_8	2.299
6.99_5		0.294_6	127.58_2	3.273_5	0.4330_7	2.309
6.75_8		0.284_5	123.02_0	3.232_2	0.4324_1	2.313
6.71_1		0.282_5	122.64_5	3.210_3	0.4341_4	2.303
6.46_4		0.272_1	115.02_2	3.249_9	0.4227_2	2.366
6.45_8		0.271_8	115.08_4	3.243_3	0.4234_1	2.362
6.27_7		0.264_2	110.74_1	3.219_1	0.4213_9	2.373
5.85_0		0.246_3	100.15_8	3.262_7	0.4066_5	2.459
5.66_9		0.238_6	98.59_6	3.178_3	0.4132_3	2.420
5.50_3		0.231_6	95.59_6	3.152_9	0.4127_6	2.423
5.32_6		0.224_2	91.97_2	3.142_2	0.4102_2	2.438
4.80_6		0.202_3	83.78_7	3.026_8	0.4141_7	2.414
4.65_5		0.196_0	83.06_8	2.934_7	0.4238_2	2.359
4.39_1		0.184_8	78.56_9	2.885_3	0.4251_6	2.352
3.90_4		0.164_3	71.91_4	2.733_8	0.4377_0	2.285
3.42_0		0.144_0	64.41_6	2.611_5	0.4473_3	2.235
3.34_0		0.140_6	62.10_4	2.634_3	0.4417_1	2.264
0.0000		0.0000	3.01_6	—	—	—

Table 11. Adsorption isotherm data, second cycle

p mm Hg	p_o mm Hg	p/p_o	q, $\frac{gm}{gm} \times 10^{-3}$	$\frac{p/p_o}{q(1-p/p_o)}$	$\frac{q}{p/p_o}$	$\frac{p/p_o}{q}$
0.03_8	23.756	0.001_6	5.67_9	0.28_1	3.5_5	0.28_2
0.04_9		0.002_1	5.67_7	0.37_1	2.7_0	0.37_0
0.13_8		0.005_8	13.40_3	0.43_5	2.31_1	0.43_3
0.14_6		0.006_1	13.40_3	0.45_8	2.19_7	0.45_5
0.18_5		0.007_9	13.40_3	0.59_4	1.69_6	0.58_9
0.64_3		0.037_1	28.69_5	0.971	1.05_9	0.944_2
0.66_7		0.028_1	28.62_0	1.010	1.018_5	0.981_8
1.29_0		0.054_3	40.11_9	1.431	0.7401	1.351
1.29_2		0.054_4	40.21_0	1.431	0.7391	1.353
1.79_1		0.075_4	47.85_6	1.704	0.6347	1.576
2.45_9		0.1035	55.44_2	2.082_6	0.5356_7	1.867
3.11_3		0.1310	62.09_9	2.426_7	0.4740_7	2.109
3.82_5		0.1610	69.83_5	2.747_9	0.4337_5	2.305
4.53_6		0.1909	79.64_0	2.961_9	0.4171_8	2.397
5.14_6		0.2166	89.89_4	3.076_4	0.4150_2	2.409
6.03_0		0.2538	101.28_9	3.357_9	0.3990_8	2.506
6.87_9		0.2896	110.52_4	3.688_4	0.3816_4	2.620
6.91_4		0.2910	110.70_4	3.707_5	0.3809_2	2.624
7.66_2		0.3225	117.54_0	4.049_8	0.3644_6	2.743
8.62_8		0.3632	124.42_2	4.583_9	0.3425_7	2.919
9.49_8		0.3998	131.38_4	5.069_9	0.3286_2	3.043

Table 11. (Continued)

p mm Hg	p_o mm Hg	p/p_o	q; $\frac{gm}{gm} \times 10^{-3}$	$\frac{p/p_o}{q(1-p/p_o)}$	$\frac{q}{p/p_o}$	$\frac{p/p_o}{q}$
10.41_8		0.4385	138.42_5	5.6416	0.31567	3.167
11.35_4		0.4779	144.51_2	6.3340	0.30238	3.307
12.21_2		0.5141	150.38_9	7.0353	0.29253	3.418
13.14_8		0.5531	157.25_8	7.8701	0.28432	3.517
14.12_1		0.5944	163.29_7	8.1382	0.27473	3.640
14.91_1		0.6277	168.54_5	10.003	0.26851	3.724
15.79_6		0.6649	175.14_1	11.328	0.26341	3.769
16.67_2		0.7018	182.63_7	12.883	0.26024	3.843
17.66_1		0.7434	181.71_4	15.270	0.25520	3.918
18.44_8		0.7766	195.89_1	17.745	0.25224	3.964
19.10_7		0.8043	204.43_2	20.203	0.25293	3.953
19.86_3		0.8361	211.77_5	24.087	0.25329	3.948
20.52_8		0.8641	219.41_4	28.977	0.25392	3.928
21.07_8		0.8872	227.30_0	34.602	0.25620	3.903
21.67_2		0.9123	237.45_0	43.799	0.26028	3.843
22.08_0		0.9295	249.96_8	52.727	0.26893	3.718
22.08_5		0.9297	257.82_4	51.275	0.27732	3.606
22.09_3		0.9299	251.30_2	52.805	0.27025	3.700
22.72_4		0.9566	267.25_5	82.468	0.27938	3.579
23.75_6		1.0000	324.66_0	———	0.32446	3.080

Table 12. Desorption isotherm data, second cycle

p mm Hg	p_o mm Hg	p/p_o	q (gm/gm)x10^{-3}	$\frac{p/p_o}{q(1-p/p_o)}$	$\frac{q}{p/p_o}$	$\frac{p/p_o}{q}$
23.75_6	23.756	1.000	324.66_0	———	0.32466	3.080
23.34_0		0.9825	323.61_1	173.48	0.32938	3.036
23.29_1		0.9804	323.61_1	154.57	0.33008	3.030
23.26_8		0.9795	318.27_4	150.12	0.32494	3.077
23.07_1		0.9712	313.56_6	107.54	0.32286	3.097
23.05_6		0.9705	323.31_1	101.76	0.33314	3.002
23.04_9		0.9702	311.76_7	104.44	0.32134	3.112
23.01_9		0.9690	293.56_6	106.48	0.30296	3.301
22.91_9		0.9648	320.67_2	85.477	0.33237	3.009
22.83_7		0.9613	286.22_0	86.786	0.29774	3.359
22.53_5		0.9486	274.52_6	67.243	0.28940	3.455
22.02_0		0.9269	261.18_3	48.548	0.28178	3.549
21.60_5		0.9095	247.27_0	40.644	0.27187	3.678
20.70_9		0.8717	234.88_6	28.925	0.26946	3.711
19.85_4		0.8357	223.46_2	22.760	0.26739	3.740
18.75_7		0.7896	212.96_7	17.622	0.26972	3.708
17.74_5		0.7470	204.99_1	14.406	0.27442	3.644
16.99_1		0.7152	200.70_3	12.511	0.28063	3.563
16.03_1		0.6748	194.04_7	10.693	0.28756	3.478
14.82_2		0.6239	187.75_0	8.8362	0.30093	3.323
13.71_6		0.5774	181.00_3	7.5468	0.31348	3.190

Table 12. (Continued)

p mm Hg	p_o mm Hg	p/p_o	q, $(\frac{gm}{gm})x10^{-3}$	$\frac{p/p_o}{q(1-p/p_o)}$	$\frac{q}{p/p_o}$	$\frac{p/p_o}{q}$
12.69_1		0.5342	175.75_6	6.5261	0.32901	3.039
11.36_4		0.4784	168.59_0	5.4404	0.35240	2.838
10.69_5		0.4502	164.09_2	4.9899	0.36449	2.744
9.53_2		0.401_2	156.74_6	4.274_4	0.3906_9	2.560
8.53_8		0.359_4	149.21_9	3.759_6	0.4151_9	2.409
7.87_9		0.331_7	141.75_3	3.501_2	0.4273_5	2.340
6.82_2		0.287_1	130.08_9	3.095_6	0.4531_1	2.207
6.67_6		0.281_0	129.24_5	3.023_7	0.4599_5	2.174
6.19_2		0.260_6	119.23_5	2.955_5	0.4575_4	2.186
5.68_6		0.239_0	104.87_2	2.995_1	0.4387_9	2.279
5.59_7		0.235_6	107.27_1	2.873_1	0.4553_1	2.196
5.54_9		0.233_6	103.37_2	2.948_6	0.4425_2	2.260
5.414		0.227_9	105.83_1	2.789_4	0.4643_7	2.153
5.23_2		0.220_2	98.99_5	2.852_7	0.4495_7	2.224
5.18_3		0.218_2	101.09_4	2.760_8	0.4633_1	2.158
5.18_1		0.218_1	101.87_3	2.737_7	0.4670_9	2.141
4.86_1		0.204_6	92.09_8	2.792_7	0.4501_4	2.222
4.22_4		0.177_8	80.61_4	2.681_9	0.4534_0	2.206
3.30_0		0.138_9	69.00_3	2.337_6	0.4967_8	2.013
2.64_5		0.111_3	58.92_8	2.1246	0.5294_5	1.889
2.05_0		0.0863	49.39_2	1.912	0.5723	1.747

Table 12. (Continued)

p mm Hg	p_o mm Hg	p/p_o	q, $(\frac{gm}{gm})x10^{-3}$	$\frac{p/p_o}{q(1-p/p_o)}$	$\frac{q}{p/p_o}$	$\frac{p/p_o}{q}$
1.70_1		0.0716	43.45_5	1.775	0.6069	1.648
1.10_6		0.0466	28.15_3	1.736	0.6041	1.655
0.00_0		0.000	2.59_9	0.000	———	0.000

tion, and the free energy change for the second cycle were computed from the isotherm beginning at q = 0 and using the end point of the first desorption cycle as the new reference point.

The isotherms show equilibrium moisture contents for the clay as the relative water vapor pressure increases or decreases. In the low relative pressure region, the isotherm is concave to the pressure axis whereas in the high relative pressure region it is convex to the pressure axis. In an intermediate pressure range the isotherm exhibits a somewhat linear portion, the length and slope of which Brunauer (16) states is dependent on the adsorbent, the adsorbate, and the temperature selected for the investigation. Orchiston (64, 65) points out that the multimolecular adsorption theory is based on an adsorption on localized sites rather than on the

Figure 23. Sorption isotherms of calcium montmorillonite, first cycle

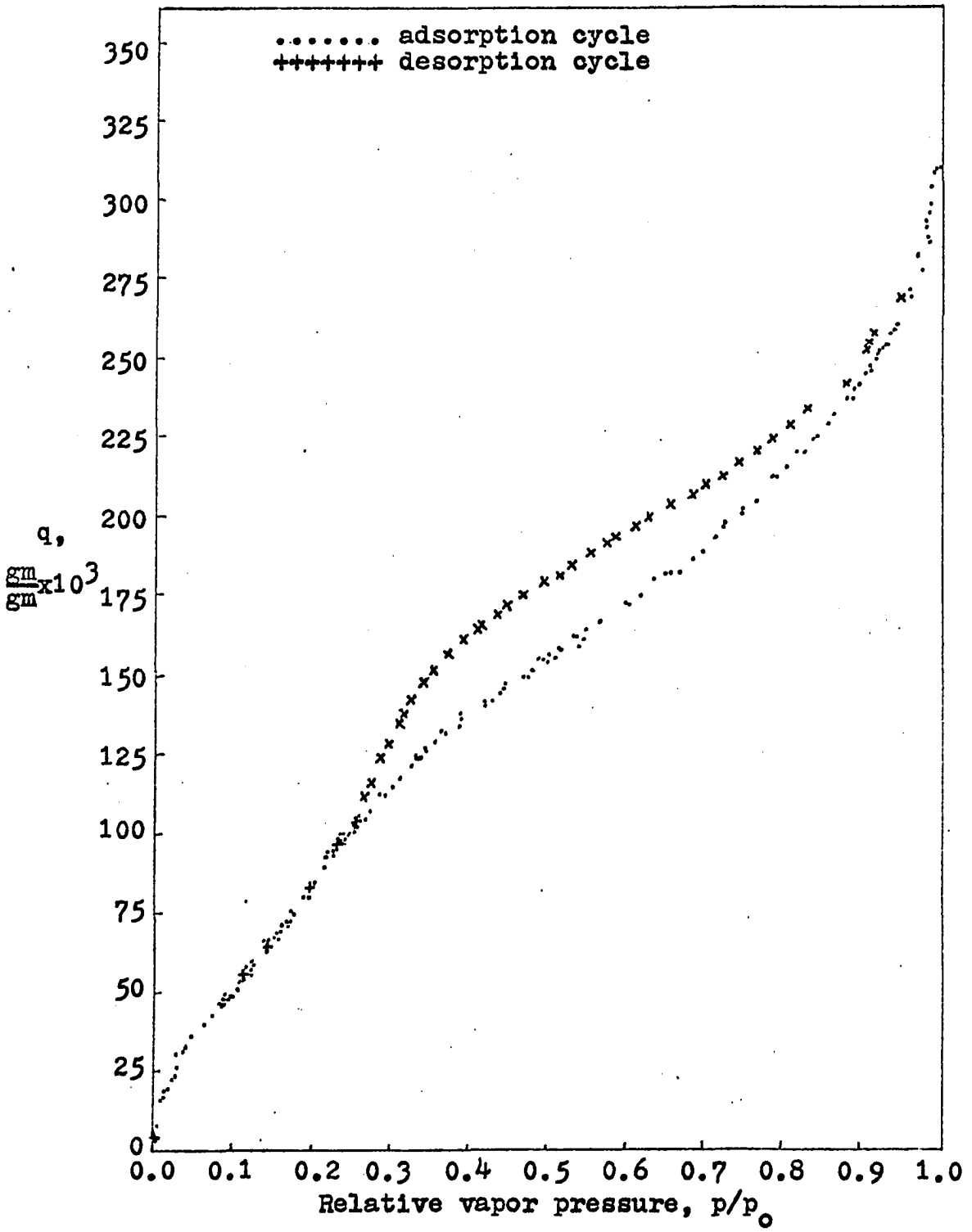
..... adsorption cycle
+++++++ desorption cycle
q, gm/gm x10^3
350
325
300
275
250
225
200
175
150
125
100
75
50
25
0
0.0
0.1
0.2
0.3
0.4
0.5
0.6
0.7
0.8
0.9
1.0
Relative vapor pressure, p/p_o

Figure 24. Sorption isotherms of calcium montmorillonite, second cycle

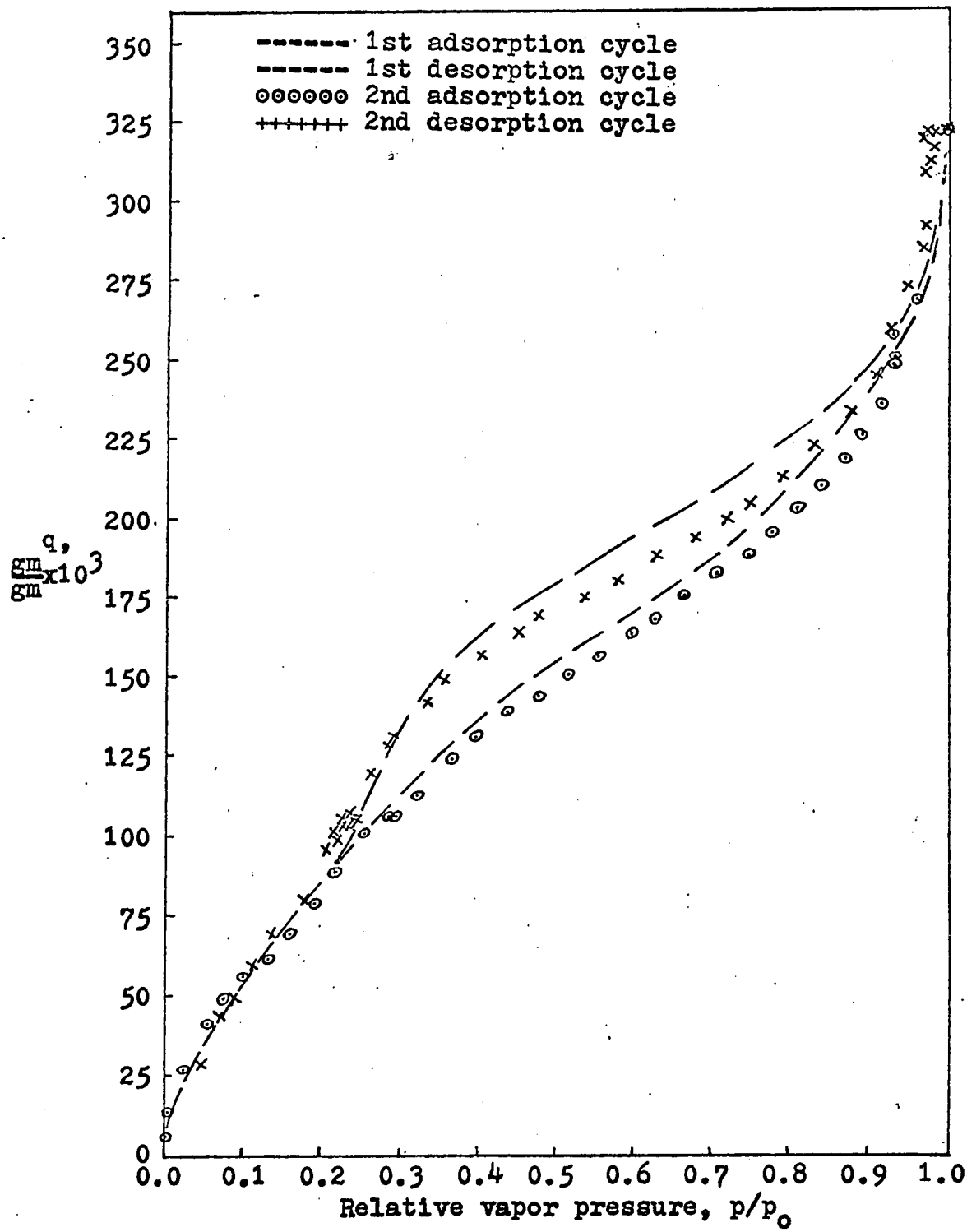
1st adsorption cycle
1st desorption cycle
2nd adsorption cycle
2nd desorption cycle
q, gm/gm x10^3
350
325
300
275
250
225
200
175
150
125
100
75
50
25
0
0.0
0.1
0.2
0.3
0.4
0.5
0.6
0.7
0.8
0.9
1.0
Relative vapor pressure, p/p_o

formation of a mobile adsorbed layer. Using the Orchiston (65) approach, the concave section of the section of the isotherm explains the completion of the first layer on these sites which may grow vertically and horizontally. The convex section of the isotherm shows a running together of the clusters of water molecules around the active sites.

It can be seen that there is a drift on successive cycles with the same adsorbent, and the isotherms do not coincide. The shift in the curve is probably due to a rearrangement of the surface areas as well as the changes due to pore size and shape during the first adsorption cycle. In the relative pressure range from $p/p_o = 0.85$ to saturation, the effects due to capillary condensation are pronounced.

A large portion of the sorption chamber, namely the large vacuum bottle containing the electrobalance, was exposed to room temperature (Figures 4 and 5), and fluctuations in room temperature would affect the pressure in the sorption chamber. When the Kelvin equation is employed to determine the capillary condensation, it can be seen that little change in pressure at high relative pressures due to slight room temperature fluctuations can have a pronounced effect on adsorption. The effect of slight room temperature variations at low and intermediate relative vapor pressures ($p/p_o = 0$ to $p/p_o = 0.85$), however, have little effect on the stability of the system at equilibrium since capillary effects and the

differences in pressure due to room temperature fluctuations are minimal. The instability of the system at high relative pressure range probably results in a rearrangement of the pores of the adsorbate, causing drifts in successive sorption cycles. After a relative pressure of 0.90 the effect of room temperature variations on the stability are especially pronounced and manifested as an oscillating or "hunting" of the recorder pen. This oscillation was associated with a change of relative pressure of 0.01 and a change of q equal to 5.0 mg/gm of clay.

Between relative pressure of 0.97 and 0.99 the "hunting" was due to the condensation of the water around the hangdown tube in the thermostat. To eliminate this effect, the water level was raised in the thermostat so that the water level extended up onto the heavy glass protrusion of the electrobalance, and a thin film of oil was placed on the surface to reduce condensation. At saturation although the bath temperature was maintained at 25.00$\pm$ 0.01° C and the sample was suspended approximately 20 centimeters below the surface of the bath, equilibrium was difficult to maintain. The sample weight oscillated very slightly due to random condensation and evaporation due to room temperature fluctuations of 1/2° C causing a pressure difference in the vacuum flask of the electrobalance. Regardless of the variations during adsorption at the high relative pressure range, when equilibrium was established, a

smooth curve was obtained.

Several interesting facets concerning the rate of adsorption were observed during the investigation. The spontaneity and instantaneousness of adsorption was indicated by the automatic recording device attached to the electrobalance. As soon as a small increment of water vapor entered the system, the response of the pen was immediate. At low relative pressures, the slope of the line described by the marking pen was very steep and the slope decreased as the relative vapor pressure approached saturation. During desorption studies, this trend was reversed at high relative vapor pressures. If it is assumed that only a small fraction of the impinging water vapor molecules are reflected back elastically by the solid, the rate of adsorption on a free surface would be quite rapid. If, however, the adsorbent contains long, very narrow pores and the vapor must diffuse into them, the adsorption would take a longer time to reach equilibrium. If the incoming water molecules must displace either previously adsorbed molecules already there, the rate of adsorption may become very slow. In these studies, equilibrium was reached four hours after introduction of vapor and eight hours after removal of vapor for adsorption and desorption respectively. At low pressure, approximately 90% of adsorption took place within the first 24 minutes after the stopcock controlling the water reservoir was closed.

A similar trend was observed with the X-ray diffraction studies. After introducing a small amount of water vapor, the goniometer was set in motion, starting at a 2θ angle two to four degrees lower than the apparent basal spacing for the previous transfer. The shift to the new vapor transfer peak position was observed within two minutes after stopcock S-1 was closed (Figure 9). At all relative vapor pressures up to $p/p_o = 0.98$, the new peak position determined within 30 minutes after closing the stopcock did not change in position or intensity during the next 24 hours. This would indicate that the basal spacing and intensity bath change rapidly with the introduction of vapor. The shift in basal spacing was dependent on the amount of water adsorbed.

During adsorption in the X-ray chamber from $p/p_o = 0.98$ to saturation, stopcock S-1 was left open and sufficient time alloted to assure saturation, and X-ray diffraction traces were run intermittantly for a period of 342 hours. The driving force was very small and adsorption proceeded very slowly. No appreciable change in basal spacing, intensity, or line breadth was observed until 80 hours after introduction of the vapor. After 80 hours there was an increase in line breadth preceding a change in basal spacing. The shift in d_{001} continued very slowly during the next 120 hours and was accompanied by a line breadth and intensity variation as shown in Figures 13 and 14. During desorption, a cooling bath was

provided to condense the water adsorbed on the clay back into the water reservoir. The bath temperature reached an equilibrium condition within one hour after start of the transfer. Although variation of line breadth, intensity, and basal spacing were observed during the first 16 hours, equilibrium conditions were determined after a minimum of 24 hours. At relative pressures between p/p_o = 0.65 and 0.60, there was a sharp basal spacing change from 19 Å to 16 Å. This shift was accompanied by a line breadth increase and then decrease as indicated in dashed line on Figure 13. For the final expansion or initial collapse of highly hydrated calcium montmorillonite there is either a force or strain to be overcome and/or the pores must be sufficiently filled or evacuated.

Barrer and MacLeod (7) studied the sorption of non-polar and polar gases and vapors on montmorillonite. They reported that in theory van der Waals adsorption should take place instantaneously, but that conducting of heat away from the sample causes a slight time lag. Additional slowing down is due to diffusion of vapors between particles of adsorbent, and redistribution of sorbed vapors by evaporation and condensation which proceeds until a uniform distribution of adsorbed material throughout the sample is achieved.

Brunauer (16), Foster (32), and McBain (54) have shown that hysteresis can be expected with porous adsorbents. As can be seen, the adsorption and desorption isotherms fall on

different curves forming a hysteresis loop which closes in the range of $p/p_o = 0$ to $p/p_o = 0.25$. The hysteresis loop indicates more adsorbate during desorption than adsorption at a given pressure. Physical adsorption on the surface of the adsorbent is usually completely reversible, whereas the hysteresis shown by the desorption branch may or may not be reversible. If on repeating the experiment the desorption isotherm is completely reproduced, the desorption hysteresis can be considered as reversible; or it is irreversible if the second investigation gives a different curve. We may note that the hysteresis begins in the region of multimolecular adsorption.

The first explanation for hysteresis was advanced by Zsigmondy in terms of capillary condensation (16, p. 394). He assumed that during adsorption the vapor does not wet the walls of the capillaries in which adsorption takes place. As the adsorption reaches saturation, the impurities are displaced and at saturation complete wetting takes place.

The hysteresis due to trapped gases or adsorbed water molecules should be eliminated or reduced by effective evacuation of the system prior to investigation. However, pore size and distribution probably remain as the chief causes of hysteresis, as explained in following paragraphs.

McBain (54) proposed what is called the "ink bottle" theory of hysteresis. He pointed out that as p/p_o increases,

the condensed adsorbate will occupy the narrowest cross-section and will extend to wider cross-sections only as p/p_o increases. When the vapor is sufficiently close to saturation, the pores will be completely filled. On desorption, no evaporation will occur from filled pores until the relative vapor pressure has fallen to a value sufficient to cause evaporation from the largest orifice or passage leading to the larger enclosed cavity. In this theory, the true equilibrium corresponds to the adsorption points since the important part of the liquid, that contained in the body of the pore, is in equilibrium with the vapor only on the adsorption side but not on the desorption side.

Foster (32) suggested that hysteresis can be explained by the "open pore" theory, and showed that a meniscus should be formed in order that condensation may occur in a capillary. However, this condensation can not take place until there is sufficient liquid present to block the pore at its narrowest point. Initally, the surfaces of capillaries are covered by a strongly adsorbed layer so that the forces tending to form an additional layer are much smaller than those attracting the molecules. As the layer formation proceeds, the capillaries become smaller so that a point is reached where the cohesive forces would be able to produce a greater lowering of equilibrium vapor pressure than the adsorption forces. In the pores that are already blocked at their narrowest point

and in which the meniscus is formed condensation can proceed without delay. During desorption, the adsorbed liquid is bounded by the menisci and the pressure corresponding to the point at which the Kelvin equation is satisfied is that observed during adsorption for a lesser amount of water adsorbed producing a hysteresis.

Barrer and MacLeod (7) have explained hysteresis by stating that the desorption branch is the delay of the development of an adsorbate-poor phase in the interlayer regions caused by strain and interfacial free energy until the pressure of the system has fallen below that for true equilibrium, whereas, for adsorption, the development of an adsorbate-rich phase in the interlayer regions is delayed due to strain and interfacial tensions and the pressure exceeds the value for true equilibrium between the vapor and separated montmorillonite layers with or without interlayer adsorbate.

Hirst (40) has shown that the forces tending to hold platelets together also prevents penetration of the adsorbate. Interlayer adsorbate can only enter after a sufficient pressure is reached which would overcome the attractive forces and allow penetration. As the solid swells on adsorption, the free energy lowering of the solid may not be equated to the free surface energy since some energy will be used as work of expansion. As the interlayer attraction is reduced by the expansion, less energy is necessary to expand the unit

for additional penetration of vapor. He further points out that when capillary condensation occurs, pores tend to shrink. As a result, on desorption when the vapor pressure is lowered slightly, liquid will remain in the tube. When the platelets are fully expanded, the forces of attraction are weakened and the forces tending to keep them apart are high. Collapse of the structure will proceed only after the amount of interlayer adsorbate and swelling pressures are reduced. Brunauer (16) points out that even though adsorbents are usually regarded as rigid bodies, the adsorption process causes a change in pore volume, shape, and a rearrangement of the surface of the sample.

The plots in Figures 23 and 24 tend to produce a completely reproducible isotherm up to p/p_o 0.20, after which a well defined hysteresis is observed. This is consistent with the studies conducted by Bering et al. (10) on bentonite using hydrocarbons as well as water vapor. Demirel (26) and Roderick (70) observed that the adsorption branch of the homoionic bentonites investigated gave better reproducibility, and they chose the adsorption branch as the true equilibrium curve. Mooney et al. (60) observed that during their water vapor montmorillonite studies, the adsorption isotherm was not reproducible, and they apparently used the initial water content at which the adsorption was begun. The desorption isotherm had a hysteresis which was reproducible, and because of

the irreversibility of hysteresis and the close reproducibility of the desorption curves, they chose the desorption curves as the true equilibrium curves.

Adsorption models

According to Martin (57), the adsorption of water vapor on montmorillonite is a very complex process and it is very difficult to properly ascribe the phenomena to one single model of adsorption such as the Langmuir model or the multimolecular adsorption model for the entire range. It can be seen that the repeated cycles do not give a straight line for the Langmuir model, indicating that equation 1 is not obeyed. The isotherm was therefore subdivided into a number of straight line portions to determine if in the region between p/p_o equal to 0.0 to 0.28 any substantial information could be obtained concerning unimolecular adsorption. Brunauer (16) has pointed out that a similar technique was applied to the adsorption of chlorine by silica gel, and attributed straight line relationships for the various sections to adsorption on fractions of the surface that had roughly the same heat of adsorption. The sample under investigation had a crystalline surface, and one should expect several surface types corresponding to the different developed crystal faces.

The subdivision of straight lines gives rise to a discontinuous distribution of heat of adsorption values. Various

experimental straight lines were evaluated considering that the X-ray studies indicate one complete expansion in the region of p/p_o from 0.09 to 0.22.

Van Olphen (79) conducted water vapor experiments on a sodium vermiculite to give clues for the interpretation of the intercrystalline swelling of montmorillonite. He determined that the second monomolecular layer of water entered only after the first layer was completed, and his isotherms showed a definite stepwise trend. Van Olphen's Langmuir plot gave linear relations, and "one layer" and "two layer" Langmuir plots were defined from the data. However, plots for the present investigation, Figures 25 and 26, indicate that for Wyoming calcium bentonite, the Langmuir treatment does not give reasonable results.

The BET multimolecular adsorption model gives a reasonably straight line in the region of p/p_o from 0.11 to 0.27. The region normally expected for the multimolecular adsorption model to be obeyed is between $p/p_o = 0.05$ to $p/p_o = 0.35$. Roderick (70), studying sodium bentonite, used the BET function $\frac{p/p_o}{q(1-p/p_o)}$ to determine the multimolecular adsorption on external surfaces in the ranges of relative pressures normally expected.

Hendricks et al. (39) conducted isotherm and X-ray diffraction studies on various treated montmorillonites; their BET parameters are tabulated in Table 13.

Figure 25. Langmuir plot for the adsorption of water vapor on calcium montmorillonite, first cycle

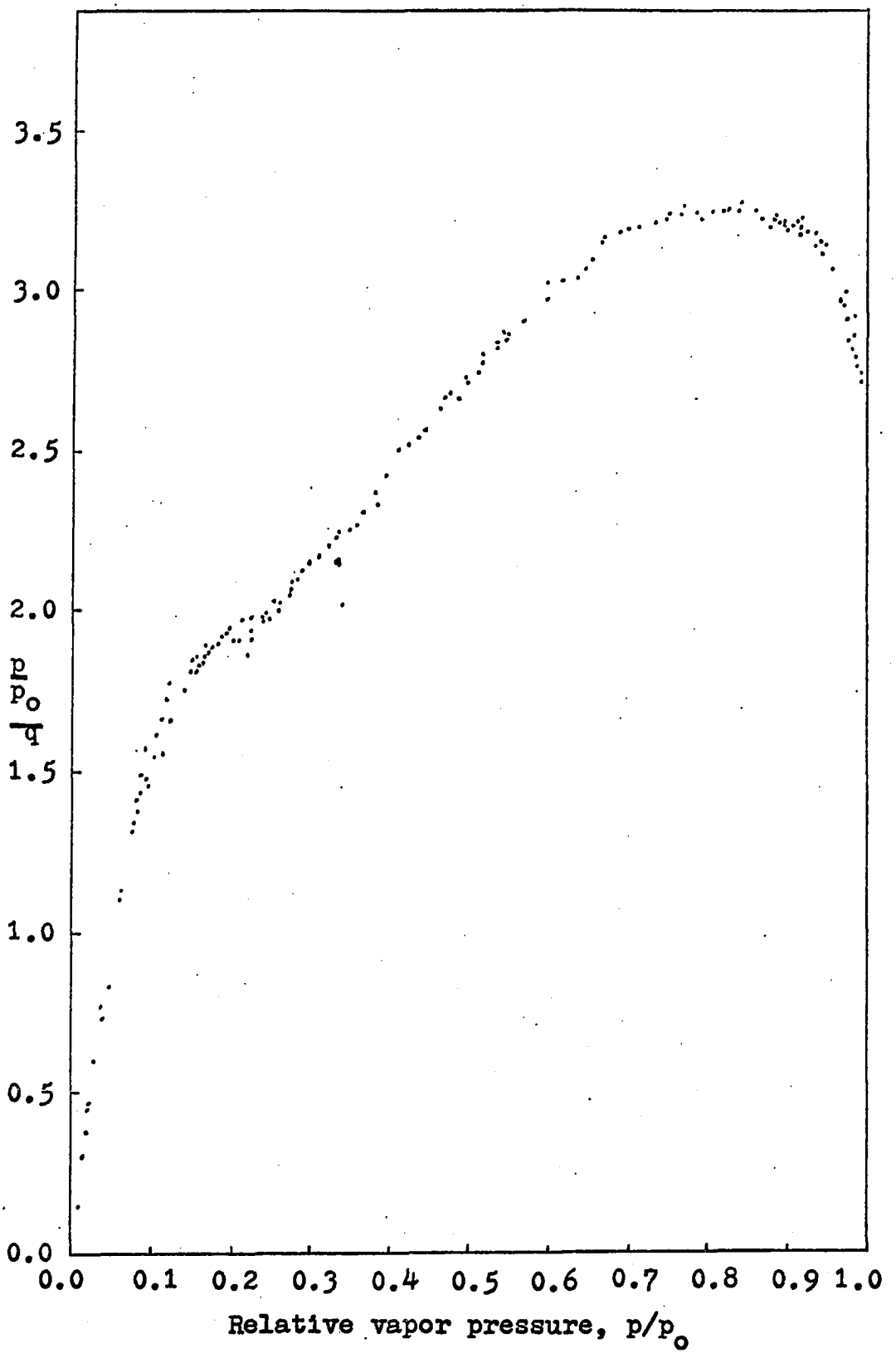
3.5
3.0
2.5
2.0
1.5
1.0
0.5
0.0
p/p_o q
0.0 0.1 0.2 0.3 0.4 0.5 0.6 0.7 0.8 0.9 1.0
Relative vapor pressure, p/p_o

Figure 26. Langmuir plot for the adsorption of water vapor on calcium montmorillonite, second cycle

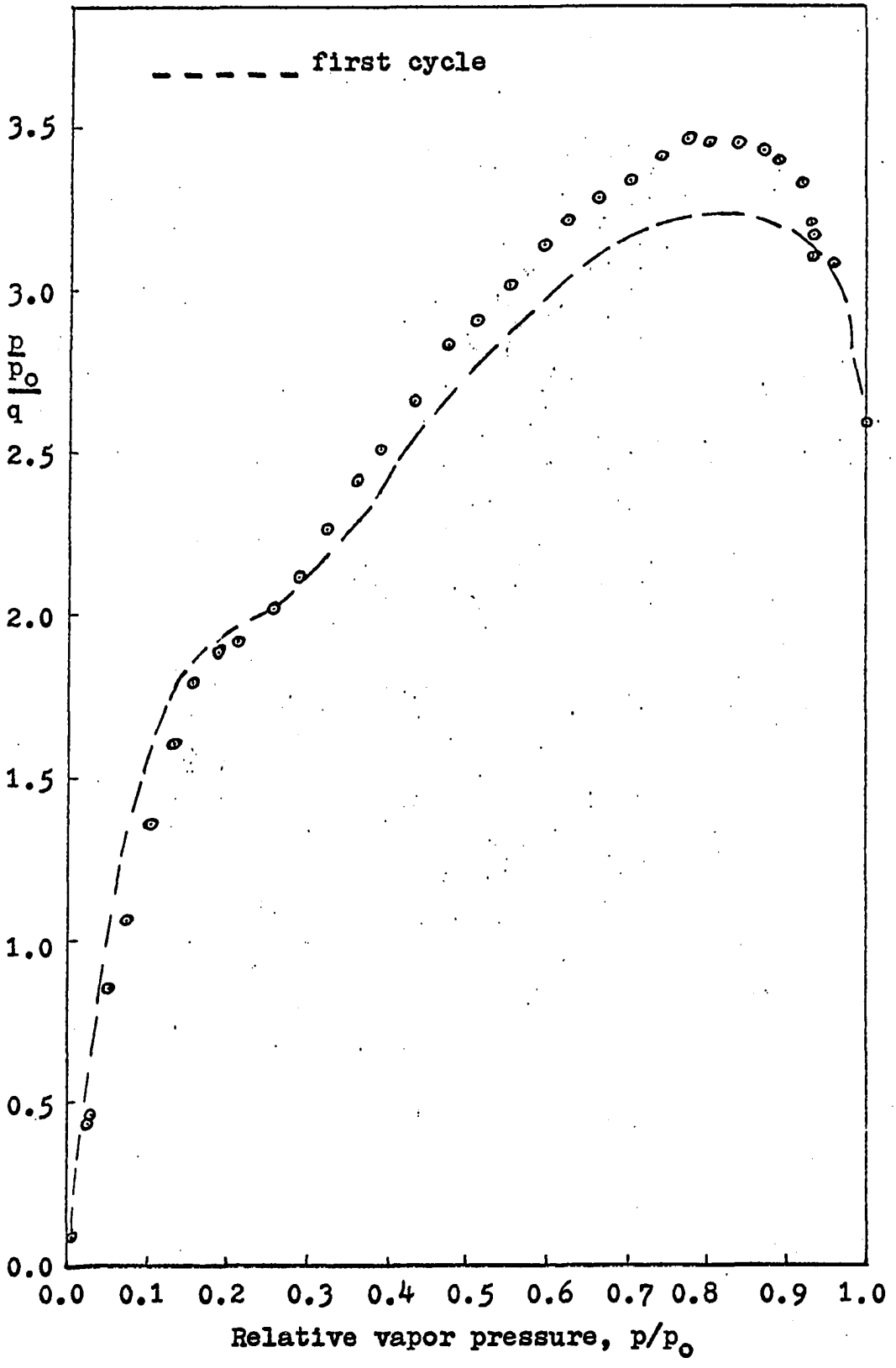
first cycle
3.5
3.0
p/p_o q
2.5
2.0
1.5
1.0
0.5
0.0
0.0 0.1 0.2 0.3 0.4 0.5 0.6 0.7 0.8 0.9 1.0
Relative vapor pressure, p/p_o

Table 13. The BET parameters q_m and C calculated from data for various montmorillonites reported in literature[a]

Mineral	q_m	C
Cesium Mississippi montmorillonite	0.052	19
Potassium Mississippi montmorillonite	0.059	7
Sodium Mississippi montmorillonite	0.070	8
Lithium Mississippi montmorillonite	0.101	26
Hydrogen Mississippi montmorillonite	0.129	10
Magnesium Mississippi montmorillonite	0.138	29
Calcium Mississippi montmorillonite	0.130	23
Strontium Mississippi montmorillonite	0.133	11
Barium Mississippi montmorillonite	0.090	22
Sodium Wyoming montmorillonite	0.023	13
Calcium Wyoming montmorillonite	0.125	6
Sodium California montmorillonite	0.091	8
Calcium California montmorillonite	0.133	15

[a]Data obtained from Demirel (26, Figures 23, 24 and 25).

Demirel (26) has shown that the BET method may be utilized in the relative pressure range from 0.1 to 0.3 for calcium montmorillonite. The values of the parameters he obtained were $q_m = 0.130 \pm 0.005$ gm and $C = 6.68 \pm 0.77$. He points out

that by using the data obtained by the BET method, the cross sectional area for a water molecule adsorbed on the clay mineral can vary between 16.3 Å and 17.9 Å. These cross sectional areas were comparable with the geometric arrangement of water molecules in an ice-like structure.

As previously mentioned, the BET plots in Figures 27 and 28 give reasonably good straight lines within the range of applications from 0.11 to 0.27 relative pressures. The parameters q_m and C were calculated by a least square treatment of all the experimental data for both cycles. In order to estimate the accuracy of the values in the equation, the method proposed by Topping (76, p. 105) was used. The equation of the line obtained is:

$$y = (6.523 \pm 0.0625)x + (1.682 \pm 0.0120)$$

When the slope of the line and the intercept are known, equation 3 enables one to determine q_m and C. The values of these parameters are 0.1219 gm and 4.878 respectively. The errors in q_m and C were calculated from the principle of superposition of errors with the relationship (76, p. 20):

$$\delta Q^2 = \left[\frac{\partial Q}{\partial x} \times e_1\right]^2 + \left[\frac{\partial Q}{\partial y} \times e_2\right]^2$$

where δQ is the square root of the sum of the squares of the greatest errors due to an error in each variable separately, and e_1 and e_2 are the errors in the slope and the intercept respectively. The values of q_m and C corrected for the errors

Figure 27. BET plots for the adsorption of water vapor on calcium montmorillonite, first cycle

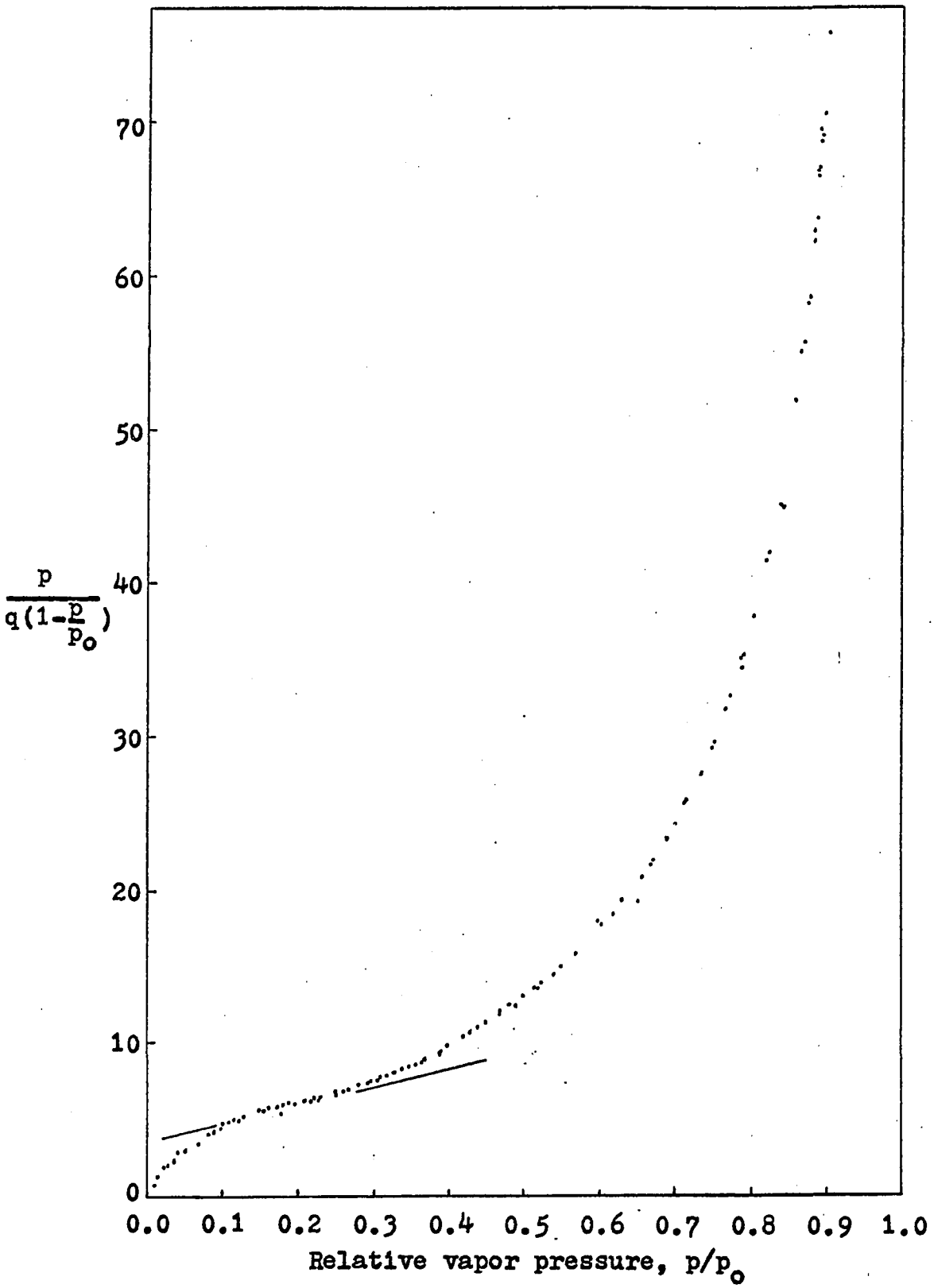
70
60
50
40
30
20
10
0
$\frac{p}{q(1-\frac{p}{p_o})}$
0.0 0.1 0.2 0.3 0.4 0.5 0.6 0.7 0.8 0.9 1.0
Relative vapor pressure, p/p_o

Figure 28. BET plots for the adsorption of water vapor on calcium montmorillonite, second cycle

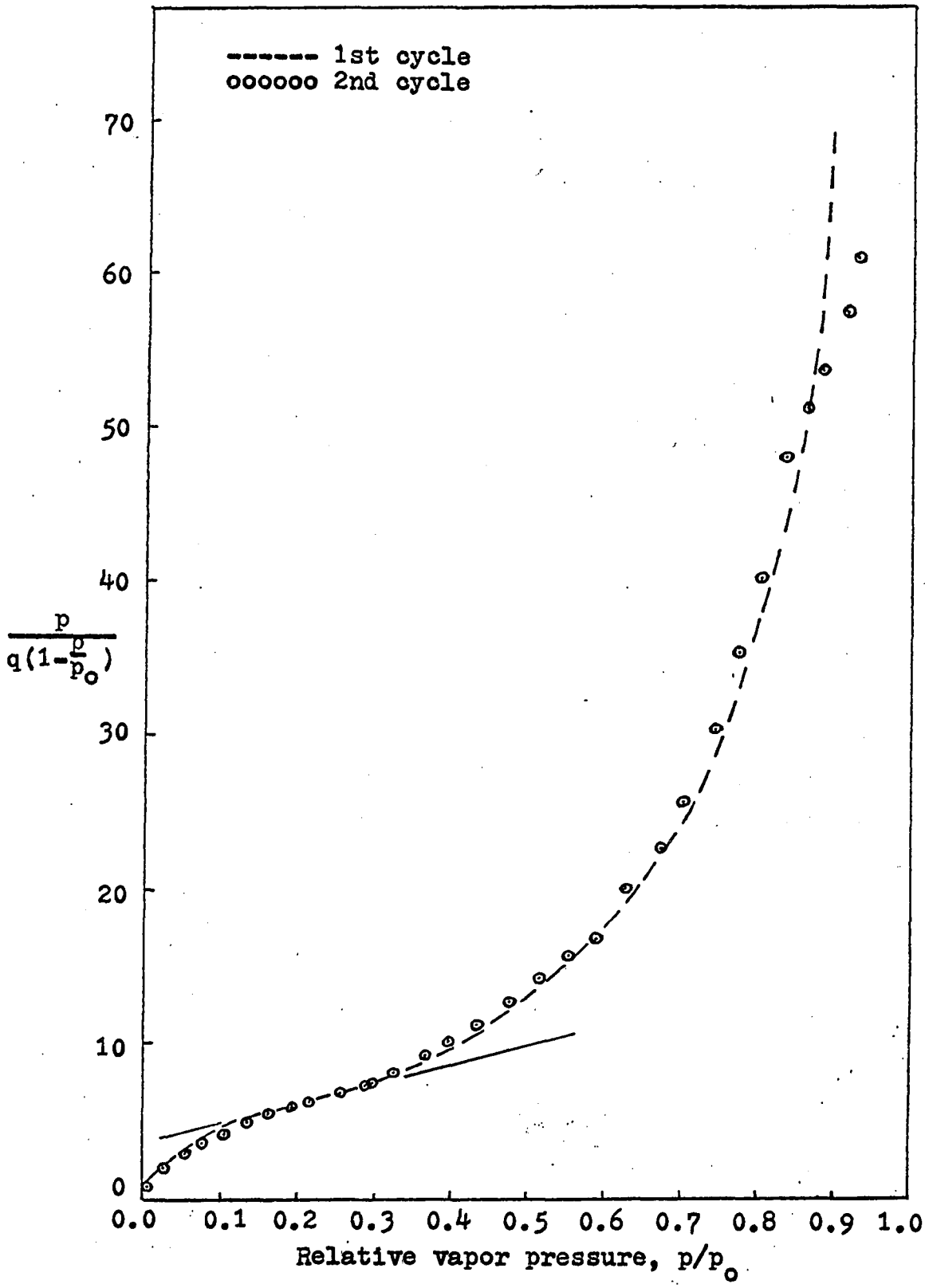
------ 1st cycle
oooooo 2nd cycle
70
60
50
40
30
20
10
0
$\frac{p}{q(1-\frac{p}{p_o})}$
0.0
0.1
0.2
0.3
0.4
0.5
0.6
0.7
0.8
0.9
1.0
Relative vapor pressure, p/p_o

noted above are 0.1219 ± 0.0009 gm and 4.878 ± 0.042, respectively. The data show very little error from a straight line determined by the least squares method for the BET data; departures from the straight line after p/p_o of 0.27 are probably somewhat complicated by capillary condensation, although of a minimal nature at this low range of p/p_o.

The X-ray data indicate that initial separation of the platelets starts almost immediately as the relative pressure increases from zero. However, from p/p_o of 0.00 to 0.02 there is very little increase in spacing, indicating perhaps initial adsorption on the external surfaces. After 0.02, the spacing starts to increase rapidly with an increase in pressure, indicating that the preponderance of water adsorbed is interlayer water.

Of interest is the comparison of the q_m values of the straight lines between 0.00 and 0.08 relative vapor pressure given by the slopes plotted according to both the BET and Langmuir methods. These are tabulated in Table 14. Both of the methods agree reasonably well for adsorption of the first monomolecular layer. However, after a p/p_o of 0.08, the values of the parameters vary considerably, supporting a multimolecular adsorption.

The problem of external area coverage as applied to the montmorillonite system might better be termed the areas accessible to polar and non-polar gases and vapors. As pointed

Table 14. The q_m values for calcium montmorillonite, determined by Langmuir and BET methods

p/p_o range	Langmuir		BET	
	1st cycle	2nd cycle	1st cycle	2nd cycle
0.00 - 0.02	0.0259	0.0281	0.0294	0.0344
0.02 - 0.08	0.066	0.058	0.0526	0.0629
0.05 - 0.18[a]			0.023[a]	0.027[a]

[a]Roderick (70) for sodium montmorillonite

out previously, nitrogen is adsorbed only on external surfaces. If a single non-swelling platelet is considered, then the area available to nitrogen and water vapor would be the same as indicated in Figure 29a. On the other hand, if the system is constituted of a porous swelling powder, as is the system under investigation, then the area available to water might be considerably greater than that available to nitrogen, as in Figure 29b. The smaller water molecules perhaps can either be accomodated in narrower intercrystalline channels or can penetrate into tapered channels that are unaccessible to nitrogen molecules. By using the Kelvin equation, one can see that as the relative pressure increases, the capillary radius available to a molecule for capillary condensation increases. Therefore, the following situation may occur with respect to montmorillonite powders.

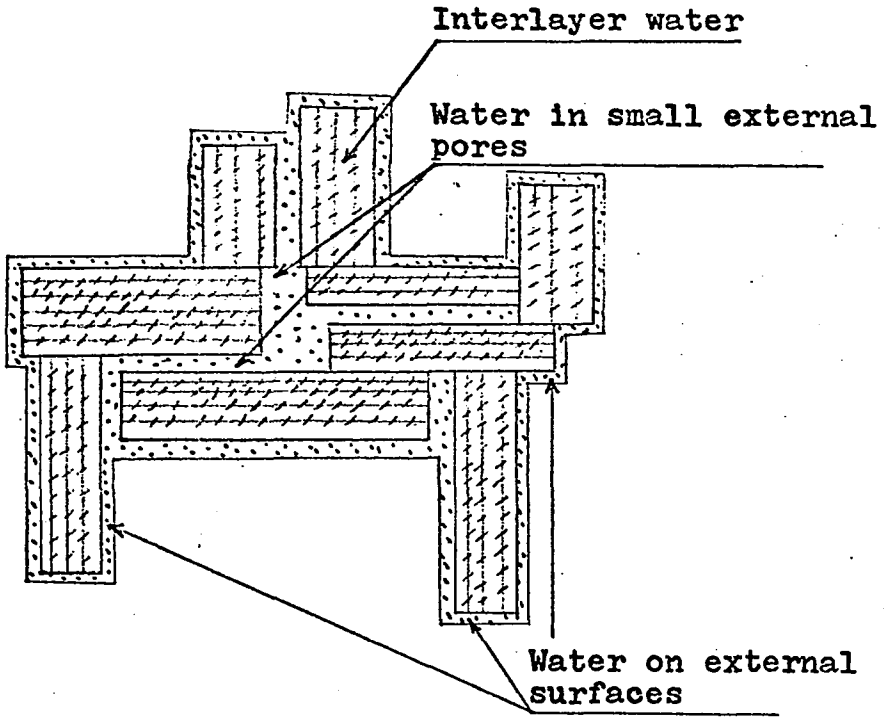

Figure 29a. Idealized diagram of possible areas accessible to water

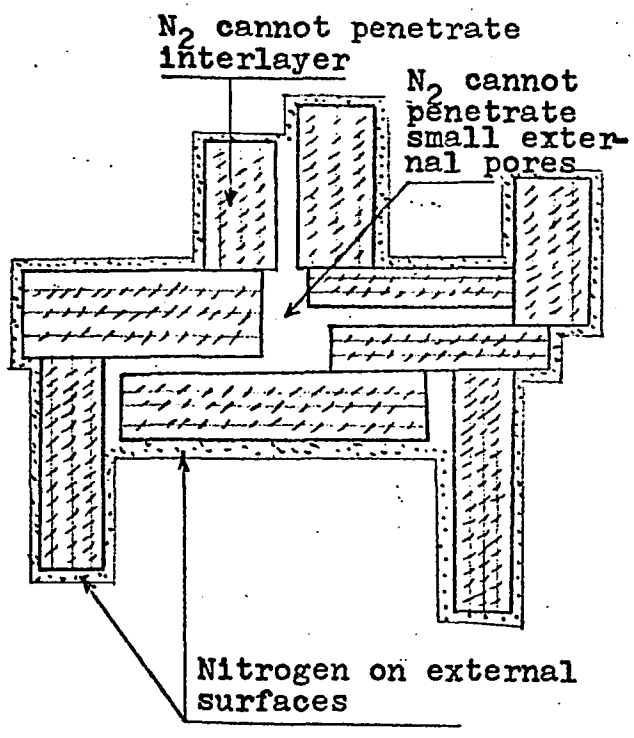

Figure 29b. Idealized diagram of possible areas accessible to nitrogen

In Figures 29a and 29b, the pore spaces between the platelets act as capillaries and are accessible to water molecules when the diameter of the pore spaces is such as to allow the passage of a water molecule with diameter of 2.76 Å. The water will penetrate between platelets as well as external areas, and the area available to water would be the total external area as well as the internal area of the agglomerate of platelets. In the case of nitrogen adsorption, when the pore spaces are too small in diameter to pass the 4.5 Å nominal diameter nitrogen molecule, the areas within the platelets agglomerate would not be accessible to the molecule. Therefore, the area associated with the nitrogen would be the external area of the agglomerate only. Roderick (70) found that the montmorillonite area determined by water adsorption varied from 83 to 145 m^2/gm to 172 m^2/gm. Both the values of Roderick and those in his study are considerably larger than those reported by others as determined from nitrogen adsorption, i.e. 41 to 71 m^2/gm by Emmett (29) 33 m^2/gm by Mooney et al. (61), and 34.5 m^2/gm by Zettlemoyer et al. (82).

Heat of adsorption

Brunauer (16) points out that the criteria of the application of the BET theory was based on the reasonableness of the two parameters q_m and C evaluated from the straight lines. The average heat of adsorption less the heat of liquification

Table 15. Average heat of adsorption of monomolecular water adsorbed on calcium montmorillonite, calculated from BET parameters listed

Mineral	BET parameters q_m	C	Average heat of adsorption less heat of liquification E_1-E_L, Kcal/mole	
			According to Brunauer (16)	Corrected according to Clampitt and German (23)
Hendricks et al. (33)[a]				
Mississippi Ca-montmorillonite	0.130	23	1.9	3.6
California Ca-montmorillonite	0.133	15	1.6	3.3
Wyoming Ca-montmorillonite	0.125	6	1.1	2.9
Demirel (26)				
Wyoming Ca-montmorillonite	0.130	6.7	1.1	2.8
Wyoming Ca-montmorillonite[b]	0.1219	4.878	0.94	2.6

[a]BET parameters calculated by Demirel (26, Figures 24 and 25).

[b]BET parameters calculated by data in this study.

of the first observed monomolecular layer was calculated by using equation 5 to obtain:

$$E_1 - E_L = R\ T\ \ln\ C = 1.987 \times 298.16 \times \ln\ C \text{ cal/mole}$$

However, as pointed out previously, this value for the heat of adsorption required a correction when C was rederived by Clampitt and German (23). By using their correction the equation for calculation of E_1 becomes:

$$E_1 - E_L = R\ T\ \ln\ C + (\Delta H_s - E_L)$$

where $(\Delta H_s - E_L)$ is equal to 1.7 Kcal/mole. Both corrected and uncorrected values are listed in Table 15 for several calcium montmorillonites for which water vapor adsorption data are available, and show reasonably good uniformity.

Roderick (70), studying a Wyoming sodium montmorillonite, determined values of 1.0 and 2.7 for $E_1 - E_L$ uncorrected and corrected for Clampitt and German, respectively. Takizawa (74) obtained an uncorrected value for $E_1 - E_L$ of 0.84 Kcal/mole using Niigata bentonite tested at 25° C. He further showed the effect of temperature by obtaining $E_1 - E_L = 1.430$ Kcal/mole at 15° C, and $E_1 - E_L = 0.410$ Kcal/mole at 35° C. Zettlemoyer *et al.* (82) used heat of immersion and adsorption isotherm data to determine heats of adsorption or desorption of water from bentonite at 25° C, and show good agreement with the adsorption branch of Takizawa. This may indicate that the adsorption branch is nearer the true equilibrium curve than is the desorption isotherm.

Free energy changes

The values of the function $\frac{q}{p/p_o}$ versus p/p_o used to determine the free energy changes are plotted in Figures 30 and 31 for the first and second adsorption cycles respectively. Demirel (26) and Roderick (70) used similar plots to determine the free energy of wetting in their studies of montmorillonites. The data of Demirel (26) are plotted on Figure 30 for comparison of shape and values. In general, the shapes of the curves are similar and the values of the function vary due to the amount of water vapor adsorbed at similar values of relative vapor pressures. The differences most probably are due to method of preparation of the sample; Demirel's sample was a loose powder, while the sample in this investigation was a compressed powder.

The second adsorption cycle agrees with the first cycle up to approximately $p/p_o = 0.3$. From $p/p_o = 0.3$ to 0.9, the first cycles points were from 0-12 mg/gm higher than the second cycle. Between $p/p_o = 0.9$ and saturation, the second cycle points passed through the curve of the first cycle. Slight changes in the pore size and shapes would cause this difference. However, since the second adsorption points agree with the first cycle in the low pressure region and very nearly agree up to $p/p_o = 0.40$, any slight swelling of the pores or material after the first cycle would not materially change the calculated free energy of wetting because the low

Figure 30. Plot for graphical integration of equation 12 for the adsorption of water vapor on calcium montmorillonite, first cycle

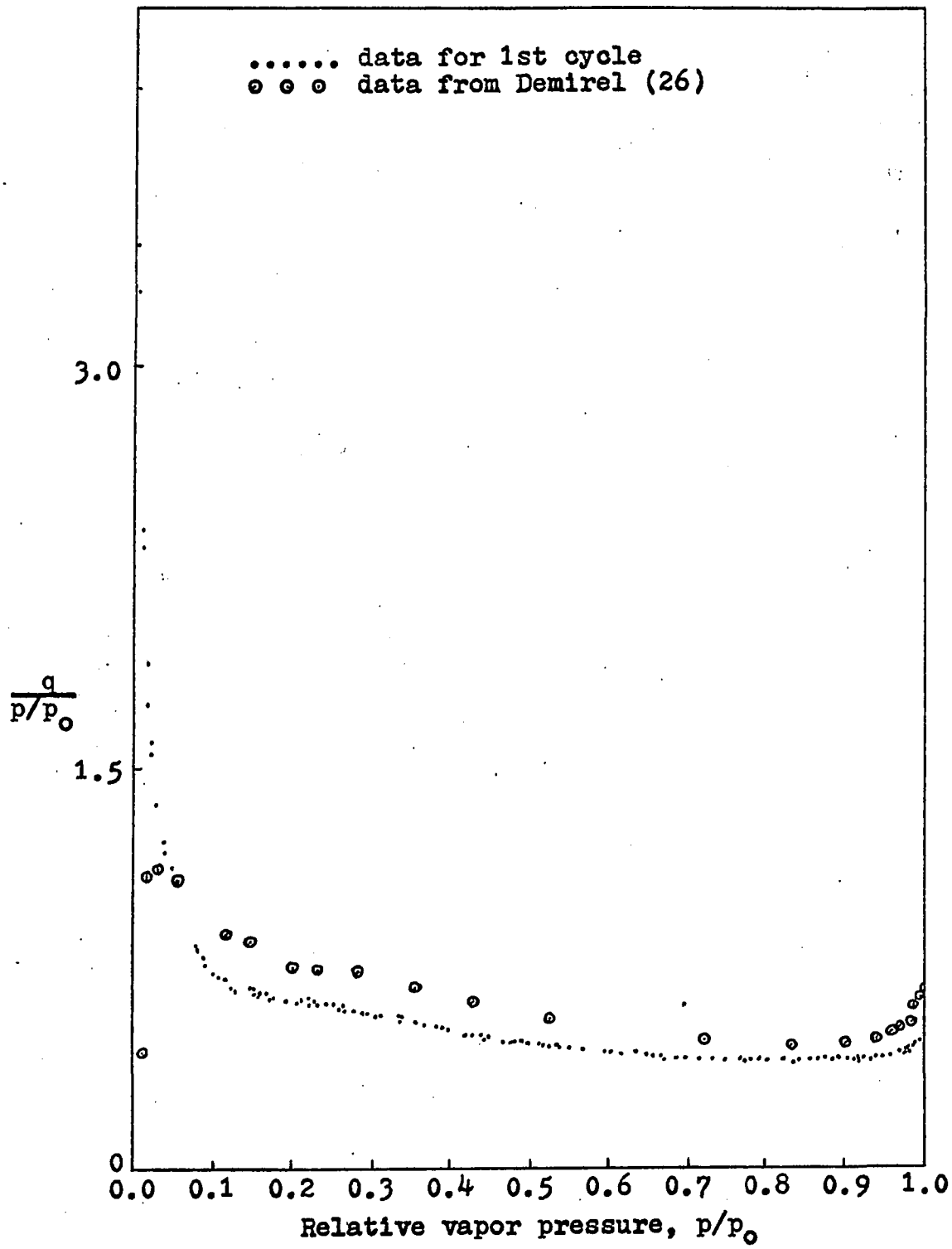
..... data for 1st cycle
o o o data from Demirel (26)
3.0
1.5
0
q / p/p_o
0.0 0.1 0.2 0.3 0.4 0.5 0.6 0.7 0.8 0.9 1.0
Relative vapor pressure, p/p_o

Figure 31. Plot for the graphical integration of equation 12 for the adsorption of water vapor on calcium montmorillonite, second cycle

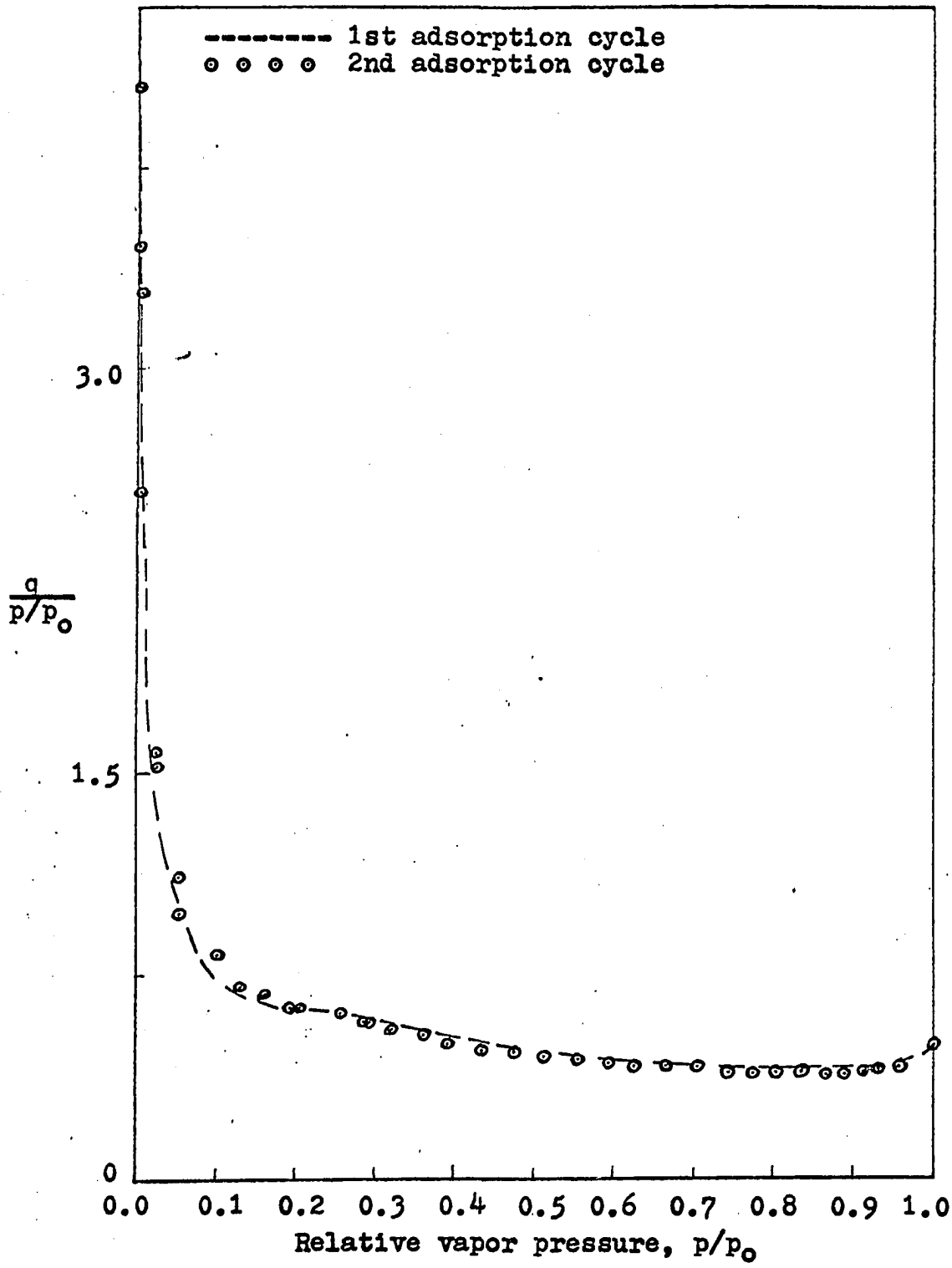
1st adsorption cycle
2nd adsorption cycle
3.0
1.5
0
$\frac{q}{p/p_o}$
0.0 0.1 0.2 0.3 0.4 0.5 0.6 0.7 0.8 0.9 1.0
Relative vapor pressure, p/p_o

pressure data are of the most importance in the energy change calculations. The free energy of wetting may be expressed by Demirel's equation:

$$\Delta F = (\gamma sl - \gamma so) \not\propto \Delta V$$

for the system investigated. But as can be seen, there are three unknowns $(\gamma sl - \gamma so)$, $\propto$, and ΔV. The values of $\propto$, the interstitial area, may be determined from the external area and total crystallographic area of the mineral and the known cross sectional area of the adsorbed molecule. However, $(\gamma sl - \gamma so)$ and ΔV can only be determined by: a) solving simultaneous equations available from experiments on two samples having different known values of $\propto$, b) by determining the value of one of the unknowns independently, or c) by determining another independent relationship between $(\gamma sl - \gamma so)$ and ΔV. Roderick (70) points out that the large error in determination of the specific surfaces by the BET method would tend to rule out the solution of the unknowns by simultaneous equations, and up to the present time the other alternatives have not been possible.

The free energies of wetting were actually calculated by using equation 12 and a graphical integration of the curves presented in Figures 30 and 31. The errors in the function were estimated to be ± 0.013 and ± 0.015 for the first and second adsorption cycles respectively. The numerical values for the integral $\int \frac{q}{p/p_o} d\left(\frac{p}{p_o}\right)$ were found to be 0.3858 and

0.3844 ± 0.015 gm/gm of calcium montmorillonite respectively for the first and second adsorption, cycles, respectively. The specific surface Σ, for equation 12 was determined from crystallographic data (77) for calcium montmorillonite by the relationship:

$$\Sigma = \frac{N_A \sigma}{M_{ca}} \qquad (20)$$

where N_A is Avogadro's constant, M_{ca} is the weight of the calcium montmorillonite unit cell, and σ is the area exposed by one unit cell layer. M_{ca} is equal to 732. The value of may be determined from the unit cell dimensions $a_o = 5.16$ Å and $b_o = 8.94$ Å. Substituting these values in the expression above, Σ, the specific area is found to be:

$$\Sigma = \frac{6.02 \times 10^{23} \times 2 \times 5.16 \times 8.94}{732 \times 10^{10}}$$

$$\Sigma = 759 \text{ m}^2/\text{gm}$$

Using the value of the parameter q_m obtained in the BET solution, the specific surface was also calculated using equation 9. Substituting the values of $q_m = 0.1219$ and $s = 17.5$ Å^2/molecule of water vapor in equation 9 the specific surface was found to be:

$$\Sigma = \frac{N_A \, q_m \, s}{M}$$

$$\Sigma = \frac{6.02 \times 10^{23} \times 0.1219 \times 17.5}{18.02 \times 10^{10}}$$

$$\Sigma = 714 \text{ m}^2/\text{gm}$$

The value obtained by using the BET parameter is a reasonable value and compares very well with the theoretical crystallographic data. When Σ obtained from equation 20 above is substituted in the equation, the free energy of immersion in saturated vapor or liquid, also referred to as the free energy of wetting, is calculated as follows:

$$\Delta F = -\frac{RT}{M\Sigma}\, 0.3858$$

$$= -\frac{8.314 \times 10^7 \times 298.16}{18.02 \times 759 \times 10^4} \times 0.3858$$

$$= 69.91 \pm 2.36 \text{ ergs/cm}^2$$

$$\Delta F = -\frac{RT}{M\Sigma}\, 0.3844$$

$$= -\frac{8.314 \times 10^7 \times 298.16}{18.02 \times 759 \times 10^4} \times 0.3844$$

$$= 69.66 \pm 2.72 \text{ ergs/cm}^2$$

Demirel (26) reported a value of 76.61 ± 4.30 ergs/cm^2 for calcium montmorillonite. He used a loose powder in his study, yet the values obtained in both studies are in very good agreement. Craig et al. (22) found similar results in their studies of compressed and uncompressed graphite powders, pointing out the importance of accurate low pressure range data.

Expansion energies

As pointed out in equation 3, the free energy change of

adsorption may be expressed as:

$$\Delta F = -\frac{RT}{M\Sigma} \int_{o}^{p/p_o} \frac{q}{p/p_o} d(p/p_o)$$

Fu and Bartell (33), studying the surface areas of porous absorbents, evaluated this equation and found that the change in free energy could be expressed by the relationship:

$$\Sigma \Delta F = \alpha (p/p_o)^{\beta}$$

where ΔF is the decrease in the free energy per unit area, α and β are constants, p/p_o is the relative vapor pressure, and Σ is the area on which the adsorption takes place. They point out that this method can be utilized to study the expansion and deformation of porous materials caused by adsorption of various vapors (33, 674). For a given adsorbate-adsorbent system, α and β remain constant so long as there is no change in the mechanism of adsorption. If changes in the mechanism of adsorption, such as capillary condensation or swelling occur, values of α and β change to another set of constant values. If only the external surface areas of the clay are involved in adsorption of the vapor, the relationship can be made to read:

$$\Sigma_{ext} \Delta F = \alpha (p/p_o)^{\beta}$$

The change in slope of the $\Sigma \Delta F$ curve, observed by Fu and Bartell (33) was attributed to capillary condensation in the pores of the adsorbents. The exact point at which capillary condensation takes place can not be determined, but it

may be assumed to show its most pronounced effects at p/p_o values greater than 0.9 to saturation. For clay minerals, while capillary condensation undoubtedly has some effect, swelling (interlayer expansion) manifests itself more profoundly throughout the entire adsorption range.

The values of the integral $-\frac{RT}{M}\int_{o}^{p/p_o=1} \frac{q}{p/p_o}\, d(p/p_o)$ for increasing values of p/p_o from zero to saturation for the second adsorption were plotted on log-log paper with $\Sigma\Delta F$ on the vertical axis and p/p_o on the horizontal axis, Figure 32. A close examination of the plot indicates six straight line portions, the breaks occurring at $p/p_o = 0.065$, $p/p_o = 0.19$, $p/p_o = 0.85$, and $p/p_o = 0.98$. From the X-ray data, the initial adsorption at low relative pressures from zero to approximately 0.02 occurs on the external surface areas. Therefore, the straight line portion of the log-log plot corresponding to a p/p_o range of 0-0.02, Figure 32, was extrapolated to saturation as indicated by a dashed line assuming that the free energy relationship of Fu and Bartell (33) was obeyed. The differences between the extrapolated curve and the plot $\Sigma\Delta F$ is the free energy change of internal surfaces (expansion energy). This relationship may be expressed as:

$$\Sigma_{int}\,\Delta F_i = \Sigma\Delta F - \Sigma_{ext}\,\Delta F_e$$

where Σ_{ext} is the external surface area, Σ_{int} is the internal surface area, Σ is the specific surface area, and ΔF_i is the expansion energy per cm^2 of internal surface. ΔF_i may be ex-

Figure 32. Log-log plot of the free energy change versus relative vapor pressure, first cycle

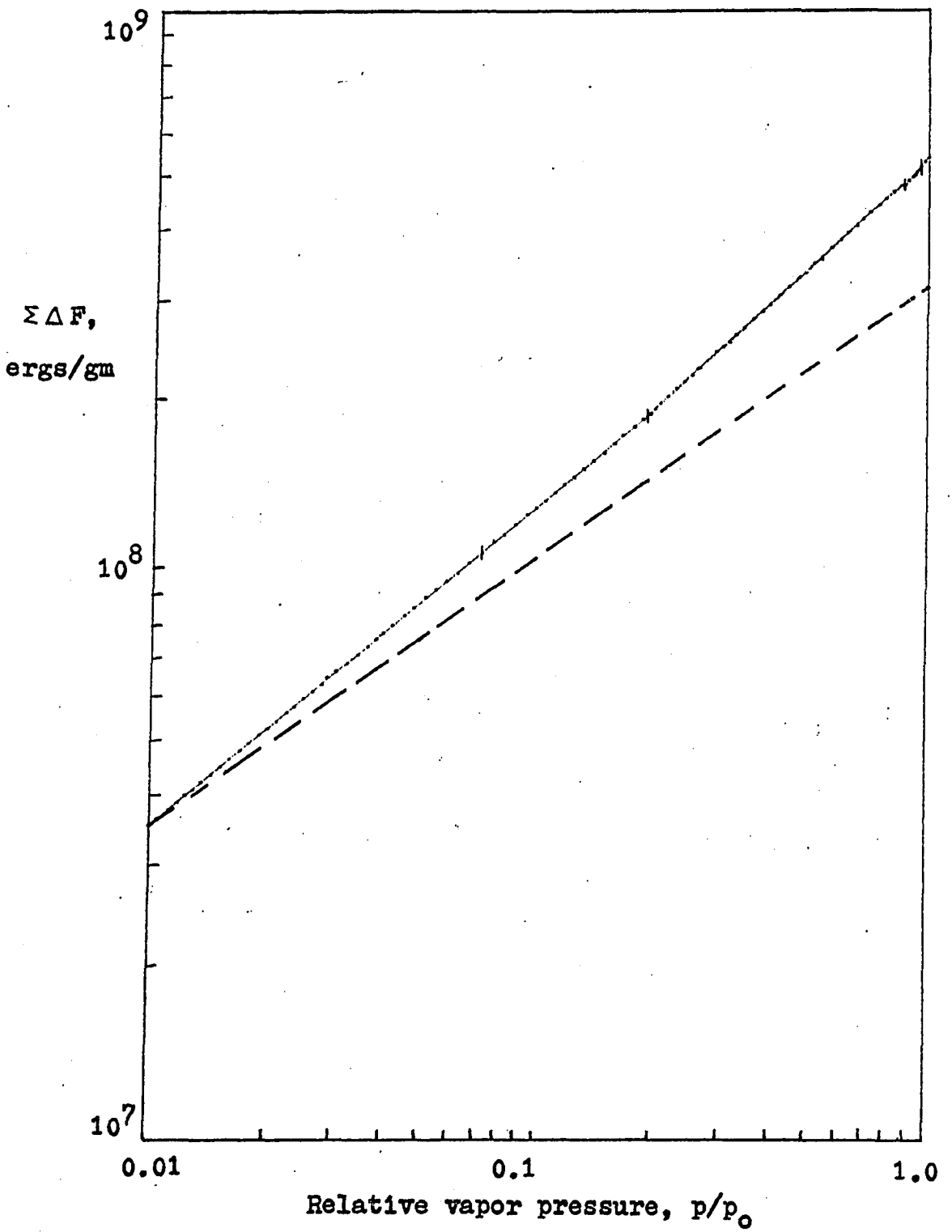
10^9
$\Sigma \Delta F$,
ergs/gm
10^8
10^7
0.01
0.1
1.0
Relative vapor pressure, p/p_o

pressed in terms of equation as follows:

$$\Delta F_i = (\gamma_{S1} - \gamma_{So}) + \Delta V$$

where ΔV is the free energy change per cm^2 of internal surface due to the separation of the particles against the force of interaction.

ΔF_i can be calculated by the expression:

$$\Delta F_i = \frac{\Sigma \Delta F - \Sigma_{ext} \Delta F_e}{\Sigma_{int}} \qquad (21)$$

and may be obtained from Figure 32 as the difference between the plot of $\Sigma \Delta F$ and the dashed line extended to saturation, indicating the change in free energy due to adsorption on external surfaces.

Figure 33 presents a plot of $\Sigma_{int} \Delta F_i$ versus platelet separation h for the second adsorption cycle. It can be seen that the changes in slope of the free energy change with increasing relative vapor pressure, Figure 32, correspond in general to variations in d_{001} spacing at increasing relative vapor pressure, Figure 13. Figure 33 can be conveniently divided into four major segments as follows: segment I from 0-2.6 Å, segment II from 2.6 Å to 5.1 Å, segment III from 5.1 Å to 6.2 Å, and segment IV from 6.2 Å to 9.1 Å. The free energy change in segments I and II is about equal. The free energy change for segment III is substantially greater than a combination of the three other segments.

The expansion energy of the first segment is the free

Figure 33. Plot of free energy change due to adsorption on and separation of internal surfaces versus interlayer separation, second adsorption cycle

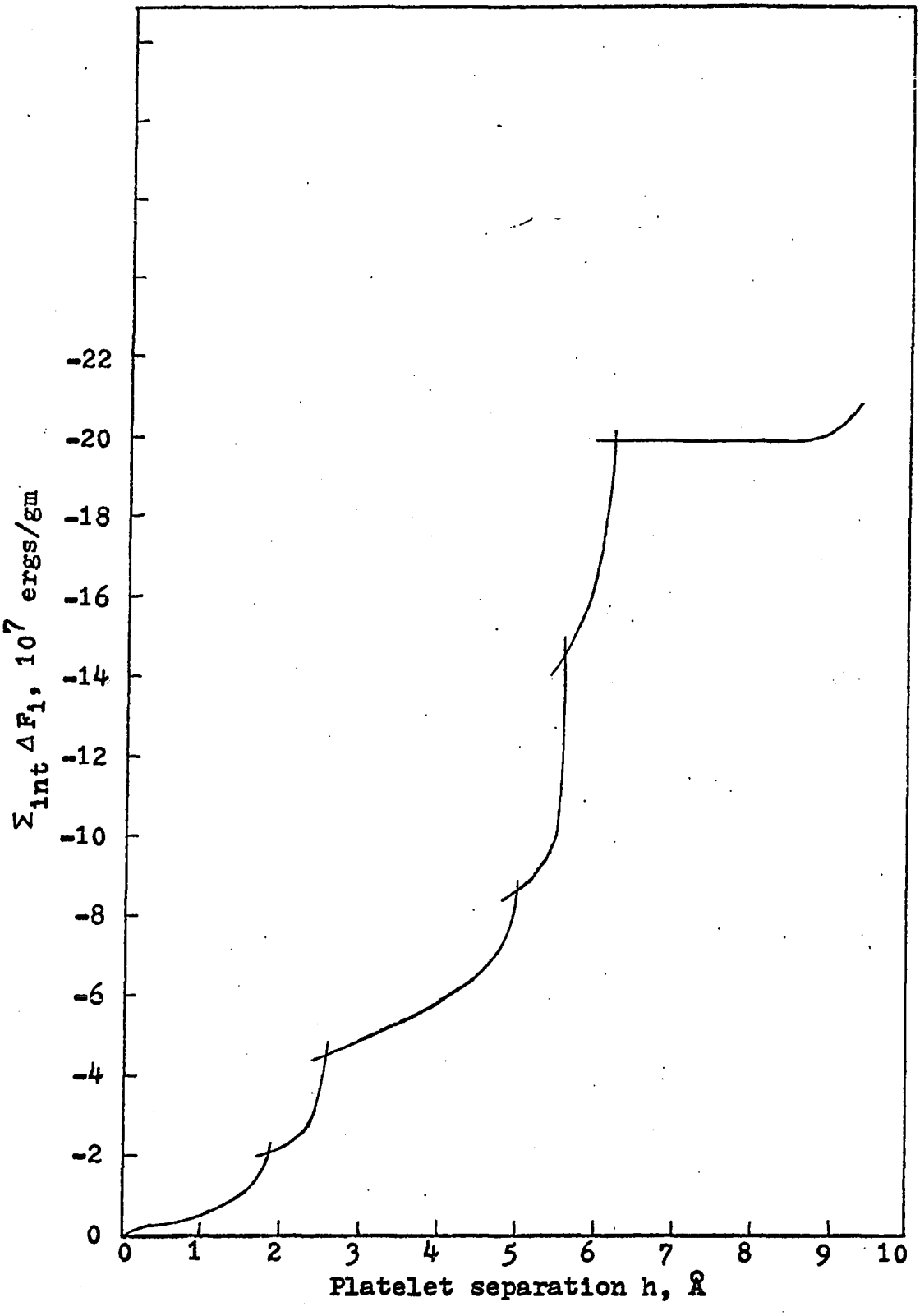
-22
-20
-18
-16
-14
-12
-10
-8
-6
-4
-2
0
$\Sigma_{int} \Delta F_1$, 10^7 ergs/gm
0
1
2
3
4
5
6
7
8
9
10
Platelet separation h, Å

energy change which includes the disappearance of the solid surface forming a solid-adsorbed film interface, and the partial hydration of the adsorbed cation plus the contribution due to separation against the force of interaction between platelets. This latter term will decrease the magnitude of the free energy change. As the adsorption continues (segment II), the second layer of water penetrates between the first layer and the surface, and the free energy change is due to the extension of the film thickness and is probably less than that for disappearance of the solid surfaces and formation of a solid-adsorbed film interface. However, since the distance between the platelets is greater than that corresponding to the previous step, the interaction between platelets is decreased. In segment III, additional vapor is adsorbed in the interlayer region, further slightly reducing the interaction forces. In this segment, the free energy change is quite large because of the arrangement of the water molecules covering the active sites. No new surfaces appear or disappear. The free energy on adsorption for the final expansion, segment IV, is due to penetration of additional water molecules between the layers. The forces of interaction between the platelets being reduced as the platelets are relatively far removed from each other.

Since the free energy change for segment IV is the smallest of any of the segments, the energy for penetration of

water molecules between the water complexes existing must be less than for penetration between the clay surfaces, or due to hydration of the cations and arrangement of water molecules in the interlayer regions.

Swelling pressures

The change in free energy at constant temperature can be expressed as:

$$dF = V\,dp \tag{21}$$

where V is the molar volume of the adsorbed water and p is the external pressure. However, if we consider that the expansion is due only to the adsorption of vapor on the interlayer surfaces, the expression may be made to read:

$$\Sigma_{int}\, dF_i = V\,dp \tag{22}$$

Since water is incompressible this equation becomes:

$$dF_i = \frac{V}{\Sigma int}\,dp = h_o\,dp \tag{23}$$

where dF_i is the expansion energy per cm^2, V is the total volume of the interlayer at saturation per gm of calcium montmorillonite, h_o is the maximum platelet separation, and p is the applied pressure. When equation 23 is integrated, we obtain the following:

$$\Sigma_{int}\int_{\Delta F = \Delta F_s}^{\Delta F_i} dF_i = \Sigma_{int}\int_{p=0}^{p} h_o dp$$

$$p = \frac{\Sigma_{int}\Delta F_i - \Sigma_{int}\Delta F_s}{h_o\,\Sigma int} \tag{24}$$

where ΔF_s is the expansion energy when clay is in equilibrium with saturated vapor, p is the pressure required to prevent any platelet separation, and p = 0 is the pressure when the maximum separation is obtained. From Figure 33 the expression $\Sigma_{int}{}^{\Delta F_i} - \Sigma_{int}{}^{\Delta F_s}$ for the expansion energy may be obtained for platelet separation h and h_o respectively. The swelling pressure may now be found by dividing the expression by the maximum platelet separation and the calculated internal surface area. Table 16 is a computation of expansion energies and swelling pressures for the calcium montmorillonite under investigation.

The internal area used in the Table was calculated using three different values for the cross sectional area of adsorbed water molecules and the value of q_m for the external area obtained from the BET equation. Hendricks and Jefferson (38) reported a laminar stacking of interlayer water such that the area occupied by a water molecule is 11.5 Å^2. The area occupied per molecule of closest packing would be 10.8 Å^2. The data in the present study suggests an ice-like configuration of water similar to the one proposed by Demirel (26) which gave a cross sectional area of 17.5 Å^2. Use of these three values in equation 9 gave the calculated external surface areas. Internal areas were determined by subtracting each external area from the total surface of 759 m^2/gm obtained from crystallographic data. The values for

Table 16. Expansion energies and swelling pressures for indicated separations due to adsorption of water vapor on the interlayer surfaces of calcium montmorillonite

	Area assigned to a water molecule, Å	Internal surface, area $_{int}$, m^2/gm	Expansion energy, $ergs/cm^2$	Swelling pressure, p, dynes, cm^2	Swelling pressure, $tons/ft^2$
No interlayer water present	10.8	653	----	377	394
	11.5	646	----	382	399
	17.5	587	----	419	437
One molecular layer of interlayer water	10.8	653	3.1	370	386
	11.5	646	3.1	374	390
	17.5	587	3.4	412	430
One molecular layer of interlayer water plus start of cation hydration	10.8	653	6.9	268	280
	11.5	646	7.0	271	283
	17.5	587	7.7	298	311
Two molecules of interlayer water (laminar stacking)	10.8	653	14.7	176	184
	11.5	646	14.9	180	188
	17.5	587	16.4	198	210

Table 16. (Continued)

	Area assigned to a water molecule, Å	Internal surface, area A_{int}, m^2/gm	Expansion energy, γ, ergs/cm^2	Swelling pressure, p, dynes, cm^2	Swelling pressure, tons/ft^2
Three molecular layers interlayer water	10.8	653	22.2	83	87
	11.5	646	22.4	85	89
	17.5	587	24.7	93	97
Four molecular layers of waterlayer water in tetrahedral co-ordination (ice-like configuration)	10.8	653	30.6	37	38
	11.5	646	31.0	37	38
	17.5	587	34.1	41	43
Five layers of interlayer water	10.8	653	31.2	---	---
	11.5	646	31.6	---	---
	17.5	587	34.7	---	---

the internal areas were: 653 m^2/gm for 10.8 $Å^2$, 646 m^2/gm for 11.5 $Å^2$, and 587 m^2/gm for 17.5 $Å^2$.

Van Olphen (77) used the desorption data of Mooney et al. (60, 61) to estimate the pressure required to remove monolayer of water from clay surfaces, by dividing the free energy change by the thickness of one monolayer of water. He found that the energy required to remove the interlayer water from between clay platelets to be from 50 to 100 ergs/cm^2 or 630 to 1,260 tons/ft^2.

Roderick and Demirel (71) used the method outline above to obtain swelling pressure values from 52 tons/ft^2 to 339 tons/ft^2. Roderick (70) obtained a total free energy change of 40.55 ergs/cm^2 using a sodium Wyoming bentonite. The sodium montmorillonite did not swell initially and he was able to accurately determine an external area. Determining the external area in this study was more difficult since only a very short range of relative pressure was observed where the adsorption was chiefly on the external surfaces. The data at relative vapor pressures between zero and $p/p_o = 0.015$ is limited and the extrapolation of the straight line indicating the free energy change due to adsorption on external surfaces in Figure 33 may not be as accurate as those determined by Roderick.

By using the procedures outline above, the uplift pressures for calcium montmorillonite were found to vary 38 tons/

ft^2 to 439 tons/ft^2, higher at lower relative pressures. Engineering relevance of this will be discussed in the following section.

Practical applications in engineering

The hysteresis loops observed in this study and the calculated uplift pressures are of major importance in highway or foundation design or construction. In the United States, for example, many or most central state and western soils contain calcium montmorillonite as their dominant clay mineral; if the natural soil moisture and climatic conditions are known, it should be possible to predict the soil consolidation or swelling behavior.

On the very extensive alluvial calcium montmorillonitic clays of the Mississippi delta and Gulf Coastal Plain, the first requirement for minimum depth of a building foundation is that it be located below the depth of seasonal volume changes caused by alternate wetting and drying. By keeping the moisture constant, there is little chance of the building failing by differential settlement. However, if the climatic conditions ever are such that the moisture is depleted (desiccation) below the foundation, structures will settle, and the swelling pressures should be sufficient to raise them back up upon rehydration, since the maximum foundation on clay is ordinarily limited to 2-4 tons/ft^2 to avoid

shear failure. The engineer must insure that the clay will remain in the region of saturation if the construction is carried out at high moisture contents. On the other hand, as seen in Figure 12, if the construction is carried out when the soil has not reached saturation, he must provide a system whereby any excessive moisture will be diverted away from the structure and the soil cannot reach final hydration.

In most cases only the higher relative vapor pressure region will be important, since relative humidities in natural soils seldom reach below 60%. The field condition d_{001} spacings are therefore probably in the 15.1 to 19.2 Å range. The observed hysteresis loop will be extremely beneficial for reducing volume change problems, since a relatively large reduction from saturation p/p_o will be required before there is significant volume change. Conversely, if the clay is naturally in the 15.1 to 15.6 Å state, free water is required to cause it to expand. Since the former condition is more common than the latter, we may anticipate that most natural calcium montmorillonites are probably at the 19.6 Å spacing, and remain on the desorption branch of the hysteresis loop in the p/p_o region of 0.65 to 1.0. The occasional drying below this p/p_o is probably the source of most problems.

CONCLUSIONS

1. Upon adsorption or desorption of water, the first order basal spacing of calcium montmorillonite varies in a continuous but non-uniform manner.

2. X-ray diffraction line breadths are a minimum for basal spacings of 16.5 and 19.2 Å, suggesting uniform layer separations at these spacings. Simultaneously the diffraction intensity decreases, indicating that the interlayer water has structure. Combining X-ray with adsorption data indicates that at 16.5 Å the water has an ice-like configuration; the 19.2 Å spacing and sorption data may be explained by intrusion of one additional layer of water.

3. At vapor pressures which give basal spacings less than 16.5 Å, line breadth and intensity data suggest simultaneous existence of varying numbers of water layers between the platelets, and steps in the basal spacings appear to be directly influenced by the interlayer cations.

4. At certain vapor pressures and d_{001} spacings, strong secondary basal reflections appeared in the neighborhood of 3 Å and 5 Å, and may be explained by use of an electron density curve inferred from the mica-like structure of the clay layers.

5. Interlayer swelling and shrinkage of calcium montmorillonite due to adsorption of water exhibit a hysteresis

forming two loops; one from relative vapor pressure of zero to about 0.40 and the other from about 0.55 to saturation. X-ray diffraction line breadths during desorption suggest that at low pressures the water is very strongly attracted to the surfaces or around cation positions forming islands of water within the interlayer regions. As the sheets become undulated, the water may be trapped and the escape of water to the vapor environment is inhibited. The hysteresis in the higher relative vapor pressure region is accompanied by an increase and then decrease of line breadth as the fourth and fifth layers of water are withdrawn. This water escapes quite easily indicating that is not as strongly oriented as the water near the surface of the platelets.

6. Calcium montmorillonite shows coloration after X-radiation. This was attributed to prolonged X-radiation induced color centers.

7. The sorption isotherms are completely reversible at a relative vapor pressures between zero and 0.20. The adsorption isotherms are more closely reproducible on successive cycles and the rate of adsorption is greater than desorption as observed from the automatic recording device and X-ray diffraction pattern, suggesting that the adsorption branch is the equilibrium branch.

8. The BET multimolecular adsorption model more closely fits the experimental data than does the Langmuir monomole-

cular adsorption model.

9. The experimentally determined total surface area calculated from the BET parameter q_m is equal to 714 m^2/gm, which is in good agreement with 759 m^2/gm calculated from crystallographic data.

10. The BET parameter C was used to determine the heat of adsorption of the first molecular layer of water on calcium montmorillonite less the heat of condensation of water $(E_1 - E_L)$. The calculated value of $(E_1 - E_L)$ was found to be 2.6 Kcal/mole, which agrees favorably with previously published data.

11. The free energy of wetting, defined as the free energy of immersion less the free energy change due to particle interaction was found on a compressed calcium montmorillonite powder to be 69.91 ± 2.30 ergs/cm^2 and 69.61 ± 2.72 ergs/cm^2 for the first and second adsorption cycles, respectively. This is in good agreement with data of Demirel (26) who obtained 76.61 ± 4.30 ergs/cm^2 using a loose powder. The magnitude of the free energy change is not affected by the degree of compression of the powder. The low pressure region data are most important for determining free energy changes.

12. The X-ray diffraction data and adsorption isotherm data were used to estimate the external surface area at low relative vapor pressure regions. The free energy was divided into two components: one due to adsorption on inter-

layer surfaces and particle interaction and the second for adsorption on external surfaces. These data enable one to estimate the expansion energies and uplift pressures. The swelling pressures exerted with the platelet separation corresponding to zero to four layers of water are 440 tons/ft^2 to 40 tons/ft^2, respectively.

BIBLIOGRAPHY

1. Adamson, A. W. Physical chemistry of surfaces. New York, N.Y., Interscience Publishers, Inc. 1960.

2. American Society for Testing Materials. 1961 Book of ASTM Standards. Part 4 Cement, Lime, Gypsum, Mortar, Concrete, Mineral Aggregates Bituminous Materials, Soils. Philadelphia, Pa., author. 1961.

3. Anderson, D. M. and Low, P. F. The density of adsorbed water by lithium, sodium, and potassium bentonite. Soil Science of America Proceedings 22: 99-103. 1958.

4. Aylmore, L. A. G. and Quirk, J. P. Swelling of clay water systems. Nature (London) 183: 1752-1753. 1959.

5. Bangham, D. H. The Gibbs adsorption equation and adsorption on solids. Faraday Society Transactions 33: 805-811. 1937.

6. Bangham, D. H. and Razouk, R. I. Adsorption and wettability of solid surfaces. Faraday Society Transactions 33: 1459-1463. 1937.

7. Barrer, R. M. and MacLeod, D. M. Intercalation and sorption by montmorillonite. Faraday Society Transactions 50: 980-989. 1954.

8. Barshad, I. The nature of lattice expansion and its relation to hydration in montmorillonite and vermiculite. American Mineralogist 34: 675-684. 1949.

9. Bartell, F. E. and Bower, J. E. Adsorption of vapors by silica gels of different structures. Journal of Colloid Science 7: 80-93. 1952.

10. Bering, B. P., Dreving, V. P., Kiselev, A. V., Serpinsky, V. V., Surova, M. D., and Shcherbakova, K. D. Adsorption properties of montmorillonite clays. Colloid Journal (USSR) 14: 433-441. 1952.

11. Boyd, G. E. and Livingston, H. K. Adsorption and energy changes at crystalline solid surfaces. American Chemical Society Journal 64: 2383-2388. 1942.

12. Bradley, W. F., Grim, R. E. and Clark, G. L. A study

of the behavior of montmorillonite upon wetting. Zeitschrift fuer Kristallographie 97: 216-222. 1937.

13. Brindley, G. W. Chlorite minerals. In Brown, G., editor. The x-ray identification and crystal structures of clay minerals. Pp. 242-296. London, Mineralogical Society. 1961.

14. Brindley, G. W. Kaolin, sepentine, and kindred minerals. In Brown, G., editor. The x-ray identification and crystal structures of clay minerals. Pp. 51-131. London, Mineralogical Society. 1961.

15. Brindley, G. W. X-ray diffraction by layer lattices with random layer displacements. In Brown, G., editor. The x-ray identification and crystal structures of clay minerals. Pp. 446-466. London, Mineralogical Society. 1961.

16. Brunauer, S. The adsorption of gases and vapors. Physical adsorption. Princeton, N.J., Princeton University Press. 1943.

17. Brunauer, S. Solid surfaces and solid-gas interface. Advances in Chemistry Series 33: 5-17. 1961.

18. Brunauer, S., Deming, L. S., Deming, W. E. and Teller, E. On a theory of the van der Waals adsorption of gases. American Chemical Society Journal 62: 1723-1732. 1940.

19. Brunauer, S., Emmett, P. H. and Teller, E. Adsorption of gases in multimolecular layers. American Chemical Society Journal 60: 309-319. 1938.

20. Buerger, M. J. Crystal structure analysis. New York, N.Y., John Wiley and Sons Inc. 1960.

21. Cornet, I. Expansion of the montmorillonite lattice on hydration. Journal of Chemical Physics 18: 623-626. 1950.

22. Craig, R. G., Van Voohis, J. J. and Bartell, F. E. Free energy of immersion of compressed powders with different liquids. I. Graphite powders. Journal of Physical Chemistry 6: 1225-1230. 1956.

23. Clampitt, B. H. and German, D. E. Heat of vaporization of molecules at liquid-vapor interfaces. Journal of Physical Chemistry 62: 438-440. 1958.

24. Davis, D. W., Rochow, T. G., Rowe, F. G., Fuller, M. L., Kerr, P. F. and Hamilton, P. Electron micrographs of reference clay minerals. American Petroleum Institute project 49. Ann Arbor, Michigan, Edwards Brothers Inc. 1950.

25. Deitz, V. R. Gas adsorption, the extreme limits of surface coverage. Industrial and Engineering Chemistry 57, No. 5: 49-66. 1965.

26. Demirel, T. Adsorption of water vapor by sodium and calcium montmorillonite. Unpublished Ph.D thesis. Ames, Iowa, Library, Iowa State University of Science and Technology. 1962.

27. Dobay, D. G., Fu, Y. and Bartell, F. E. Energetics of the adsorption of aliphatic amines by silica gel. American Chemical Society Journal 73: 308-314. 1951.

28. Emerson, W. W. The swelling of Ca-montmorillonite due to water adsorption. I. Water uptake in the vapour phase. Soil Science Journal 13: 31-39. 1962.

29. Emmett, P. H., Brunauer, S. and Love, K. S. The measurement of surfact area of solids and soil colloids by the use of low temperature van der Waals adsorption isotherms. Soil Science 45: 57-65. 1938.

30. Forslind, E. Crystal structure and water adsorption of clay minerals. Swedish Cement and Concrete Research Institute Bulletin 11: 1-20. 1948.

31. Forslind, E. Some remarks on the interaction between the exchangeable ions and the adsorbed water layers in montmorillonite. 4th International Congress of Soil Science Transactions 1: 110-113. 1950.

32. Foster, A. G. The sorption of condensible vapors by porous solids. I. The applicability of the capillary theory. Faraday Society Transactions 28: 645-657. 1932.

33. Fu, Y. and Bartell, F. E. Surface area of porous absorbents. Journal of Physical and Colloid Chemistry 55: 662-675. 1951.

34. Gillery, F. H. Adsorption-desorption characteristics of synthetic montmorillonite in humid atmospheres. American Mineralogists 44: 806-818. 1959.

35. Goates, J. R. and Hatch, C. V. Standard adsorption potentials of water vapor on soil colloids. Soil Science 75: 275-278. 1953.

36. Grim, R. E. Clay mineralogy. New York, N.Y., McGraw-Hill Book Company Inc. 1953.

37. Grim, R. E. Applied Clay mineralogy. New York, N.Y., McGraw-Hill Book Company Inc. 1962.

38. Hendricks, S. B. and Jefferson, M. E. Structure of kaolin and talc-pyrophyllite hydrates and their bearing on water sorption of clays. American Mineralogist 23: 863-875. 1938.

39. Hendricks, S. B., Nelson, R. A. and Alexander, L. T. Hydration mechanism of the clay mineral montmorillonite saturated with various cations. American Chemical Society Journal 62: 1457-1464. 1940.

40. Hirst, W. The mechanical interaction between mobile insoluble adsorbed films, capillary condensed liquid and fine-structured solids. Faraday Society Discussions 3: 22-28. 1948.

41. Hodgman, C. D., Weast, R. C. and Selby, S. M. Handbook of chemistry and physics. Cleveland, Ohio, Chemical Rubber Publishing Company. 1958.

42. Hofmann, U., Endel, K. and Wilm, D. Kristallstructur und quellung von montmorillonit. Zeitschrift fuer Kristallographie 86: 340-348. 1933.

43. Inness, W. B. and Rowley, H. H. Relationship between the adsorption isotherm and the spreading forces. Journal of Physical Chemistry 45: 158-165. 1941.

44. International Union of Crystallography. International tables for x-ray crystallography. Vol. II. Birmingham, England, The Kynoch Press. 1959.

45. Jura, G. and Harkins, W. E. Determination of the decrease of free surface energy of a solid by an adsorbed film. American Chemical Society Journal 66: 1356-1362. 1944.

46. Klug, H. P. and Alexander, L. E. X-ray diffraction procedures for polycrystalline and amorphous materials. New York, N.Y., John Wiley and Sons, Inc. 1954.

47. Langmuir, I. The adsorption of gases on plane surfaces of glass, mica, and platinum. American Chemical Society Journal 40: 1361-1403. 1918.

48. Lipson, M. and Cochran, W. The determination of crystal structures. London, England, G. Bell and Sons, Ltd. 1957.

49. Livingston, H. K. The cross sectional areas of molecules adsorbed on solid surfaces. Journal of Colloid Science 4: 447-457. 1949.

50. MacEwan, D. M. C. Solvation of clay minerals in relation to crystal structure: Interlamellar adsorption by clay minerals. 4th International Congress of Soil Science 1: 107-109. 1950.

51. MacEwan, D. M. C., Amil, A. R. and Brown, G. Interstratified clay minerals. In Brown, G., editor. The x-ray identification and crystal structures of clay minerals. Pp. 393-445. London, Mineralogical Society. 1961.

52. Macey, H. H. Clay-water relationship and the internal mechanism of drying. Ceramic Society Transactions 41: 73-121. 1942.

53. Mackenzie, R. C. Hydrationseigenschaften von montmorillonit. Berichte der Deutsche Keramische Gesellschaft 41: 73-121.

54. McBain, J. W. An explanation of hysteresis on the hydration and dehydration of gels. American Chemical Society Journal 57: 699-700. 1935.

55. Maegdefrau, E. and Hofmann, U. Die Kristallstructur des montmorillonits. Zeitschrift fuer Kristallographie 98: 299-323. 1937.

56. Marshall, C. E. Layer lattice and base exchange clays. Zeitschrift fuer Kristallographie 91: 433-449. 1935.

57. Martin, T. R. Adsorbed water on clay: a review. National Conference on Clays and Clay Minerals Proceedings 9: 28-70. 1960.

58. Means, R. E. and Parcher, J. V. Physical properties of soils. Columbus, Ohio, Charles E. Merrill Books, Inc. 1963.

59. Mering, J. On the hydration of montmorillonite. Faraday Society Transactions 42B: 205-219. 1946.

60. Mooney, R. W., Keenan, A. G. and Wood, L. A. Adsorption of water vapor by montmorillonite. I. Heat of desorption and application of BET theory. American Chemical Society Journal 74: 1367-1371. 1952.

61. Mooney, R. W., Keenan, A. G. and Wood, L. A. Adsorption of water vapor by montmorillonite. II. Effect of exchangeable ions and lattice swelling as measured by x-ray diffraction. American Chemical Society Journal 74: 1371-1374. 1952.

62. Nagelschmidt, G. On the lattice shrinkage and structure of montmorillonite. Zeitschrift fuer Kristallographie 93: 481-487. 1936.

63. National Research Council of the United States of America. International critical tables. Vol. 1. New York, N.Y., McGraw-Hill Book Company, Inc. 1926.

64. Orchiston, H. D. Adsorption of water vapor. II. Clays at 25°C. Soil Science 78: 463-479. 1954.

65. Orchiston, H. D. Adsorption of water vapor. III. Homoinic montmorillonites at 25°C. Soil Science 79: 71-78. 1955.

66. Overbeek, J. T. G. The interaction between colloidal particles. In Kruyt, H. R. Colloid Science. Vol. 1. Pp. 245-277. New York, N.Y., Elsevier Publishing Company. 1952.

67. Pauling, L. The structure of the micas and related minerals. National Academy of Science Proceedings 16: 123-129. 1930.

68. Quirk, J. P. and Aylmore, L. A. G. Swelling and shrinkage of clay-water systems. 7th International Congress of Soil Science Transactions 2: 378-387. 1960.

69. Road Research Laboratory, Department of Scientific and Industrial Research (Great Britain). Soil mechanics for road engineers, London, England, Her Majesty's Stationery Office. 1954.

70. Roderick, G. L. Water-vapor sodium montmorillonite interaction. Unpublished Ph.D Thesis. Ames, Iowa, Li-

brary, Iowa State University of Science and Technology. 1965.

71. Roderick, G. L. and Demirel, T. Water vapor sodium montmorillonite interaction. Iowa State Univ. of Sci. and Tech. Engr. Expt. Sta. Progress Report. 1965.

72. Ross, S. On physical adsorption. IV. A comparison of two theories of multimolecular adsorption. Journal of Physical and Colloid Chemistry 53: 383-391. 1949.

73. Spangler, M. G. Soil engineering. Scranton, Pa., International Textbook Company. 1960.

74. Takizawa, M. Mechanism of water vapor adsorption in bentonite. Tokyo Institute of Physical and Chemical Research Scientific Papers 54, No. 3: 313-322. 1960.

75. Taylor, D. W. Fundamentals of soil mechanics. New York, N.Y., John Wiley and Sons, Inc. 1948.

76. Topping, J. Errors of observation and their treatment. London, England, The Institute of Physica. 1957.

77. van Olphen, H. An introduction to clay colloid chemistry. New York, N.Y., Interscience Publishers. 1963.

78. van Olphen, H. Interlayer forces in bentonite. National Academy of Science-National Research Council Publication 327: 418-438. 1953.

79. van Olphen, H. Thermodynamics of interlayer adsorption of water in clays. I. Sodium vermiculite. Journal of Colloid Science 20: 822-837. 1965.

80. van Olphen, H. Unit layer interaction in hydrous montmorillonite systems. Journal of Colloid Science 17: 660-667. 1962.

81. Wu, T. H. A nuclear magnetic resonance study of water in clay. Geophysical Research Journal 69: 1083-1091. 1964.

82. Zettlemoyer, A. C., Young, C. J. and Chessick, J. J. Studies of the surface chemistry of silicate minerals. Journal of Physical Chemistry 59: 962-966. 1955.

ACKNOWLEDGEMENTS

The subject matter of this investigation was obtained as a part of the research done under Project 576-S of the Iowa Engineering Experiment Station, Soils. Project 576-S is under contract with the Iowa Highway Research Board and is supported by funds supplied by the Iowa State Highway Commission. The Officer's Graduate Training Program of the U.S. Army Corps of Engineers and U.S. Army Degree Completion Program enabled the author to engage in the research described in the dissertation.

The author is especially indebted to Dr. Richard L. Handy under whose supervision this research was conducted for his guidance, advice, ever ready assistance and suggestions throughout the investigation.

I cannot adequately describe in words my appreciation for the time and help so gladly given whenever required, by my good friend Dr. T. Demirel. My thanks to Dr. R. A. Jacobson, Chemistry Department, Iowa State University for his advice on X-Ray problems. To the other members of the Engineering Experiment Station Soils Research Laboratory the author wishes to express his thanks for their help in the investigation. To Brad Moses and Bill Bauer for their aid in preparing the data included in the study.

Den Fakultaet des mineralogisches Institutes der Goethe

Universitaet, Frankfurt am Main, moechte ich meinen herzlichen Dank fuer das Priveleg mir den Gebrauch des Labors und der Roentgenangelegenheiten zu gestatten auszusprechen.

Never has one man owed so much to his dear wife, unhonored, and unsung, who has withstood the slings and arrows of outrageous demands upon her patience and immense good nature. To Dorothy.....lend me a heart replete with thoughtfulness.